FINAL REPORT
R3189-01R

EFFECT OF HIGH CP POTENTIALS ON PIPELINES

PRCI CONTRACT NO. PR-186-02107
US DOT CONTRACT NO. DTRS56-03-T-0004

PREPARED FOR
PIPELINE RESEARCH COUNCIL INTERNATIONAL, INC.
US DEPARTMENT OF TRANSPORTATION
WASHINGTON, DC

PREPARED BY
CC TECHNOLOGIES LABORATORIES, INC.
MARK YUNOVICH, MS, MBA, NACE CORROSION SPECIALIST
BRETT TOSSEY, BS

NOVEMBER 2004

CC Technologies
5777 FRANTZ ROAD
DUBLIN, OHIO 43017
614.761.1214 • 614.761.1633 fax
www.cctechnologies.com

EXECUTIVE SUMMARY

Concern over the effects of high cathodic protection potentials ("overprotection") on pipelines has been discussed for many years. The concern focuses in two areas: (1) high potentials' affecting pipeline coatings and (2) high potentials resulting in hydrogen-related damage to the steel. The primary objective of the research was to develop a set of guidelines that will assist a pipeline operator in selecting a high potential limit. The project received funding from two sources: PRCI and USDOT. Co-funding by the Department of Transportation enabled the expansion of the originally funded work plan to include additional testing conditions.

The results of the extensive experimental program show that, under the tested conditions, the imposition of the cathodic protection current had an effect on the mechanical properties of the studied steels (X65 with and without simulated "hard spots" and X100 grades). The primary observed effect is that, in response to the increase of the current density of the CP current, the brittle area on the fracture surface of the slow strain rate test specimens increased as well. The size of the brittle area serves as a proxy for the propensity to hydrogen-related damage. Similar trends were observed for the tested external pipeline coatings (mill-applied FBE and three-layer coatings and hand-applied liquid epoxy): higher imposed CP densities led to a more pronounced disbondment of the coatings (some coatings performed better than others) in the presence of a holiday. None of the coatings exhibited a propensity to blistering.

It is important to stress that whereas the increase in the cathodic protection current produced an effect on the mechanical properties of the studied steels and external coatings, there is insufficient data to draw definitive conclusions as to the quantified relationship between the CP current density and structural integrity of the operating pipelines. The CP effect on the materials' properties is material-specific and a 'one-size-fits-all' approach to choosing a 'hard and fast' criterion may not be adequate and will likely result in over- / underestimation of the potential problem in some circumstances. The assessment of the hazards of increased cathodic disbondment area at existing holidays at higher CP currents should be considered with regard to the ability of the imposed CP to mitigate corrosion at the larger holiday(s).

Laboratory tests were carried out at an ambient temperature; it should be recognized that the results may not represent pipelines at significantly different temperatures. Accurate determination of the level of conservatism inherent in the experimental results (with respect to hydrogen related damage and coating disbondment) will require further study. Notwithstanding the above, prolonged periods of 'overprotection' should be avoided.

The value of less than 2 mA/ft^2 may serve as a target value for the CP current density (and can be monitored through the use of Coupon Test Stations); at this time, the use of the polarized off-potentials as the sole criterion for the assessment of the hazards of hydrogen-related damage is discouraged. The proposed approach to monitoring for conditions conducive to cathodic disbondment should include monitoring both current density and off-potential values. As a *preliminary* and *general* guideline, the use of the -1.1V (CSE) off-potential and 2 mA/ft^2 for the upper limits of the polarized potential and

applied CP current density, respectively, may be acceptable. In order to evaluate the degree of the universality and to establish the degree of the conservatism of this criterion, further testing is necessary.

The adoption of the -1.1V off-potential value as the “overprotection” criterion should be weighed against the hazard of not complying with the NACE PR0169 protection criterion on more vast regions of the underground structure if the CP output is decreased. One possible solution for resolving the dilemma of complying with both the RP0169 CP criteria and avoiding the local overprotection is to install additional anode groundbeds to achieve a finer control of the CP potential conditions and even out the potential distribution along the protected structure. The alternatives are to reconfigure the CP system and/or to recoat selected sections of the pipeline.

TABLE OF CONTENTS

LIST OF FIGURES

LIST OF TABLES

INTRODUCTION

Concern over the effects of high cathodic protection potentials ("overprotection") on pipelines has been discussed for many years. The concern focuses in two areas: (1) high potentials' affecting pipeline coatings and (2) high potentials resulting in hydrogen-related damage to the steel.

Although coating disbondment has been examined extensively over the past several years, a systematic study to examine the specific effect of overprotection of a CP system in soil environments has not been performed. Industry still does not know the extent to which overprotection at the levels present on pipelines promotes conditions leading to coating damage (coating disbondment). This is critical since coating disbondment is a significant factor in the ability to mitigate corrosion on a pipeline by cathodic protection.

The primary reduction reactions that occur on the steel surface during cathodic protection are the reduction of oxygen and the reduction of water (accumulation of hydroxyl ions and elevation in pH are particularly important for cathodic disbondment of coatings):

$O_2 + 2H_2O + 4e^- > 4OH^-$ [Oxygen Reduction]
$2H_2O + 4e^- > H_2 + 2OH^-$ [Water Reduction]

Water reduction is the only reaction that produces hydrogen, while both reactions produce hydroxide anions and increase the pH of the environment at the steel surface. At protection potentials more positive than –0.9 V (CSE), oxygen reduction is the predominant reaction. The potential at which water reduction occurs is dependent on the pH; but typically begins to contribute to the total reduction reaction at –0.7 to –0.8 V (CSE). It is generally accepted that the rate of hydrogen production increases an order of magnitude every 120 mV (Tafel constant) of increasing negative potential. Between –0.9 and –1.1 V, the rate of water reduction is as important as oxygen reduction and at potentials between –1.0 to –1.2 V water reduction (hydrogen production reaction) is predominant. Therefore, hydrogen production typically becomes dominant at potentials greater than –1.0 V.

With the use of higher strength pipeline steels (X-60 and greater), hydrogen damage mechanisms have become a greater concern. Of greatest concern are (1) hard spots in X-60 steels and (2) newer high strength pipeline steels (X-80 and above). Hydrogen damage mechanisms that are typically a concern to the pipeline operator include HIC (hydrogen induced cracking), SOHIC (stress oriented hydrogen induced cracking), and HE (hydrogen embrittlement).

Environmental factors controlling damage (either hydrogen damage to the steel or coating disbondment) due to overprotection are those factors that affect the rates of reduction reactions. These factors are soil type, soil moisture, and soil chemistry (pH, alkalinity, resistivity, etc.). Other critical factors include level of CP (polarized potential or current density), coating type, and type of steel and local metallurgy (hard spots [HE] or inclusions [HIC and SOHIC]).

The question of overprotection is made more complicated because of the difficulties in measuring the potential of the steel. The potentials discussed above are “polarized” potentials estimated for pipelines by interrupting the CP and measuring an off-potential. Accurate estimates of the polarized potential are difficult or impossible for many pipelines. For these pipelines, only on-potentials are available unless special monitoring, such as coupon monitoring, is employed. Some pipeline operators have adopted high potential limits based on on-potentials; the upper limits for the on-potential criteria have been reported to range from–1.2 to -3.0 V (CSE).

The preferred measurement however is based on the off-potentials, as the on-potentials may contain significant errors associated with the ohmic (IR) drop in high(er) resistivity environments. Typically, the value of –1.2 V would apply to those operators for whom off-potentials are available. Any study that develops guidelines for operators concerning overprotection limits must address the issue of off-potentials versus on-potentials in some manner. The primary difficulty is that no one has been able to estimate the IR drop of a specific application, which would allow a direct relationship between on- and off-potential measurements. It is not expected that such a relationship can be established without a significant effort.

Objectives and scope

The primary objective of the research is to develop a set of guidelines that will assist a pipeline operator in selecting a high potential limit. This set of recommendations and criteria will enable the users to choose CP potentials based on the specific properties of steel and protective external coating. The specific objectives are:

1. Establish the relationship between hydrogen damage to pipeline steels and CP overprotection.
2. Establish the relationship between pipeline coating disbondment and CP overprotection.
3. Develop practical criteria/guidelines for limiting the CP level on pipelines.

The scope of the project focused on the laboratory experiments in realistic soil conditions for both coating disbondment and hydrogen damage testing.

WORK PLAN

Project organization

The project received funding from two sources: PRCI and USDOT. Co-funding by the Department of Transportation enabled the expansion of the originally funded work plan to include additional testing conditions. Furthermore, during the course of investigation, the scope was expanded further to reflect the interim findings.

The work plan was divided into two three distinct subsets:

1. Evaluation of the impact of high CP potentials (overprotection) on the common linepipe steels (Task 1 PRCI and Task 4 USDOT), referred to as Task I in this report.
2. Evaluation of the impact of high CP potentials (overprotection) on cathodic disbondment of common external surface coatings for underground pipelines (Task 2 PRCI and Task 5 USDOT), referred as Task II in this report.
3. Preparation of a set of guidelines (Task 3 PRCI and Task 6 USDOT), referred as Task III in this report.

Task I – Hydrogen-Induced Damage to Steel

Task I consisted of laboratory testing of specimens for hydrogen-related damage. The test variables included the following:

- Type of steel (X 65 with 3 different chemistries, X70, and X100)
- Presence of hard spots (on X65 linepipe steel)
- Level of CP (three different levels)
- Soil environment (one type)

The specimens were evaluated using slow strain rate tests (SSRT) on notched cylindrical specimens. Prior to conducting the SSRT tests, the specimens were subjected to testing in the environment prescribed in NACE International TM0284-96 "Evaluation of Pipeline and Pressure Vessel Steels for Resistance to Hydrogen-Induced Cracking" to select the materials susceptible to the hydrogen damage.

In addition, control SSRT tests were carried out on specimens exposed to air. Specific details of the Task I testing are described in the Experimental Approach section.

Task II – Coating Disbondment

Task II consisted of laboratory testing of several coating types in actual soil environments. The testing protocol was an amalgamation of ASTM G8, ASTM G95, and the CAN/CSA Z245 standards for coating disbondment testing with the exception of the testing environment and the applied potentials/currents. The test variables included the following.

- Coating type (FBE with two thicknesses, liquid epoxy, and three-layer system)
- Coating thickness (two thicknesses for FBE)
- Level of CP (three different levels)
- Soil environment (three different soil environments)

Specific details of the Task II testing are described in the Experimental Approach section.

Task III – Guidelines

The goal of Task III was to develop a set of practical criteria to assist a pipeline operator in selecting a maximum acceptable output high potential limit for operating a CP system. These criteria are based on the relationships developed in Tasks I and II.

TASK I – HYDROGEN-INDUCED DAMAGE TO STEELS

Testing of the effect of high CP potentials on mechanical properties and metallurgy of several common and recently introduced pipeline steel grades was carried under the activities stipulated by Task I (combining Task 1 and Task 4 of the PRCI- and USDOT-funded effort, respectively.

Approach

Testing was carried out in two steps: preliminary screening tests (immersion tests in accordance with standard NACE procedures) were followed by evaluating selected materials at different levels of cathodic protection current densities under applied stress. The details of the testing approach are described below.

Tested materials

The effect of high CP on the material properties of commonly used pipeline steels was evaluated using the following materials:

- X65 (linepipe steel with two carbon concentrations and vessel plate with similar composition)
- X65 with simulated (by heat treatment) 'hard spots'
- X70 (linepipe steel)
- X100 (plate)

The X65 linepipe steel had two carbon concentrations (denoted LC for 'low carbon' and HC for 'high carbon'). The vessel plate was chosen to verify the aggressiveness of some of the screening tests (see next section); this material had been used in other studies and had exhibited considerable propensity to hydrogen damage. The X70 material was supplied as X80; however, mechanical testing has shown that its properties were closer to the API 5L specification for the X70 steel. The lack of availability of X100 linepipe steel prompted the use of the X100 steel plate.

The chemical composition and mechanical properties of the tested materials are shown in Table 1 and Table 2, respectively. The chemical composition and the mechanical properties were found to be in compliance with API 5L (July 2000), where applicable (with the noted exception for X80 steel).

Microstructures of the steels in as-received condition are shown in Figure 1 through Figure 4.

Table 1. Chemical composition of tested materials.

	Concentration, % wt.			
API 5L	**Carbon**	**Manganese**	**Phosphorus**	**Sulfur**
X65	0.26	1.45	0.03	0.03
X70	0.26	1.45	0.03	0.03
X100	Not specified			
Material designation				
X65 (LC)	0.049	1.06	0.013	0.005
X65 (HC)	0.16	1.23	0.015	0.005
X65 (Vessel plate)	0.23	1.05	0.007	0.014
X70	0.083	1.12	0.011	0.004
X100	0.064	1.91	0.007	0.004

Table 2. Mechanical properties of tested materials.

API 5L	**Tensile strength, psi**	**Yield strength, psi**	**Elongation, %**
X65	77,000	65,000	20
X70	82,000	70,000	22.3
X100	Not specified		
Material designation			
X65 (LC)	71,250	67,000	39.5
X65 (HC)	87,350	65,350	30
X65 (Vessel plate)	81,000	65,000	21
X70	86,250	73,750	53.5
X100	127,500	96,250	27.5

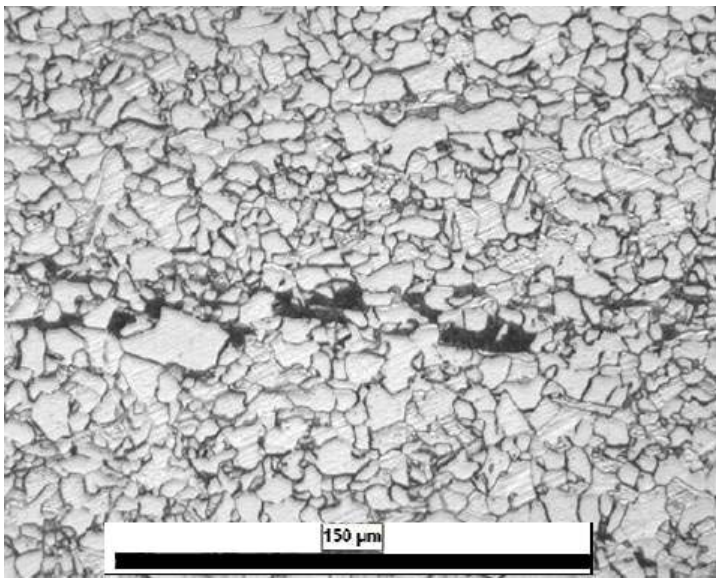

Figure 1. X65(LC) steel, 0.049% carbon, microstructure.

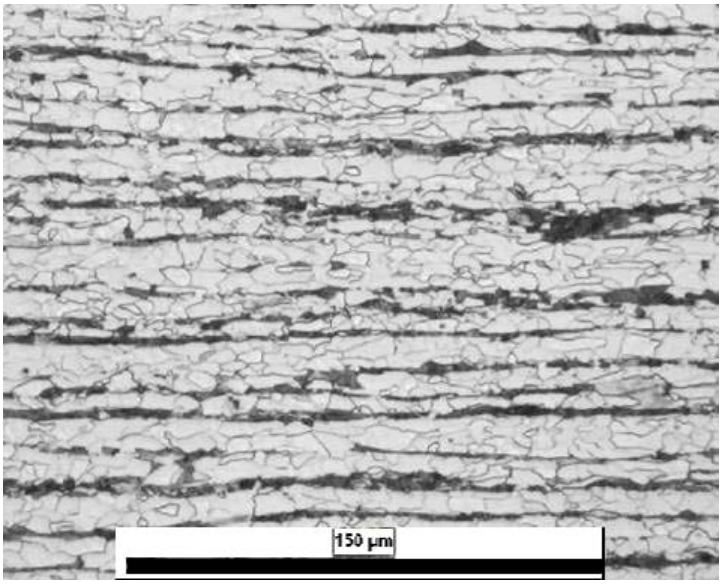

Figure 2. X65(HC) steel, 0.16% carbon, microstructure. Note pearlite banding.

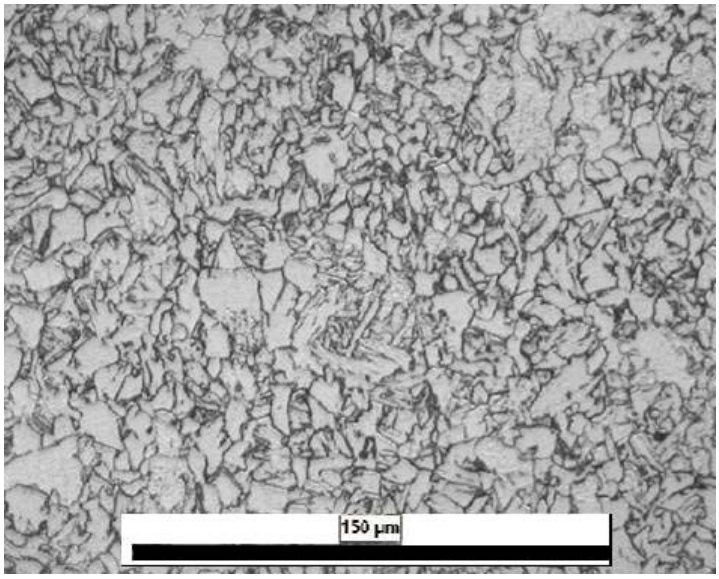

Figure 3. X70 steel microstructure.

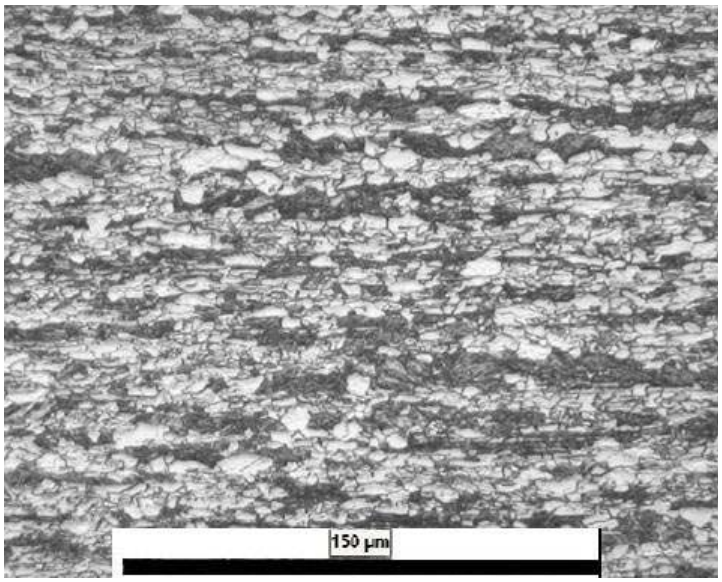

Figure 4. X100 steel microstructure.

Hard Spots: Heat Treatment Technique.

The X65(HC)[1] steel (0.16% carbon) was subjected to a single-stage heat treatment to simulate hard spot conditions. The details of the heat treatment procedure are given in Appendix A1.

Screening tests for hydrogen-related damage

As a first step, in order to establish whether any of the materials are likely to exhibit propensity to hydrogen-related damage, X65, X70, and X100 steels were subject to screening tests. Both HIC and SOHIC tests were used as a screening procedure for the' susceptibility to hydrogen damage. The presence of hydrogen sulfide (used in the screening tests) 'poisons' or reduces the efficiency of the atomic hydrogen recombination reaction at the steel surface, resulting in a much higher flux of atomic hydrogen diffusing into the steel matrix. The high rate of hydrogen charging in the screening tests was expected to exceed the amount of hydrogen charging found at a steel surface under high cathodic protection conditions thus allowing screening the susceptible materials for further testing. The assumption was that the screening tests would be harsher than the mechanical tests used to evaluate the effect of high CP potentials. Experimental details are provided in Appendix A2.

Specific combinations of the test specimen/test protocol are shown in Table 3.

[1] Heat treated specimens are denoted as (HT) for 'heat treatment'.

Table 3. Test specimen/test protocol combinations for screening tests.

Sample ID	SOHIC	HIC
X65(Vessel plate) 0.23%C	Y	Y
X65(LC) 0.049%C	Y	Y
X65(HC) 0.16%C	Y	N
X65(HC)(HT) 0.16%C, heat treated	Y	N
X70	Y	Y
X100	Y	Y

Slow Strain Rate Testing

The pipeline steels that failed the screening tests were subjected to slow strain rate testing (SSRT). Also, as the SSRT results were being analyzed, it was decided to expand the scope of the testing and include the X65(LC) steel which did *not* exhibit susceptibility to hydrogen damage in the screening tests. Furthermore, the tests on both X65(LC) and X65(HC) included current density of 0.2 mA/ft^2 to evaluate the effect of the CP currents of the magnitude referenced as an approximate requirement for the underground coated pipelines in low resistivity soils.

With the exception of the control samples (tested in air), all specimens were tested in the saturated RNM soil (slurry consistency)[2]. Cathodic protection was applied immediately after the samples had been exposed to the soil[3]; the CP current was controlled galvanostatically throughout the test duration. The specimens were charged for 24 hours prior to applying the tensile stress. The test duration was determined by the complete failure of the test specimen.

The test matrix is shown in Table 4.

Table 4. Experimental matrix for SSRT evaluation.

Steel	Environment	Current density, mA/ft^2
X100	Air	na
	RNM	2, 200
X65(HC)	Air	na
	RNM	0[2], 0.2, 2, 200
X65(HC)(HT)	Air	na
	RNM	2, 200
X65(LC)	RNM	0.2, 2, 200

[2] For description of soil properties, see Table 12.
[3] One X65(HC) specimen was tested without CP.

Tested current densities
The choice of the current densities was predicated on two goals:

- to establish the presence/absence of the impact of varying CP currents on the mechanical properties of the tested linepipe steels and external coatings

- to evaluate the effect of the current densities which may be encountered in the field

The lower values of 0.2 and 2.0 mA/ft^2 are representative of the range suggested as a general guideline by the NACE Corrosion Engineer's Reference Book[4] and Peabody's Control of Pipeline Corrosion[5], respectively. The value of 0.2 mA/ft^2 represents CP requirement suggested for a coated pipe and 2.0 mA/ft^2 is the suggested requirement for a bare pipe underground. Whereas these current densities assume the total area of the pipe, it is likely that locally, current densities are considerably higher (e.g., at a holiday in a coating). The highest value (200 mA/ft^2) was chosen because it was believed to be near the high range of currents that could exist on a pipeline coating flaw. This high value was chosen to ensure that any detrimental effect would be identified in the overall test program, but the number was not considered so high that it would fall outside of a practical range. From a CP design standpoint, 200 mA/ft^2 is not a realistic target for applied current density; however, this high current may occur near a CP groundbed, especially if the rectifier output is high[6]. The choice of 20 mA/ft^2 follows the same reasoning; it also provides a 'mid-point' value for the tested CP currents.

When the current was applied to SSRT specimens, the total area of the bare specimen was taken into account to achieve the desired current density.

The readers should note that the selected range allows establishing the presence/absence of the impact of varying CP currents on the mechanical properties of the tested linepipe steels and external coatings. Although the experimental matrix serves as a basis for preliminary practical guidelines with regard to overprotection/upsets, in order to evaluate the effect of CP currents/potentials commonly found in the field, further experimentation is required, which would focus on the lower end of the studied range of currents.

Test specimens
Longitudinal steel blanks approximately 12 in. long and 1 in. wide were removed from the pipe wall. SSRT specimens were machined from the blanks to the specifications presented in Figure 5. The notch was machined into the center of the gauge section in each specimens using electrical discharge machining (EDM). The notch depth was 0.010 inch with a notch root radius of 0.005$\pm$0.002 in. The purpose of the standardized defect (notch) was to create a region of triaxial stress and localize the hydrogen ingress to the notched area. The strain rate was 5×10^{-7} s^{-1} during all of the SSR tests.

[4] NACE Corrosion Engineer's Reference Book, 3rd Edition, NACE, 2002, p. 162.
[5] Peabody's Control of Pipeline Corrosion, A.W. Peabody, Second Edition, NACE, 2001, p. 93.
[6] During a field investigation in 2003, CC Technologies has observed CP current densities in excess of 450 mA/ft^2 on a coated pipeline (using coupon test stations).

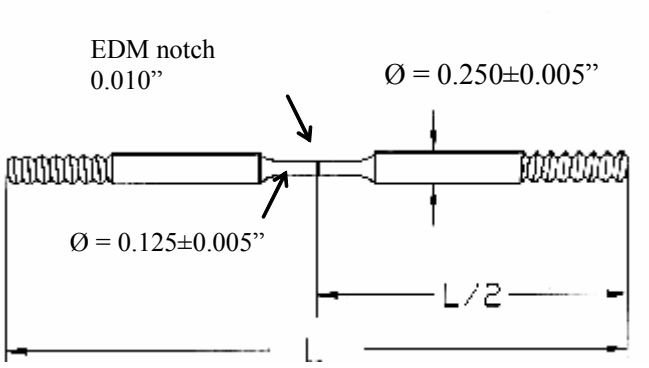

Figure 5. SSR specimen dimensions and EDM notch location.

Figure 6 shows the hardness profile of the metal bar used to manufacture the SSRT specimen from the X65(HC)(HT). As seen, the surface hardness at the root of the notch in the gauge section of the sample is approximately 32 HRC (denoted by red star).

The polarized off-potentials were measured several times during the test; the accuracy of the measurement was enhanced by the use of Luggin probe placed close to the notch in the gauge section. The experimental setup is shown in Figure 7.

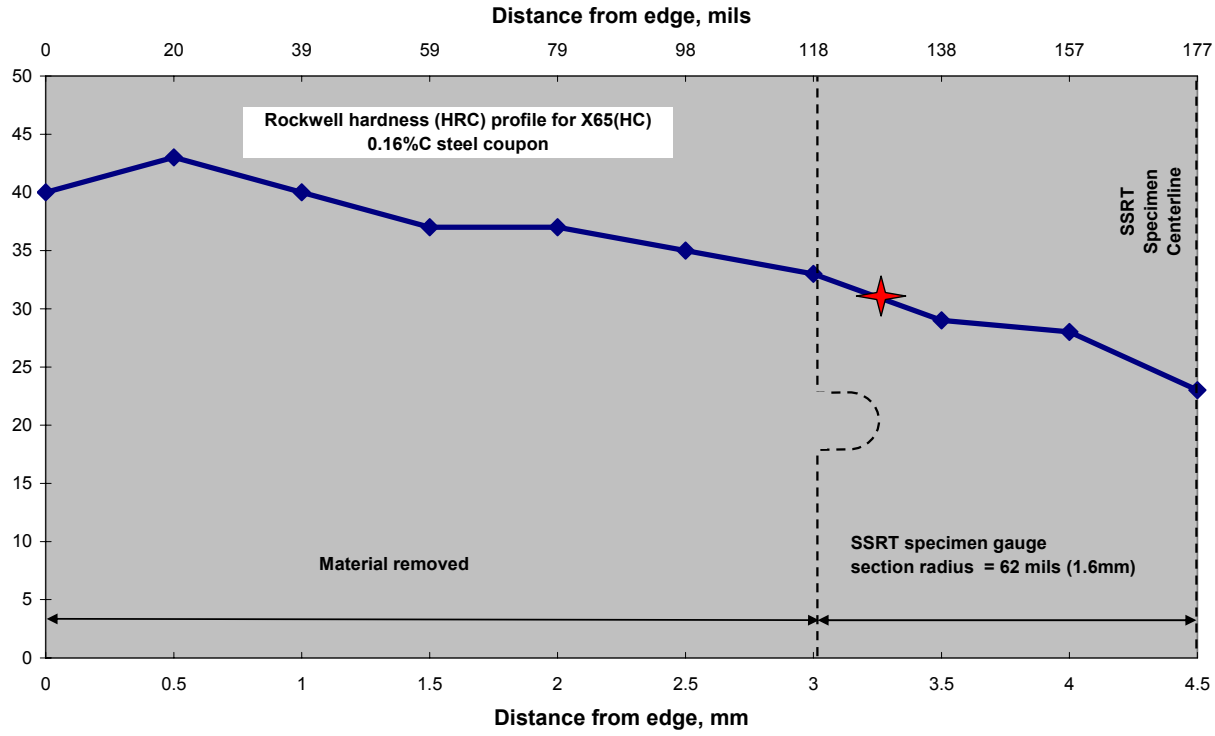

Figure 6. Hardness profile measurements on the metal bar used for fabrication of SSRT specimen from heat treated X65(HC) (HT) steel.

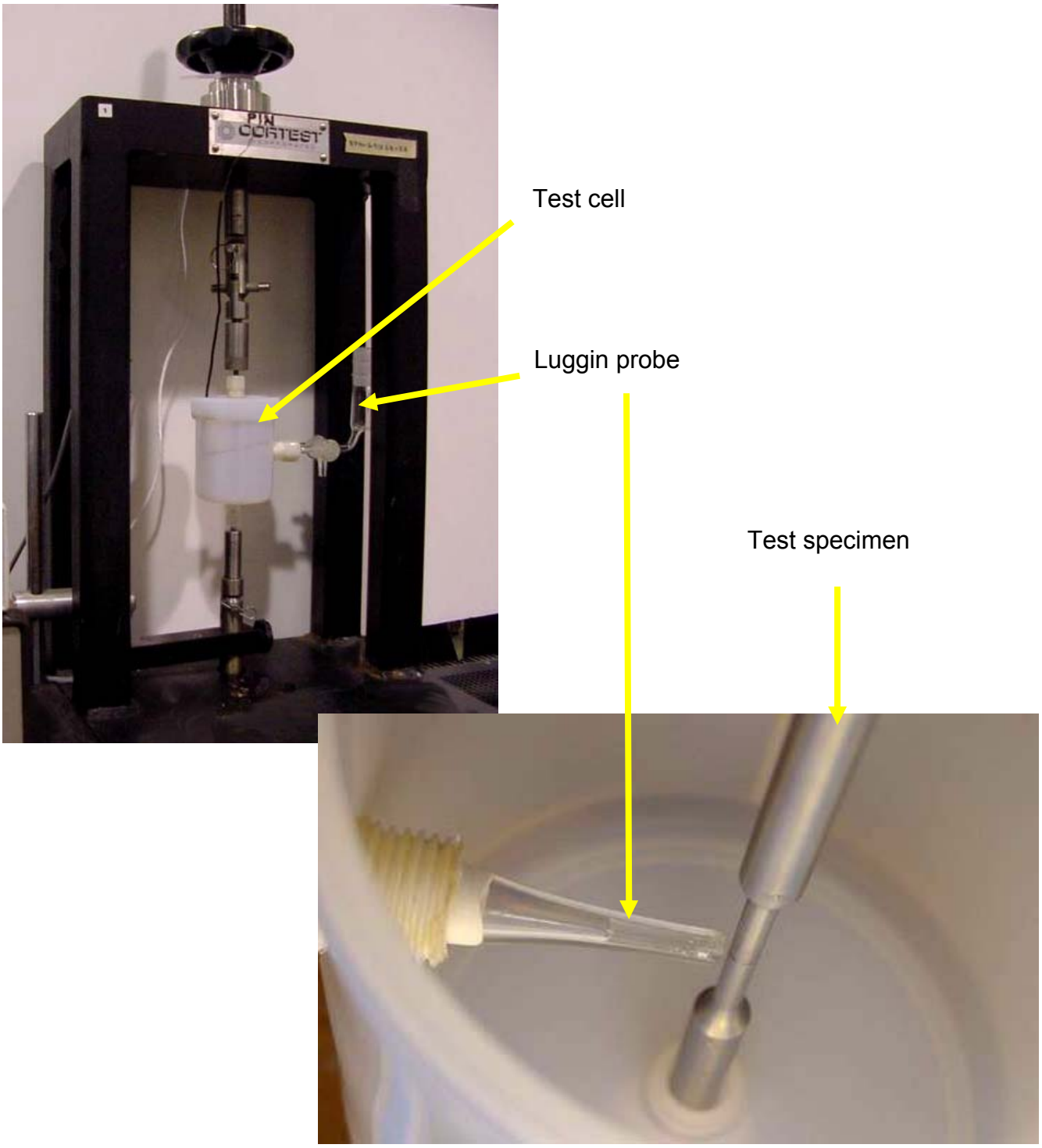

Figure 7. SSRT setup. The inset shows Luggin probe tip next to the EDM notch in the gauge section of the specimen prior to filling the cell with soil

Results and Discussion

Short Introduction to Hydrogen in Metals

Hydrogen production at steel surface

Hydrogen diffuses into the metal because the concentration of hydrogen adsorbed to the surface is higher than in the bulk. Generically, diffusion occurs as a result of a concentration gradient (i.e., Fick's 1st law). Hydrogen can adsorb to the surface of a metal directly from a gas phase or by electrochemical reaction in an electrolyte. The concentration of hydrogen through the electrochemical mechanism is greater than by gaseous absorption, and the amount of hydrogen on the surface increases with current density.

Hydrogen absorption can occur when a metal (such as carbon steel) is exposed to an atmosphere containing gaseous hydrogen. Although this effect has been observed in systems with high temperatures and hydrogen partial pressures (e.g., refineries), it is not typically significant in gas transmission systems. Through this mechanism, the hydrogen concentration inside the metal is proportional to the square root of the partial pressure of hydrogen in the atmosphere, and the equilibrium constant depends on temperature. A small fraction of the molecular hydrogen in the atmosphere adsorbs onto the metal surface, dissociates into atomic hydrogen (MH_{ad}) and absorbs into the metal matrix (MH_{ab}), as seen in the following simplified equations:

$$H_{2\,(gas)} + M \leftrightarrow 2MH_{ad}$$
$$2MH_{ad} \leftrightarrow 2MH_{ab}$$

A thermodynamic equilibrium occurs between the hydrogen concentration absorbed in the metal and the partial pressure of hydrogen in the atmosphere, and an unrealistically high partial pressure of hydrogen is necessary in a carbon steel gas transmission pipeline for damage to occur.

The concentration of hydrogen is elevated by hydrogen production on the metallic surface by electrochemical reaction (e.g., through corrosion process or cathodic protection). Consequently, the driving force for diffusion into metals much higher. This can be explained by breaking the hydrogen evolution reaction into several steps. The first reaction step in neutral to basic media (e.g., soils) is:

$H_2O + M + e^- \leftrightarrow MH_{ad} + OH^-$ (Hydrogen Discharge - Volmer reaction)

The adsorbed hydrogen can then take the path of hydrogen evolution (i.e., gas) by one of two reactions:

$MH_{ad} + H_2O + e^- \leftrightarrow H_2 + OH^- + M$ (Hydrogen Evolution – Heyrovsky reaction)
$2MH_{ad} \leftrightarrow H_2 + 2M$ (Hydrogen Evolution – Tafel reaction)

The adsorbed hydrogen can also take the competing path of absorption to the bulk metal:

$MH_{ad} \leftrightarrow MH_{ab}$ (Hydrogen Absorption)

In general, higher cathodic current results in more hydrogen absorbed in the metal. As cathodic current increases, the amount of produced atomic hydrogen (Volmer reaction) also increases. However, the rate at which the atomic (i.e., adsorbed) hydrogen is consumed depends on the other three competing parallel paths (reactions). Two of these reactions produce molecular hydrogen (gas) and the other results in hydrogen absorption. The relative rates of these reactions will control the concentration of hydrogen in the metal.

It has been experimentally observed that the Hydrogen Absorption Efficiency (defined as the ratio of produced atomic hydrogen to the absorbed hydrogen concentration) is a complex function of environmental, superficial and metallurgical factors. This efficiency is usually higher at lower cathodic currents, but the net flux of absorbed hydrogen tends to increase with cathodic currents (but with lower efficiencies) until reaching a saturation value.

Hydrogen in linepipe steels

When hydrogen is absorbed inside a metal, it forms a so-called "solid solution," where the atomic hydrogen occupies interstitial sites in the metal crystal structure, generally producing a distortion.

For an ideal homogeneous and isotropic metal, the distribution of hydrogen absorption and distribution inside the metal is governed by simple diffusion (i.e., Ficks' laws). However, the application of Fick's laws is just an approximation in real metals, where the energy barriers and potential wells are not uniform due the presence of grain boundaries, carbides, inclusions, dislocations, and other discontinuities in the crystalline structure. These sites may act as hydrogen "traps", thus reducing the overall hydrogen flux rate through the metal, since the residence time of hydrogen atoms at these traps is higher than in normal interstitial sites.

Traps may be classified as attractive traps, physical traps or mixed traps. Attractive traps have a net force acting on the diffusing atomic hydrogen, such as those produced by electrical field gradients (e.g., some metallic impurities), internal stress gradients (e.g., dislocations, grain boundaries, crack tips), and heterogeneous temperature distribution. Physical traps, on the other hand, are modifications in the crystalline structure where the hydrogen is more energetically stable (e.g., cavities). Mixed traps have a combination of both attractive and physical trap characteristics. For example, hydrogen atoms can be attracted to dislocations due to changes in the stress field, and get trapped inside the distorted crystalline structure.

In linepipe material, the most common types of damage induced by hydrogen are Hydrogen Induced Cracking (HIC) and Stress Oriented Hydrogen Induced Cracking (SOHIC). HIC occurs in low strength steel (generally less than 80 ksi yield strength). HIC cracks form parallel to the rolling direction and may be linear, stacked, or both. Stringers of MnS or other elongated inclusions serve as hydrogen traps where atomic

hydrogen collects and combines to form hydrogen gas molecules. As internal gas pressure builds, blisters form resulting in internal cracks.

SOHIC is a type of HIC that forms a stacked array of cracks in the presence of externally applied stress and residual stress. Internal cracks orient in the direction normal to the applied stress. The stacked array is often located near a notch or pit, which acts as a stress riser. The plastic strain field at the notch root is a preferential location for hydrogen ingress, and the notch vicinity is often where SOHIC is found.

Several mechanisms have been proposed to explain these types of damage, and they all coincide in accumulation of hydrogen in traps. The crack initiation occurs when the hydrogen concentration in some of these preferential sites increases beyond a critical value, inducing stresses higher than the metal yield strength. In ferrous alloys (e.g., steel) the adsorption of hydrogen (e.g., at the crack tip) facilitates crack propagation, reducing the cohesive forces of the metal.

It has been shown that HIC or SOHIC susceptibility of a specific material depends on the absorbed hydrogen concentration. There is a threshold absorbed hydrogen concentration below which, hydrogen damage does not occur. Any condition (e.g. higher cathodic protection current) that increases the hydrogen absorption above this value will increase HIC and SOHIC susceptibility (other factors constant).

Screening tests

The results of the screening HIC and SOHIC tests are summarized in Table 5 and Table 6.

Table 5. Results of HIC testing

Sample ID	**Surface Blisters**	**HIC**
X65(Vessel plate) 0.23%C	N	Y
X65(HC) 0.16%C	N	Y
X65(HC)(HT) 0.16%C, heat treated	N	Y
X65(LC) 0.049%C	N	N
X70	N	N
X100	Y	Y

Table 6. Results of SOHIC testing

Sample ID (Load, %SMYS)	**Surface Blisters**	**Internal Cracks**	**SOHIC**
X65(Vessel plate) 0.23%C (72%)	Y	Y	Y
X65(LC) 0.049%C (72%)	Y	N	N
X65(LC) 0.049%C (90%)	Y	N	N
X70 (72%)	N	N	N
X70 (90%)	N	N	N
X100 (72%)	Y	Y	Y

The findings show that X100 experienced the most extensive attack, which includes blistering and both HIC and SOHIC cracks. The X65 steels with higher carbon content

(the vessel plate, X65(HC) and X65(HC)(HT)) have failed HIC testing; the vessel plate also suffered from SOHIC. Neither X70 nor X65(LC) were found to contain any HIC or SOHIC cracks. Examples of the HIC and SOHIC cracks are shown in Figure 8 and Figure 9, respectively; an expanded set of pictures can be found in Appendix B1.

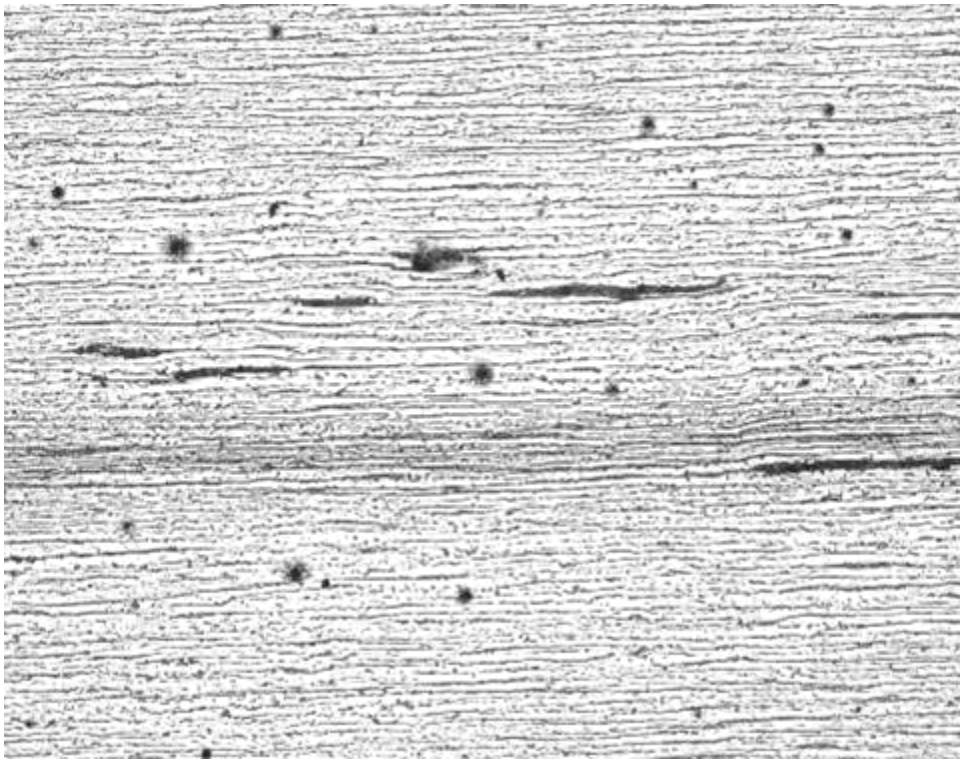

Figure 8. X65 (HC), 0.16% C, HIC, 50X magnification

Figure 9. X100, SOHIC cracks, 25X magnification.

Slow strain rate tests (SSRT)

Based on the results of the screening tests, the following materials were selected for the SSRT evaluation:

- X65(HC)
- X65(HC)(HT)
- X100

Upon completion of the tests involving the above-listed steels, it was decided to include the X65(LC) material in the testing to evaluate the response to the imposed CP current density of this common linepipe steel with different carbon content. Specific testing protocol for each material is shown in Table 4 (see earlier in the report).

The results of the SSRT experiments are summarized in Table 26 (shown as time-to-failure) and also presented in a graph format in Figure 40 to Figure 43 (see Appendix B1).

Effect of current density

Initial analysis showed that for the lower-strength X65 steel, the impact of the CP current was much more pronounced than for X100, as manifested by reduction of the times-to-failure (TTF) at CP compared to TTF in the air. Also, in a similar fashion, the heat treated material, X65(HC)(HT) exhibited a sharp reduction in TTF in the tests under CP. However, there were several notable inconsistencies in the TTF vs. current density trend, particularly at the lower current densities. (The TTF curves are shown in Appendix B1)

The analysis of the fracture surfaces yields a more consistent correlation between the applied CP currents and its effect on the materials' behavior. Scanning electron microscopy (SEM) evaluation of the fracture surfaces shows that the primary difference between the samples is the size of the area showing a ductile failure versus the area showing a brittle failure. The fraction of the brittle area is regarded as a metric linked to the susceptibility of the material to hydrogen-related damage.

Thus, all steel specimens tested in the air contained essentially only ductile fracture (99%+ of the total area). However, the specimens tested in soil have shown a much greater proportion of the brittle area on the fracture surface. Examples of mostly ductile and mostly brittle failures are shown in Figure 10 and Figure 11; the complete set of pictures of the fracture surfaces of the SSRT specimens is in Appendix B3.

The area fractions (ductile and brittle) were quantified using image analysis software. An example of the approach to the area computation is shown in Figure 12. The results of the measurements are summarized in Table 7. Then, the relative fractions (in percent of total area) were plotted against the current density.

Figure 10. X65(HC) steel, 0 mA/ft^2, 31X magnification. Note mostly ductile failure.

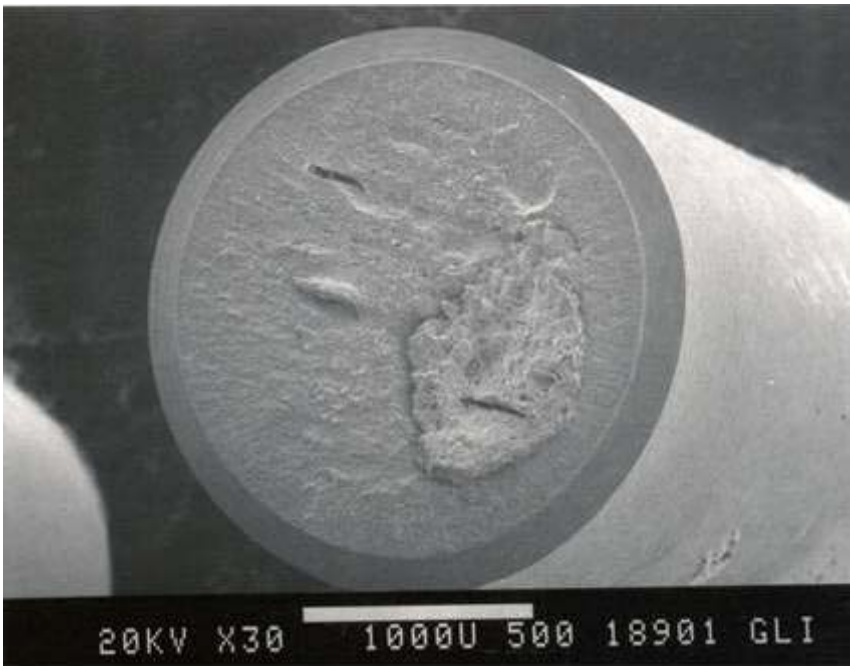

Figure 11. X65(HC) steel, 200 mA/ft^2, 30X magnification. Note mostly brittle failure.

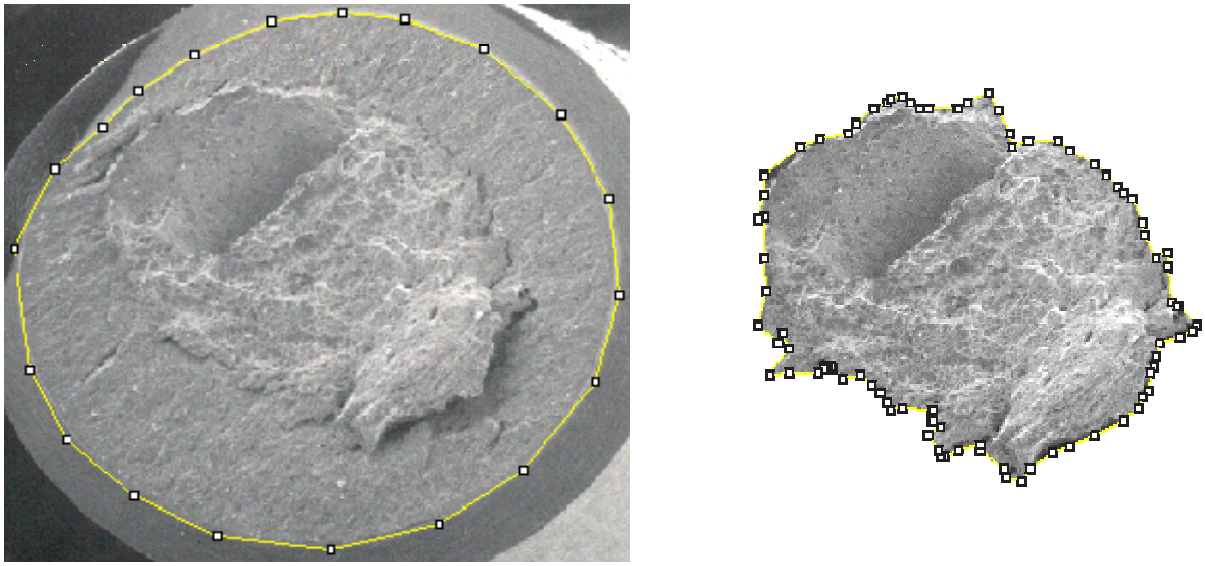

Figure 12. Example of ductile (right photo) and brittle area measurements

Table 7. Ductile and brittle area fractions.

Material	Current density, mA/ft^2	Ductile area (percent of total)	Brittle area (percent of total
X65(HC)	0	84.7%	15.3%
	0.2	58.0%	42.0%
	2	42.4%	57.6%
	200	23.6%	76.4%
X65(LC)	0.2	69.1%	30.9%
	2	60.2%	39.8%
	200	13.6%	86.4%
X65(HC)(HT)	2	48.0%	52.0%
	200	20.0%	80.0%
X100	2	53.7%	46.3%
	200	45.4%	54.6%

The tabulated data above is presented in graphs in Figure 13 and Figure 14. As seen, testing at the corrosion potential (0 mA/ft^2) resulted in some of the fracture becoming brittle in nature. However, it is in the tests with applied CP current where the impact of the current density on the material properties is particularly evident.

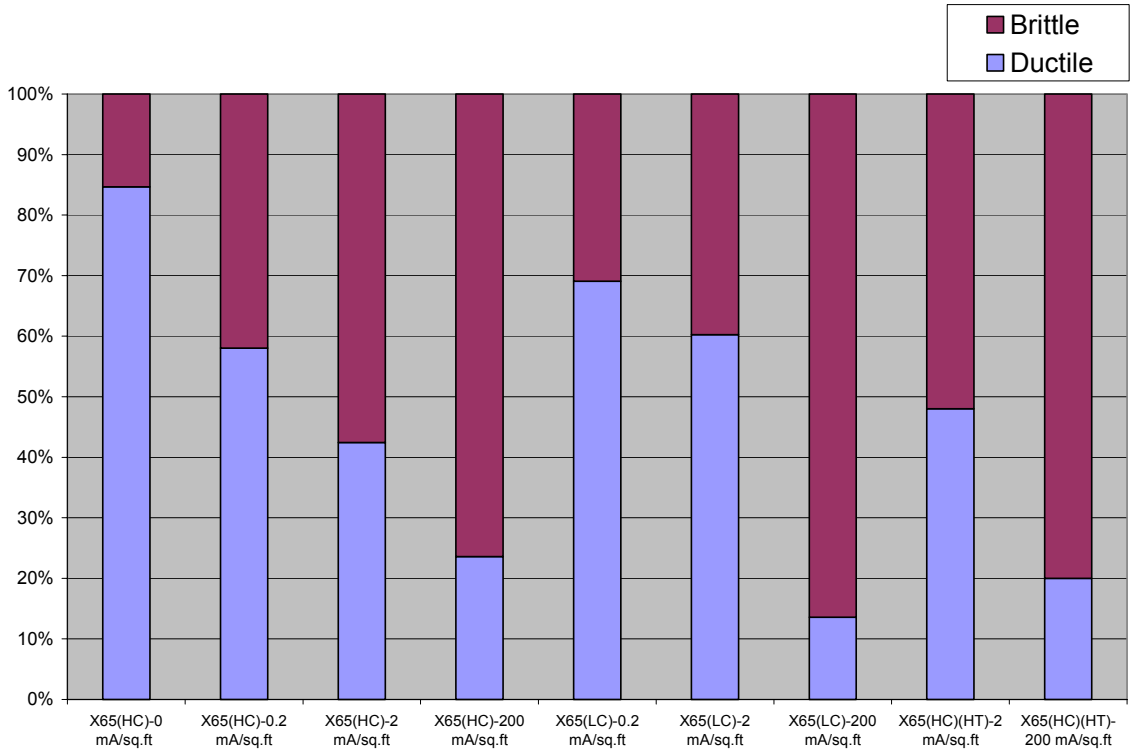

Figure 13. Areas of ductile and brittle failures for X65 steels in RNM soil.

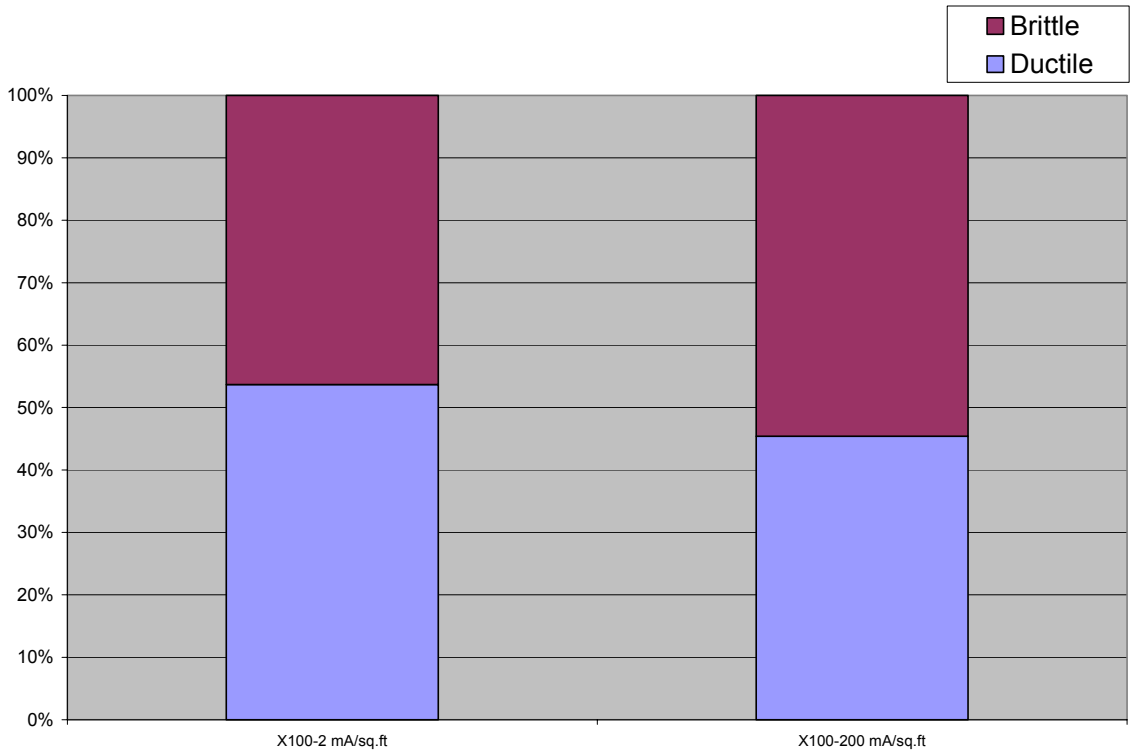

Figure 14. Areas of ductile and brittle failures for X100 steel in RNM soil.

The data indicates that under the testing conditions, all tested materials have shown almost 40% and higher of the brittle fracture at 2 mA/ft^2 of CP current density[7].

To illustrate the manner is which different materials responded to the increases in current density, the data was analyzed from the standpoint of the changes in the size of the ductile and brittle areas relative to the stepped up CP current. The results are given in Figure 15. The results do not include the data from the tests without CP current.

[7] Once it was discovered that the effect of CP current on the extent of the brittle fracture was quite pronounced at what was originally planned to be the 'low' current density (2 mA/ft^2), a decision was made to extend the tests to include even lower CP currents (0.2 and 0 mA/ft^2).

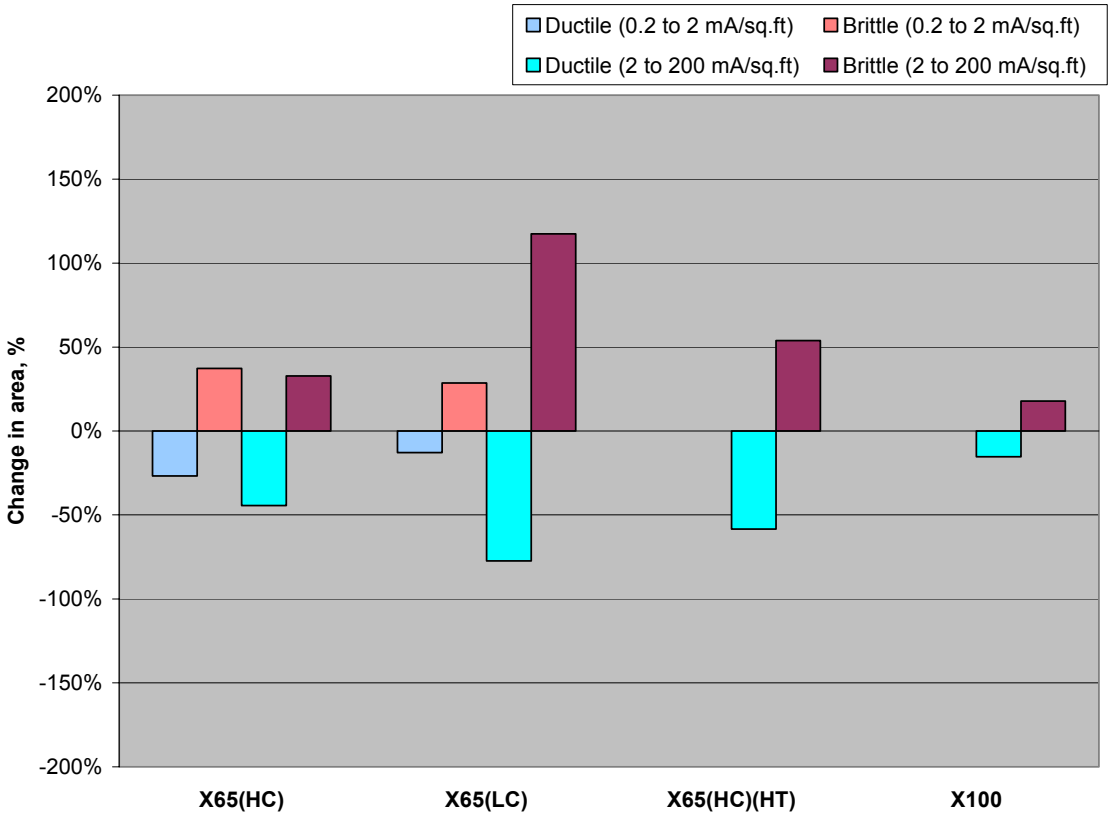

Figure 15. Change in ductile and brittle areas in response to change in impressed CP current density.

It should be emphasized that the analysis is based on a limited set of data and its primary purpose is to evaluate the 'order of magnitude' of the impact of CP current. The graph shows that, in general, the change in the ductile/brittle areas in response to the incremental increase from 0.2 to 2 mA/ft^2 or from 2 to 200 mA/ft^2 for X65(HC) steel, whereas considerable (30%+ percent), remains relatively flat. In contrast, X65(LC) steel appears to respond more dramatically to the change in current when the density is increased from 2 to 200 mA/ft^2.

The material with the simulated hard spots (X65(HC)(HT)) responded with an increase in the brittle area/decrease in the ductile area which was less pronounced than that for the X65(LC), but more significant than for the X65(HC) material. Consistently with the data in Table 7, the X100 steel showed a much more muted effect to the change in the current density from 2 to 200 mA/ft^2.

The degree to which the materials exhibited an incremental change in the brittle area as a consequence of the increase in the current density is likely the function of the concentration of the atomic hydrogen in the metal. The hydrogen concentration, in its turn, is the function (among other parameters) of the microstructure/chemical composition of the material. Therefore, the behavior of the X100 material may be explained by the supposition that the atomic hydrogen traps had been saturated or nearly saturated by the time of the failure for the lower (2 mA/ft^2) current density;

conversely, the hydrogen concentration in the X65 material apparently continued to increase to a more significant extent with the increase in the current density.

Effect of potential

The effect of potential is discussed for the purpose of relating a commonly measured field-based value (through close interval surveying of a CP-protected pipeline) and the observed effect of CP on the susceptibility to hydrogen-related damage.

The off-potential values observed in the SSRT experiments in saturated RNM soil are summarized in Table 8 and also graphed in Figure 16; Table 9 displays the Tafel slopes for the graphed range. The low slope values are likely indicative of the accelerated rate of cathodic reaction of hydrogen production. [For a more extended discussion of this subject, please see "Effect of potential" discussion in Task II of this report.]

Table 8. Per-soil average off-potential values in saturated RNM soil.

0.2 mA/sq.ft.	2 mA/sq.ft.	200 mA/sq.ft.
-0.733	-0.888	-1.007

Table 9. Potential-current density slopes based on average off-potentials.

Slope 0.2-2 mA/ft^2, mV/decade	Slope 2-200 mA/ft^2, mV/decade
-155	-60

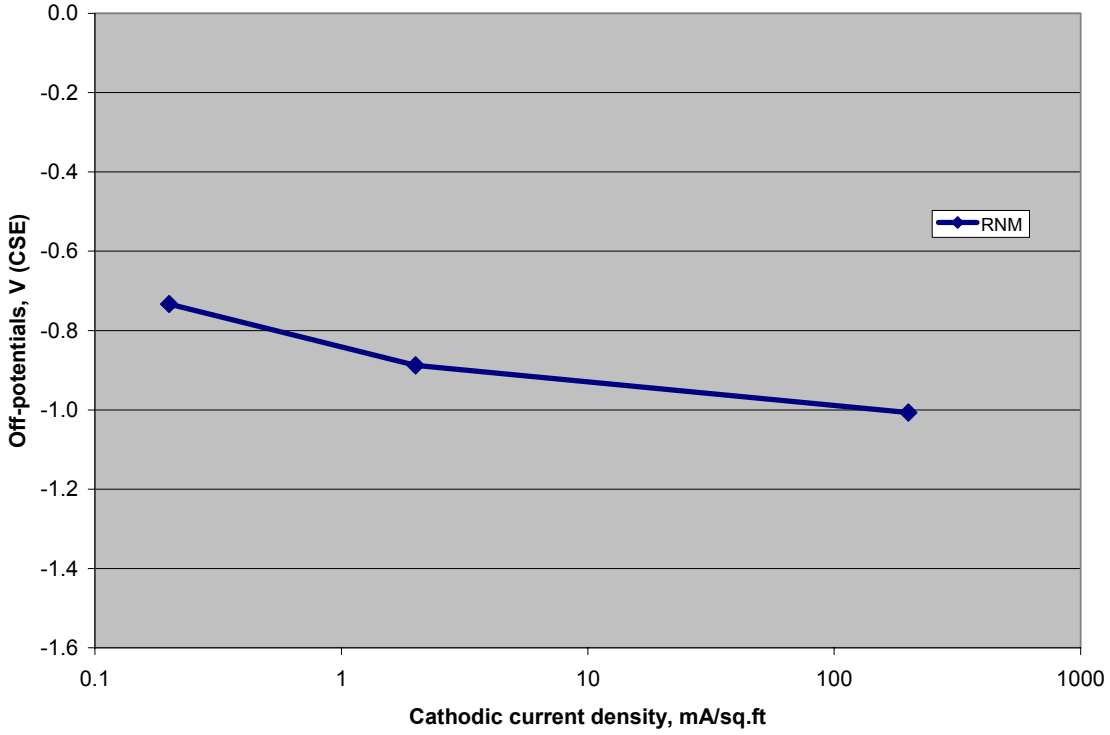

Figure 16. Average off-potential vs. current density for RNM soil.

It should be emphasized again that the CP potential, being a derivative of the applied current density, environmental characteristics, and material properties, serves merely as a convenient metric to assess the danger of the overprotection and not as the primary cause of the possible damage caused by overprotection. The discussion is therefore offered as an illustration for the argument that the heavy reliance on the potential measurements alone may lead to errors in the assessment of the actual threat of overprotection.

Testing temperature considerations

Temperature influences the rates of electrochemical reactions (e.g., cathodic hydrogen reduction). In this work, a single test temperature (ambient) was used to represent the value commonly used in laboratory experiments and stipulated by many ASTM procedures (including the ones used in this project). Although the test temperature is expected to represent a large portion of pipeline in the field and results can be compared to those of other researchers, it should be recognized that the results may not represent pipelines at significantly different temperatures.

Temperature affects both the rate of corrosion reactions (including cathodic reaction of hydrogen evolution) and the rate of diffusion of atomic hydrogen into the metal matrix. Further, the equilibrium potential of hydrogen evolution on the Pourbaix diagram for iron, is also a function of temperature (in degrees Kelvin):

$$e_{H^+/H_2} = -0.318 - 2.3 \times \frac{RT}{nF} \times pH = -0.318 - 2.3 \times \frac{8.31 \times T}{1 \times 96{,}500} \times pH = -0.318 - 0.198 \times 10^{-3} \times pH \times T$$

Hence, lower temperatures lead to more positive potentials at which hydrogen evolution becomes thermodynamically possible for a given pH (see Table 10).

Table 10. Equilibrium hydrogen evolution potentials for iron in water at pH 12.

T, ºF	T, ºC	$E(H^+/H_2)$, V (CSE)
41	5	-0.979
50	10	-0.991
59	15	-1.003
68	20	-1.015
77	25	-1.027
86	30	-1.039
95	35	-1.051

The lower temperatures also affect the cathodic reaction kinetics, leading to lower polarized potentials if the CP current density remains the same. However, if the rectifier output is increased to maintain the polarization at its previous level, the surface concentration of hydrogen would be increased.

The changes in temperature also affect changes in both the hydrogen flux through the metal and the diffusion coefficient of hydrogen atoms. The dependence of the diffusion

coefficient on temperature generally follows the Arrhenius equation ($D \propto \exp(-Q/T)$), where the Q value is the activation energy for the diffusion process. The equation indicates that at lower temperatures, the diffusion coefficient is lower. The literature data ("Application Of Hydrogen Permeation For Monitoring Sulfide Stress Cracking Susceptibility", Concepción Méndez, Isabel Martínez, Luis Melián, José Vera, NACE Paper 342, NACE International, 2002) shows that for a high-strength P110 steel the drop in temperature from 58ºC to 30ºC produced a 3.36-fold decrease in the hydrogen diffusion coefficient. However, it should be pointed that the effect of temperature is different for different materials; the same publication shows that the diffusion coefficient for a 5LB steel was reduced to a lesser extent (2.8-fold reduction). The chart shown in Figure 17 shows the change in the diffusion coefficient with temperature (relative to that at 40F) using the activation energy value for the 5LB steel.

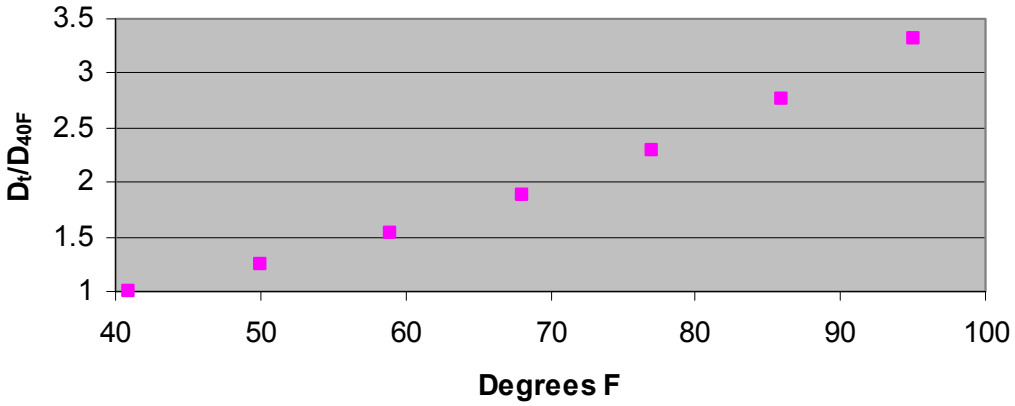

Figure 17. Change in hydrogen diffusion coefficient relative to 40F.

Therefore, the reduction in temperature produces two effects: reduction in the cathodic reaction kinetics and the reduction in diffusion coefficient for hydrogen. Based on the previous literature, the total effect on the likelihood of hydrogen-related damage may be minimal. However, if the rectifier output is adjusted upward (higher CP currents), the build-up of hydrogen at the immediately underneath the steel surface at the lower temperatures may produce conditions that will be more conducive to HRD. To ascertain this hypothesis, further testing is required. It should be pointed that the temperature effects are likely to be secondary to the effects of the changes in current density, environmental parameters (e.g., surface chemistry, moisture content, soil type, etc.), and material properties.

Summary

- The results indicate that the imposition of the cathodic protection current has an effect on the mechanical properties of the studied steels under the examined conditions. The primary observed effect is the increase of the brittle area on the fracture surface in response to the increase of the current density of the CP current, which is a proxy for the propensity to hydrogen-related damage (HRD).

- Compared to the tests in the air, the exposure of the X65 steel specimens to soil environment (without an imposed CP) also led to an increase in HRD, although the effect was relatively small.

- Incremental increase in the CP current density, however, produced variances in HRD. It appears that in the X100 steel, stepping up of the current from 2 to 200 mA/ft^2 caused a disproportionally smaller increase in HRD when compared to the X65 material.
- X65 steels, which were tested under a wider range of CP current densities, continued to exhibit an increase in HRD in response to continued incremental increase in CP currents.

- The presence of hard spots, simulated by the heat treatment of the X65(HC) steel did not cause an appreciably different behavior regarding the susceptibility to the hydrogen-related damage when compared to the un-treated material. This unexpected result (in contrast to the field-based observations) is likely caused by the insufficient sensitivity of the testing method. Whereas the chosen test (SSRT) has established the effect at the 'first degree approximation' level, further, more discriminating tests are necessary, which would use a different approach – compact tension specimens under a constant load (stable flaw).

- Whereas the increase in the cathodic protection current produced an effect on the mechanical properties of the studied materials, there is insufficient data to translate the observed effect into what could be expected in the field. In other words, the experimental program has demonstrated the 'order-of-magnitude' relationship between CP and material response. At this stage, it is not possible to draw definitive conclusions as to the quantified relationship between the CP current density and structural integrity of the pipelines. The effect of the hydrogen cathodic reaction on steel depends on a variety of parameters, which include environmental factors and material-specific factors; furthermore, being a diffusional phenomenon, hydrogen build-up in the trap sites inside the steels is time-dependent. Further studies are mandatory to establish the influence of time on the observed effect, which includes the impact of the CP potential cycling.

- The findings point out that the phenomenon is material-specific and a 'one-size-fits-all' approach is not expected to be adequate and will result in over-/underestimation of the danger in some circumstances (as manifested by the differences in behavior between the X65 and X100 specimens). Notwithstanding the above, prolonged periods of 'overprotection' should be avoided.

  Considering that the CP current-vs.-HRD charts appear not to have a "critical" cut-off point (i.e., the density at which HRD accelerates considerably), it is difficult to offer a definitive criterion for the upper limit without further experimentation, particularly in the region of the lower CP currents commonly expected in the field. If one adopts a threshold value of based on the brittle/ductile area ratio of 1 (equal areas) as the criterion for the 'acceptable' CP current density (subject to the above caveat), the value of under 2 mA/ft^2 may serve as a target value. Therefore, the use of the polarized off-potentials as the

sole criterion for the assessment of the hazards of hydrogen-related damage is discouraged. It should be emphasized one more time that in order to establish the effect of CP current density on the structural integrity of the operating pipelines, this criterion would require further refinement through additional work.

- Some of the originally selected materials (X70 and X65(LC)) did not show any apparent susceptibility to hydrogen damage in the screening tests. However, their mechanical behavior in SSRT tests requires further examination to establish the degree of propensity to hydrogen damage and to compare it to the steels that were mechanically tested. Also, the differences in behavior between the X100 plate steel (tested) and the X100 linepipe steel necessitate additional examination.

TASK II – COATING DISBONDMENT

Cathodic disbondment tests were carried out under the activities stipulated by Task II (combining Task 2 and Task 5 of the PRCI and USDOT-funded effort, respectively). The approach, results and discussion are presented below.

Approach

Testing procedure

The testing protocol for cathodic disbondment is based on a procedure which adopted the concept and some of the testing parameters used in ASTM G95 (Standard Test Method for Cathodic Disbondment Test of Pipeline Coatings (Attached Cell Method)) and ASTM G8 (Standard Test Method for Cathodic Disbondment of Pipeline Coatings). The approach of both G95 and G8 is similar and consists of applying a negative potential to a coated sample, which contains an intentionally introduced defect, for a specified period of time. The primary difference between the two Standards is in the applied potential and the size of the defect. The G95 Standard uses a smaller sized defect (diameter of $1/8^{th}$ of an inch); the G8 procedure stipulates a ¼ inch diameter holiday; the G95 Standard uses -3V (CSE) of applied potential and the G8 Standard uses -1.5V (CSE).

Based on the past experience, it was decided to use a larger size holiday (to avoid potential problems with blocking of the sample by coalescing gas bubbles). The other parameters, such as the applied potential, the duration of the tests, and the testing environment followed the proposed work scope (i.e., the controlled CP variable was the current rather than potential and the duration/environment choice was dictated by the effort to conduct tests in conditions approximating those encountered on actual pipelines).

The total number of tests was 88, which included tests on multiple coatings with and without a defect in several soils and water-based sodium chloride solution. Each particular combination of a coating and an environment was tested in duplicate. The summary of the test conditions per each tested coating is shown in Table 11 (see earlier discussion on the selection of the applied CP current densities). Specific details are described in the following sections.

Table 11. Summary of test conditions per each tested coating.

Soil	Holiday	Current density/ Applied voltage/potential	Number of tests
DOH	Y	2, 20, 200 mA/ft^2	6
RNM	Y	2, 20, 200 mA/ft^2	6
RNM	N	-1.5V	2
TCO	Y	2, 20, 200 mA/ft^2	6
ASTM (NaCl)	Y	-1.5V (CSE)	2
		Total	22

Tested coatings

Cathodic disbondment tests were carried out on four (4) different coatings:

1. Fusion Bonded Epoxy (further referred to as FBE 1)
   - Thickness, mils: 16.0 (min), 20.6 (max), 17.6 (average)
   - Brand name: presumed to be Skotchkote 206N
   - Application: mill applied

2. Fusion Bonded Epoxy (further referred to as FBE 2)
   - Thickness, mils: 10.8 (min), 15.1 (max), 13.1 (average)
   - Brand name: Skotchkote 206N
   - Application: mill applied

3. Liquid Epoxy (further referred to as LE)
   - Thickness, mils: 18.3 (min), 37.6 (max), 26.4 (average)
   - Brand name: SkotchGard 201
   - Application: hand-applied to simulate field repair conditions

4. Three component (layer) pipe coating, consisting of an FBE primer first layer, followed by a polyolefin copolymer adhesive intermediate layer, and an outer, thicker layer of polyethylene (further referred to as HPCC)
   - Thickness, mils: 34.3 (min), 59.4 (max), 40.8 (average)
   - Brand name: HPCC
   - Application: mill applied; the coating materials are applied successively in powder form to heated pipe

Test cell construction

The construction of the cell for soil tests is illustrated in Figure 18. The body of the cell and its components were made of PVC. Each cell was 5” high and cut to the curvature of the test panels. The cell was attached to the coated substrate with GE845 silicone adhesive and allowed to dry tack-free before filling the cell with the test electrolyte/soil environment. The housing for the counter electrode/sacrificial anode was closed with a drilled PVC cap to permit the ionic path between the holiday and the Mg anode and filled with agar.

The test cells were filled with the test media to approximately 1/3 of the height. Then, the housing with the sacrificial anode was inserted and the test was filled out to the top. The stages of the cell setup are illustrated in Figure 19.

The construction of the test cell for the ASTM G95 Standard was as described in the Standard and is shown in Figure 20.

Testing environment

Cathodic disbondment tests were conducted in:

1. Three (3) soil types:

    - Dublin, Ohio (DOH), saturated
    - Roswell, NM (RNM), saturated
    - Trinidad, CO (TCO), saturated

2. ASTM G95 Test Method solution (3% sodium chloride)

All the soils have been extensively used on various PRCI projects in the past and are well characterized. Specific soil compositions are shown in Table 12. All soil CD tests were carried out in duplicate at ambient temperature, with soils at their saturation point.

Testing duration

All soil tests were carried on for approximately 7 months; several tests lasted for 16 months (see Summary table in the Results section). The tests based on the ASTM Test Methods lasted 30 days.

Tested conditions

Defect configuration

The tests were carried out on the coatings with:

A. Intentionally introduced defects (holidays). A single holiday was made in the center of each specimen with a drill bit having a diameter of 6.36 mm (0.25 in). The same drill bit was used to manufacture all initial holidays. The angular cone of the drill bit was 160 degrees. This group was tested in all soils and ASTM G95 Test Method solution.

B. Without holidays (to evaluate the propensity to blistering). This group was tested in RNM soil only. One cell was removed after approximately 7 months of exposure and the remaining duplicate cell remained in the test for approximately 16 months.

In addition, the disbondment was measured for each of the coatings without any soil/solution exposure (at randomly chosen locations) to serve as a control.

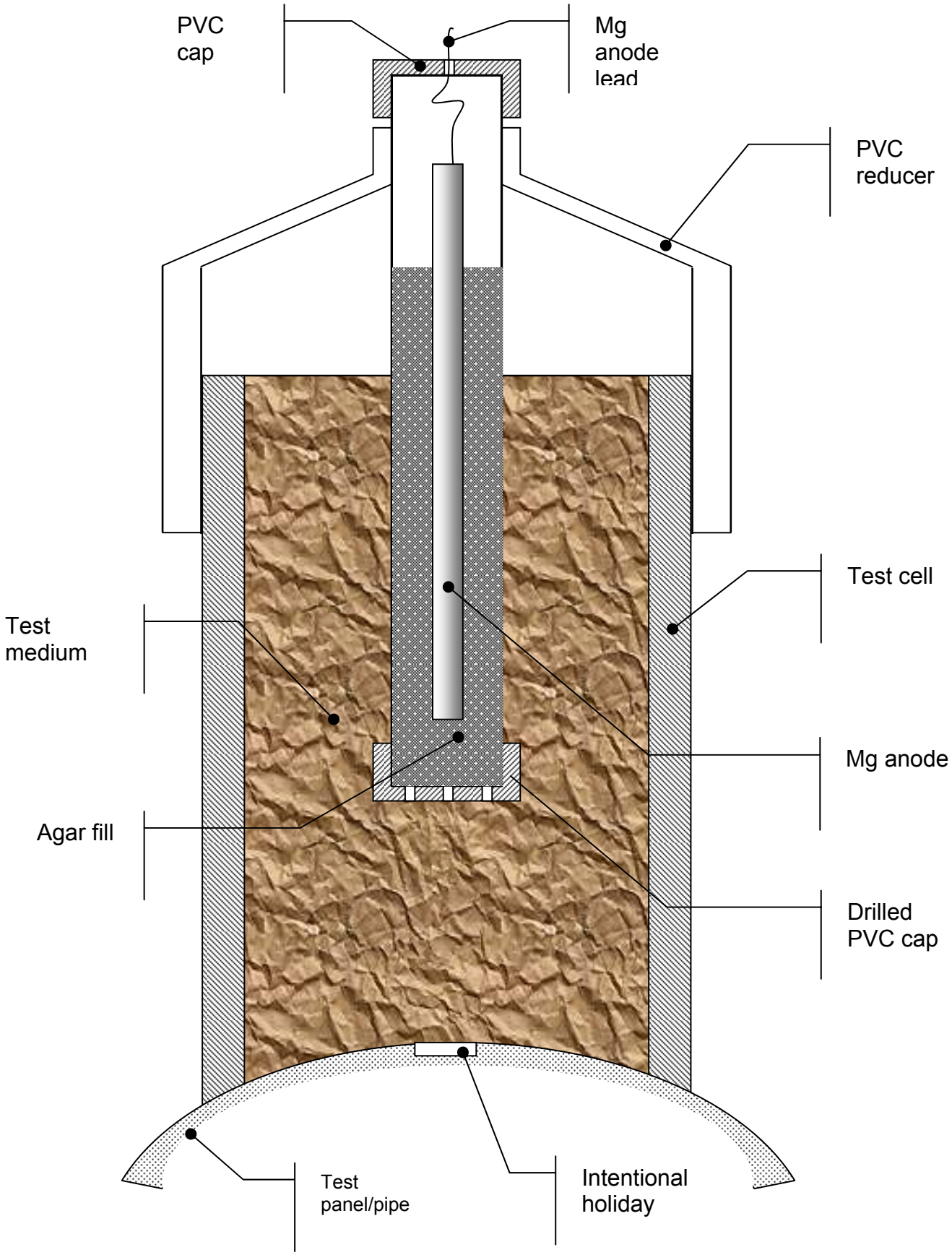

Figure 18. Test cell schematic.

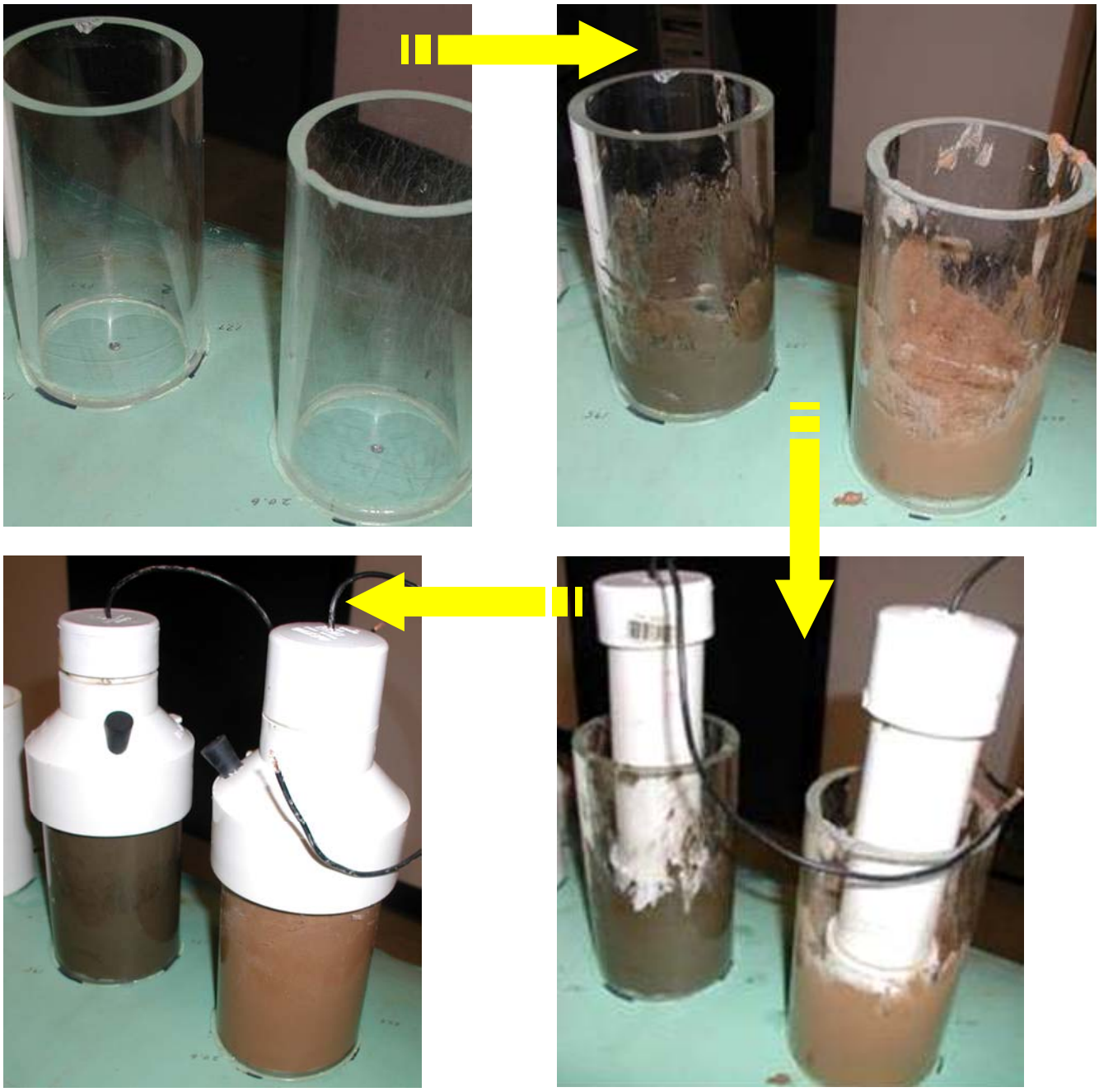

Figure 19. Test cell setup.

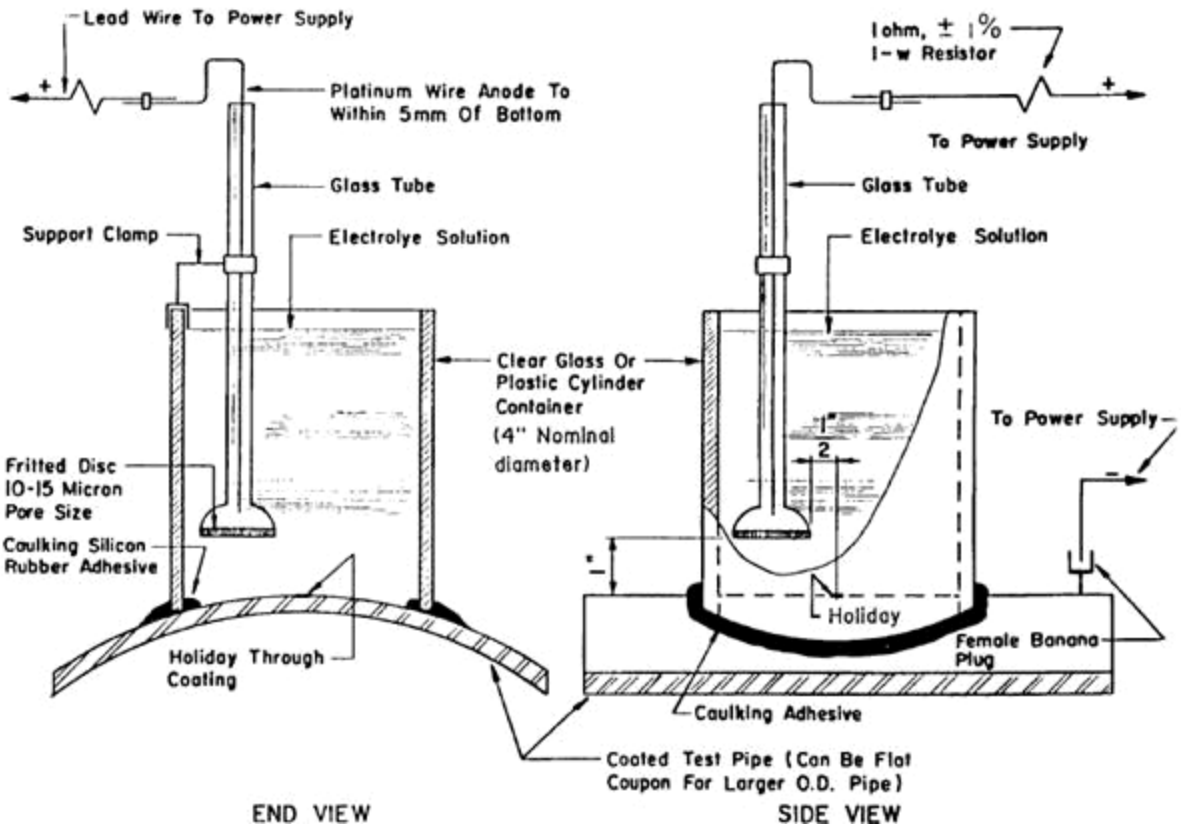

Figure 20. ASTM G95 Standard test cell setup (courtesy of ASTM).

Table 12. Soil characteristics.

Test Parameter		Units	DOH	RNM	TCO
Soluble Cations					
	Calcium, Ca	ppm	24	1362	240
	Magnesium, Mg	ppm	1394	1385	97
	Aluminum, Al	ppm	<1	<1	<1
Soluble Anions					
	Nitrite (as N)	ppm	1	<1	1
	Nitrate (as N)	ppm	10	70	75
	Chloride, Cl	ppm	39	223	86
	Sulfate, SO_4	ppm	<50	100	50
	Carbonate, CO_3	ppm	not detected	not detected	not detected
	Bicarbonate, HCO_3	ppm	111	111	549
pH		---	7.3	7.6	7.9
Total Acidity		mg/L	not detected	not detected	146
Total Alkalinity		meq/kg	3.2	2.3	3.5
Cation Exchange Capacity		cmol/kg	13	26	9
Total Dissolved Solids		g/L	0.5	3.8	1.9
Conductivity		ms/cm	0.6	3.3	1.9

Saturation Level		%	30	18	27
Resistivity					
	Initial (5% Moisture)	ohm-cm	28,000	8,600	not analyzed
	(15% Moisture)	ohm-cm	3,800	1,360	2,400
	Saturated	ohm-cm	3,000	770	720
Texture					
	% Sand	%	27	36	32
	% Silt	%	39	25	27
	% Clay	%	34	39	42
X-ray Diffraction					
	Quartz	%	32	42	36
	Plagioclase Feldspar	%	3	3	6
	K-Feldspar	%	1	2	3
	Calcite	%	9	24	3
	Dolomite	%	22	1	not detected
	Siderite	%	trace	not detected	not detected
	Gypsum	%	trace	1	trace
	Magnetite	%	not detected	not detected	not detected
	Hematite	%	not detected	1	not detected
	Hornblende	%	trace	not detected	not detected
	Geothite	%	trace	trace	not detected
	Kaolinite	%	1	1	4
	Chlorite	%	3	trace	2
	Illite/Mica	%	13	3	6
	Illite/Smectite Mixed Layer	%	16	22	40
	% Illite in Mixed Layer	%	65-75	40-60	55-75

Applied current/potential

All soil tests on the specimens with the intentionally introduced defect were exposed to three different current densities (see earlier discussion on the selection of the applied CP current densities):

- 2 mA/ft^2
- 20 mA/ft^2
- 200 mA/ft^2

The currents were controlled either through periodic adjustment with potentiometers or through galvanostatic control by a potentiostat (see Specimen Configuration below).

All tests in soil without intentionally introduced defect were conducted with an external voltage of -1.5V applied between the pipeline and the sacrificial Mg anode

ASTM G95/G8 tests were conducted using an applied potential of -1.5V (vs. copper-copper sulfate reference electrode).

Specimen configuration

Cathodic disbondment tests were conducted using two configurations:

The first group (Group 1) was tested with the cell mounted on a section of an actual pipeline. The cathodic protection current was supplied either by an individual galvanic (Mg) anode or by an external DC current source using Mg anode as a counter electrode. The current was periodically adjusted using variable resistors; in ASTM Test Method-based tests, the potential was controlled by a potentiostat.

Group 1 included FBE 1, FBE 2, LE in DOH and RNM

The second group (Group 2) was tested with the cell mounted on top of an individual panel (sized approximately 6 by 6 inches). The panels were connected in series and the impressed current, supplied by an external DC source, was galvanostatically controlled to the desired value. In ASTM Test Method-based tests, the potential was controlled by a potentiostat

Group 2 included FBE 1, FBE 2, and LE in TCO and HPCC in DOH, RNM, TCO.

Auxiliary collected data

In addition to the disbondment measurements (see below), for all soil tests, the on- and off-potential data was collected on a periodic basis.

Test Evaluation

After the test, the cells were removed from the coated panels. Evaluation of the test took place within 2 hours of removal from the test cell.

Initial radial cutting of the samples was accomplished using a Stanley Model 10-598 knife. Four cuts, approximately 4 inches long and 45 degrees apart, were made through the center of the holiday extending to the outer diameter of the test cell, in accordance with CAN/CSA-Z245.20-M92.

Cathodic disbondment was determined by measuring the average disbondment length on the four diameters, starting from the OD of the introduced defect, as illustrated in Figure 21 . Each diameter length was measured using digital calipers, and recorded to the nearest 0.1 mil. The recorded disbondment results included the lengths of the four measured diameters, the average of the four diameters rounded to the nearest 0.1 mil, and a calculated average radius of disbondment rounded to the nearest 0.1 mil.

The average radius of disbondment is defined as:

$$R_{average} = \frac{R1 + R2 + R3 + R4 + R5 + R6 + R7 + R8}{8},$$

where $R_{average}$ is the average diameter of coating disbondment measured in 8 radial directions. The measurement schematic is illustrated in Figure 21.

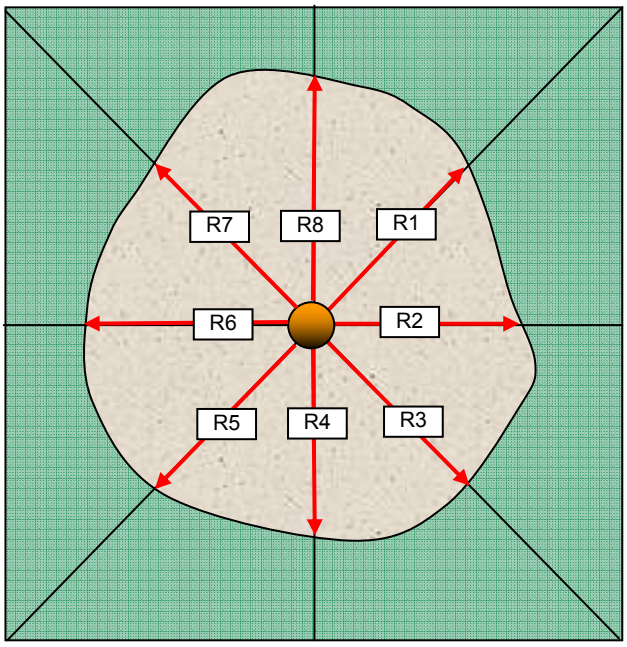

Figure 21. Disbondment distance measurement schematic.

A Stanley Model 10-598 knife and Model 5903 blade was used to remove disbonded coating. The blade was changed regularly during cutting so that at no time was a dull blade used in evaluations.

For coating performance comparisons, coating removal with the Stanley knife after CD and hot-water tests was aggressive. That is to say, all disbonded coating was removed within a reasonable time to minimize variations in technique and human error, and to allow meaningful comparisons between coating types and between laboratories. The knife blade was slid under the coating which was pried up until a definite resistance was met.

Testing conditions summary

Table 13 through Table 16 summarize the test conditions and coating characteristics for each of the tested conditions.

Table 13. Testing conditions for FBE 1

Soil	Current, mA/ft^2	Cell	Thickness, mils				Average Thickness, mils	Exposure (days)
			12 o'clock	4 o'clock	7 o'clock	Center		
Control	na	1	na	na	na	na	na	na
ASTM	na	1	17.3	16.2	17.9	na	**17.1**	30
ASTM	na	2	17.6	16.4	17	na	**17.0**	30
DOH	2	1	17.6	19.2	19.2	na	**18.7**	212
DOH	2	2	17.9	16.3	18.8	na	**17.7**	212
DOH	20	1	19.5	17.7	17.7	na	**18.3**	212
DOH	20	2	19.2	17.3	17.8	na	**18.1**	212
DOH	200	1	16.4	16	16.2	na	**16.2**	212
DOH	200	2	17.4	17.8	16.4	na	**17.2**	212
RNM	2	1	18.3	16.4	18.5	na	**17.7**	212
RNM	2	2	16.5	16.7	17.2	na	**16.8**	212
RNM	20	1	16.7	17.4	17.7	na	**17.3**	212
RNM	20	2	18.8	18.4	17.9	na	**18.4**	212
RNM	200	1	20.6	17.5	20.5	na	**19.5**	212
RNM	200	2	16.8	19.2	18.1	na	**18.0**	212
TCO	2	1	18.3	17.9	16.6	15.5	**17.1**	216
TCO	2	2	15.5	16.6	14.6	18	**16.2**	216
TCO	20	1	15.2	15.7	17.1	16.3	**16.1**	216
TCO	20	2	18.1	15.3	14.2	16.1	**15.9**	216
TCO	200	1	17.2	19.3	17.2	17.8	**17.9**	216
TCO	200	2	15.6	14.6	15.8	17	**15.8**	216
RNM	No Holiday	1	18	17.2	16.1	na	**17.1**	436
RNM	No Holiday	2	17.2	16.6	16.2	na	**16.7**	212

Table 14. Testing conditions for FBE 2

Soil	Current, mA/ft^2	Cell	Thickness, mils				Average Thickness, mils	Exposure (days)
			12 o'clock	4 o'clock	7 o'clock	Center		
Control	na	1	na	na	na	na	na	na
ASTM	na	1	11.0	12.4	10.8	na	**11.4**	30
ASTM	na	2	13.2	12.5	13.0	na	**12.9**	30
DOH	2	1	11.4	12.7	11.3	na	**11.8**	223
DOH	2	2	13.9	12.9	13.3	na	**13.4**	224
DOH	20	1	11.3	11.6	12.5	na	**11.8**	224
DOH	20	2	12.6	12.6	13.3	na	**12.8**	221
DOH	200	1	12.8	12.9	12.6	na	**12.8**	221
DOH	200	2	12.6	12.3	12.7	na	**12.5**	221
RNM	2	1	14.3	14.6	14.0	na	**14.3**	223
RNM	2	2	13.1	12.6	13.3	na	**13.0**	223
RNM	20	1	12.3	14.3	13.4	na	**13.3**	223
RNM	20	2	12.6	13.2	12.2	na	**12.7**	225
RNM	200	1	14.6	14.1	14.9	na	**14.5**	225
RNM	200	2	14.7	14.1	14.9	na	**14.6**	225
TCO	2	1	13.1	13.4	12.8	15.3	**13.7**	216
TCO	2	2	12.1	12.3	15.0	13.6	**13.3**	216
TCO	20	1	13.6	13.7	15	13.3	**13.9**	216
TCO	20	2	15	13.3	14.3	15	**14.4**	216
TCO	200	1	14.4	15.1	15	13.7	**14.6**	216
TCO	200	2	15.4	15	12.8	16.5	**14.9**	216
RNM	No Holiday	1	15.1	14.1	15.0	na	**14.7**	473
RNM	No Holiday	2	13.3	12.9	14.6	na	**13.6**	195

Table 15. Testing conditions for LE

Soil	Current, mA/ft^2	Cell	Thickness, mils				Average Thickness, mils	Exposure (days)
			12 o'clock	4 o'clock	7 o'clock	Center		
Control	na	1	na	na	na	na	na	na
ASTM	na	1	30.3	19.4	21.3	31.4	**25.6**	30
ASTM	na	2	19.8	35.4	15.2	30.3	**25.2**	30
DOH	2	1	23.0	22.9	26.2	25.1	**24.3**	227
DOH	2	2	20.3	34.4	26.2	25.9	**26.7**	227
DOH	20	1	34.3	19.8	26.8	26.6	**26.9**	227
DOH	20	2	22.6	27.8	30.1	25.7	**26.6**	231
DOH	200	1	33.3	36.1	25.1	27.9	**30.6**	227
DOH	200	2	31.7	23.7	30.1	27.9	**28.4**	226
RNM	2	1	23.1	23.4	28.4	26.7	**25.4**	227
RNM	2	2	24.2	23.0	18.3	28.5	**23.5**	227
RNM	20	1	22.7	37.6	26.2	27.9	**28.6**	227
RNM	20	2	35.7	25.1	25.9	30.2	**29.2**	227
RNM	200	1	22.4	34.1	25.5	28.4	**27.6**	227
RNM	200	2	23.2	25.6	28.7	26.3	**26.0**	227
TCO	2	1	23.3	25.1	23.1	23.7	**23.8**	211
TCO	2	2	31.3	20.1	23.1	37.1	**27.9**	211
TCO	20	1	20.2	24.5	23.1	27.9	**23.9**	216
TCO	20	2	23.5	21.8	24.7	17.2	**21.8**	216
TCO	200	1	27	24.3	20.3	22.3	**23.5**	216
TCO	200	2	35.7	32	23.5	36.2	**31.9**	216
RNM	No Holiday	1	29.0	19.8	27.9	28.3	**26.3**	226
RNM	No Holiday	2	20.0	36.0	26.3	26	**27.1**	366

Table 16. Testing conditions for HPCC

Soil	Current, mA/ft^2	Cell	Thickness, mils				Average Thickness, mils	Exposure (days)
			12 o'clock	4 o'clock	7 o'clock	Center		
Control	na	1	na	na	na	na	na	na
ASTM	na	1	36.9	42.9	35.2	38	**38.3**	30
ASTM	na	2	40.7	36.3	36.9	39.5	**38.4**	30
DOH	2	1	37.3	41.7	41.3	44	**41.1**	216
DOH	2	2	40.5	42.9	40.1	41.3	**41.2**	216
DOH	20	1	41.1	39.3	36.8	39.3	**39.1**	216
DOH	20	2	41.7	43.3	39.8	46.8	**42.9**	216
DOH	200	1	37.8	42.1	38.9	38	**39.2**	216
DOH	200	2	39.3	43.3	39.3	37.5	**39.9**	216
RNM	2	1	46.0	40.4	42.1	37.9	**41.6**	216
RNM	2	2	37.9	40.9	39.1	44	**40.5**	216
RNM	20	1	43.7	40.1	45.6	39.3	**42.2**	216
RNM	20	2	39.7	44	43.7	35.3	**40.7**	216
RNM	200	1	46.4	59.4	41.5	38.9	**46.6**	216
RNM	200	2	37	34.3	37.1	39.2	**36.9**	216
TCO	2	1	38.3	46.8	38.1	42.1	**41.3**	216
TCO	2	2	38.7	40.9	36.5	39.7	**39.0**	216
TCO	20	1	35.6	40.5	44.4	38.6	**39.8**	216
TCO	20	2	36.7	40.1	42.5	41.8	**40.3**	216
TCO	200	2	38	45.6	40.5	40.5	**41.2**	216
TCO	200	1	43.3	36.5	41.3	43.7	**41.2**	216
RNM	No Holiday	1	36.1	44	44.4	37	**40.4**	213
RNM	No Holiday	2	41.7	42.1	45.2	14.3	**35.8**	213

Results and Discussion

Disbondment measurements

The results of the cathodic disbondment measurements are summarized in Table 17. Detailed disbondment measurements and the appearance of each individual cell are shown in Appendix B4. The on- and off-potential data for each tested coating are shown in Table 18 through Table 21 (grouped by coating type).

The data is also presented in the graphic form in Figure 22 through Figure 25 (grouped by coating type) and in Figure 26 through Figure 28 (grouped by soil type). The latter group shows average off-potential values (dashed lines) for each applied current density in each of the tested soil. Note that the control and ASTM test results do not correspond to the current density values on the x-axis and are merely placed directly on the y-axis to indicate the measured disbondment.

Table 17. Summary of cathodic disbondment tests.

Soil	Current, mA/ft^2	Cell	Average Disbondment, inches			
			FBE1	FBE2	LE	HPCC
Control	na	1	0.0429	0.0347	0.1023	0.0668
ASTM	na	1	0.7643	0.3698	0.1391	0.2146
ASTM	na	2	1.0288	0.2339	0.1485	0.1946
DOH	2	1	0.1131	0.0232	0.1146	0.0829
DOH	2	2	0.0856	0.0138	0.0946	0.0916
DOH	20	1	1.2314	0.0374	0.1470	0.1324
DOH	20	2	1.0164	0.6104	0.4781	0.2914
DOH	200	1	0.3793	0.1501	0.3524	0.4184
DOH	200	2	1.3221	1.1342	0.2696	0.3133
RNM	2	1	0.0569	0.0074	0.1448	0.1306
RNM	2	2	0.0611	0.0441	0.1910	0.0684
RNM	20	1	0.3226	0.0509	0.7221	0.1178
RNM	20	2	0.4301	0.0074	0.0634	0.1053
RNM	200	1	1.1130	1.1620	0.3639	0.2844
RNM	200	2	1.1438	1.1189	0.2993	0.4521
TCO	2	1	0.3396	0.2012	0.1255	0.0998
TCO	2	2	0.1628	0.0647	0.0931	0.1116
TCO	20	1	0.3096	0.2312	0.3868	0.1079
TCO	20	2	0.1910	0.3199	0.1088	0.3314
TCO	200	1	1.2527	1.5478	0.8183	0.6104
TCO	200	2	1.3120	1.3183	0.9216	0.4230
RNM	No Holiday	1	0.1122	0.0401	0.4067	0.1041
RNM	No Holiday	2	0.1521	0.1283	0.2501	0.0484

Table 18. On/off-potential data for FBE 1.

		2 mA/sq.ft.		20 mA/sq.ft.		200 mA/sq.ft.	
		On	Off	On	Off	On	Off
RNM	Cell 1	-1.015	-0.993	-1.382	-1.206	-1.662	-1.246
	Cell 2	-1.086	-1.047	-1.454	-1.204	-1.543	-1.183
	Average	**-1.051**	**-1.020**	**-1.418**	**-1.205**	**-1.602**	**-1.215**
DOH	Cell 1	-0.938	-0.936	-1.798	-1.385	-1.488	-1.307
	Cell 2	-0.981	-0.863	-2.022	-1.296	-2.802	-1.189
	Average	**-0.959**	**-0.900**	**-1.910**	**-1.340**	**-2.145**	**-1.248**
TCO	Cell 1	-1.438	-1.047	-3.287	-1.133	-1.642	-1.339
	Cell 2	-1.624	-1.048	-2.582	-1.444	-1.606	-1.224
	Average	**-1.531**	**-1.048**	**-2.934**	**-1.288**	**-1.624**	**-1.281**

Table 19. On/off-potential data for FBE 2.

		2 mA/sq.ft.		20 mA/sq.ft.		200 mA/sq.ft.	
		On	Off	On	Off	On	Off
RNM	Cell 1	-1.023	-1.015	-1.231	-1.106	-2.880	-1.256
	Cell 2	-0.979	-0.978	-1.165	-1.122	-2.920	-1.272
	Average	**-1.001**	**-0.997**	**-1.198**	**-1.114**	**-2.900**	**-1.264**
DOH	Cell 1	-0.907	-0.902	-1.576	-1.390	-3.039	-1.254
	Cell 2	-0.947	-0.939	-1.097	-1.054	-1.551	-1.196
	Average	**-0.927**	**-0.921**	**-1.337**	**-1.222**	**-2.295**	**-1.225**
TCO	Cell 1	-1.426	-1.064	-3.117	-1.242	-2.307	-1.275
	Cell 2	-1.084	-0.995	-2.943	-1.254	-2.119	-1.292
	Average	**-1.255**	**-1.030**	**-3.030**	**-1.248**	**-2.213**	**-1.283**

Table 20. On/off-potential data for LE.

		2 mA/sq.ft.		20 mA/sq.ft.		200 mA/sq.ft.	
		On	Off	On	Off	On	Off
RNM	Cell 1	-0.949	-0.963	-1.296	-1.223	-1.590	-1.264
	Cell 2	-0.988	-0.986	-1.602	-1.382	-1.638	-1.254
	Average	**-0.968**	**-0.975**	**-1.449**	**-1.302**	**-1.614**	**-1.259**
DOH	Cell 1	-0.937	-0.929	-1.573	-1.392	-1.116	-1.061
	Cell 2	-0.949	-0.948	-1.072	-1.021	-1.526	-1.329
	Average	**-0.943**	**-0.939**	**-1.322**	**-1.207**	**-1.321**	**-1.195**
TCO	Cell 1	-1.089	-1.000	-9.084	-1.625	-3.946	-1.279
	Cell 2	-1.136	-1.018	-3.032	-1.187	-2.508	-1.345
	Average	**-1.113**	**-1.009**	**-6.058**	**-1.406**	**-3.227**	**-1.312**

Table 21. On/off-potential data for HPCC.

		2 mA/sq.ft.		20 mA/sq.ft.		200 mA/sq.ft.	
		On	Off	On	Off	On	Off
RNM	Cell 1	-1.158	-1.047	-1.092	-1.071	-1.574	-1.229
	Cell 2	-1.070	-1.043	-1.190	-1.100	-2.591	-1.234
	Average	**-1.114**	**-1.045**	**-1.141**	**-1.086**	**-2.082**	**-1.232**
DOH	Cell 1	-1.001	-0.976	-1.078	-1.023	-3.085	-1.189
	Cell 2	-1.016	-0.989	-5.360	-1.705	-2.615	-1.134
	Average	**-1.008**	**-0.983**	**-3.219**	**-1.364**	**-2.850**	**-1.161**
TCO	Cell 1	-1.103	-0.997	-2.688	-1.359	-2.116	-1.188
	Cell 2	-1.257	-1.030	-2.590	-1.490	-2.484	-1.213
	Average	**-1.180**	**-1.013**	**-2.639**	**-1.424**	**-2.300**	**-1.200**

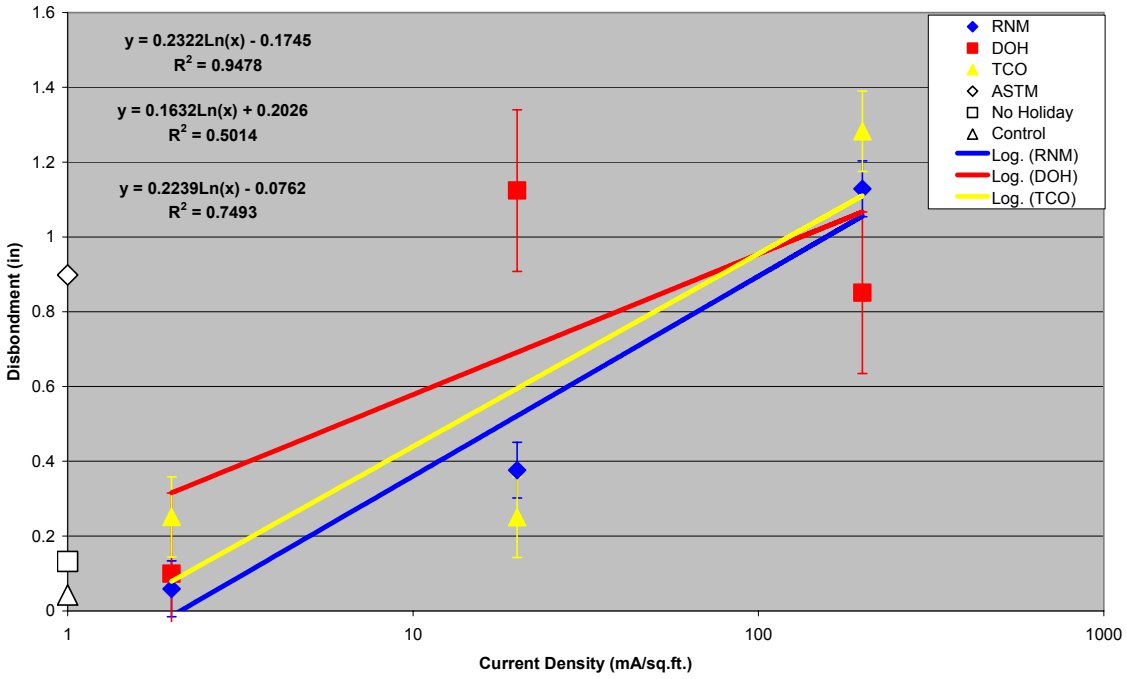

Figure 22. Cathodic disbondment vs. CP current density for FBE 1 coating. Color coded lines illustrate regression analysis results.

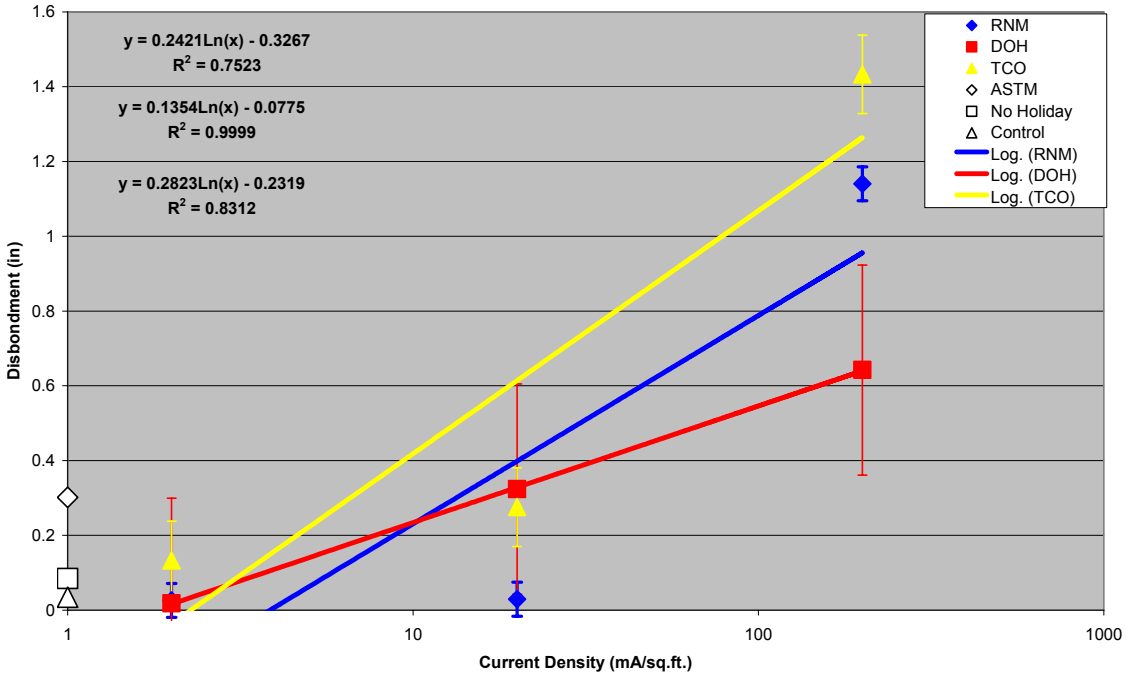

Figure 23. Cathodic disbondment vs. CP current density for FBE 2 coating. Color coded lines illustrate regression analysis results.

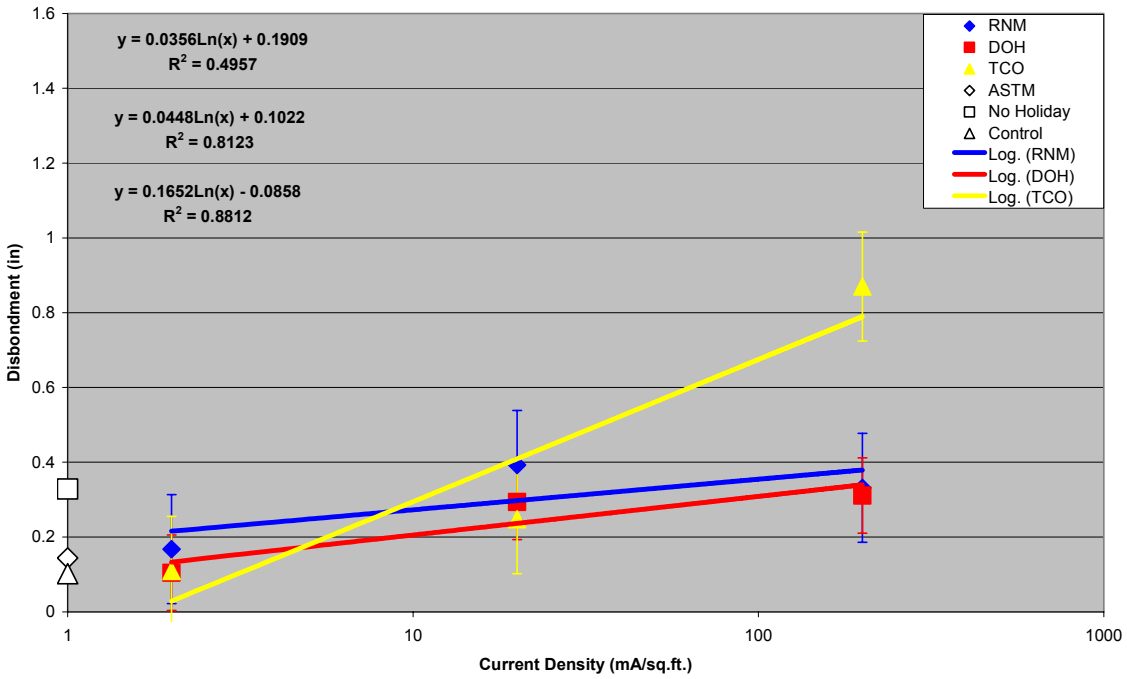

Figure 24. Cathodic disbondment vs. CP current density for LE coating. Color coded lines illustrate regression analysis results.

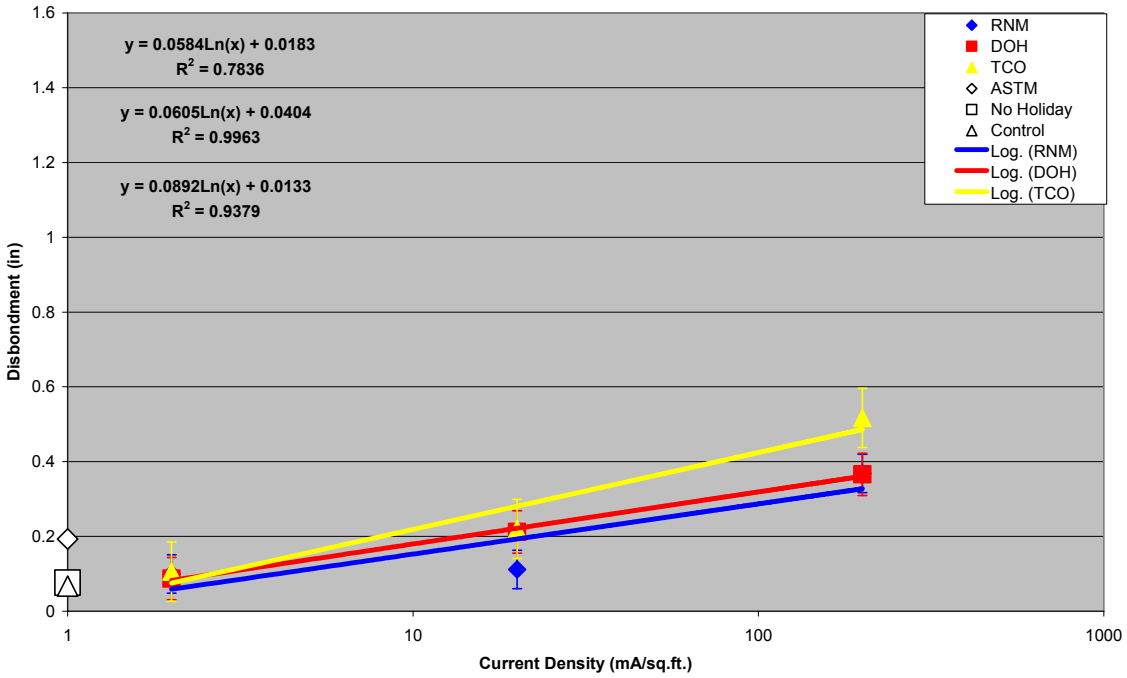

Figure 25. Cathodic disbondment vs. CP current density for HPCC coating. Color coded lines illustrate regression analysis results.

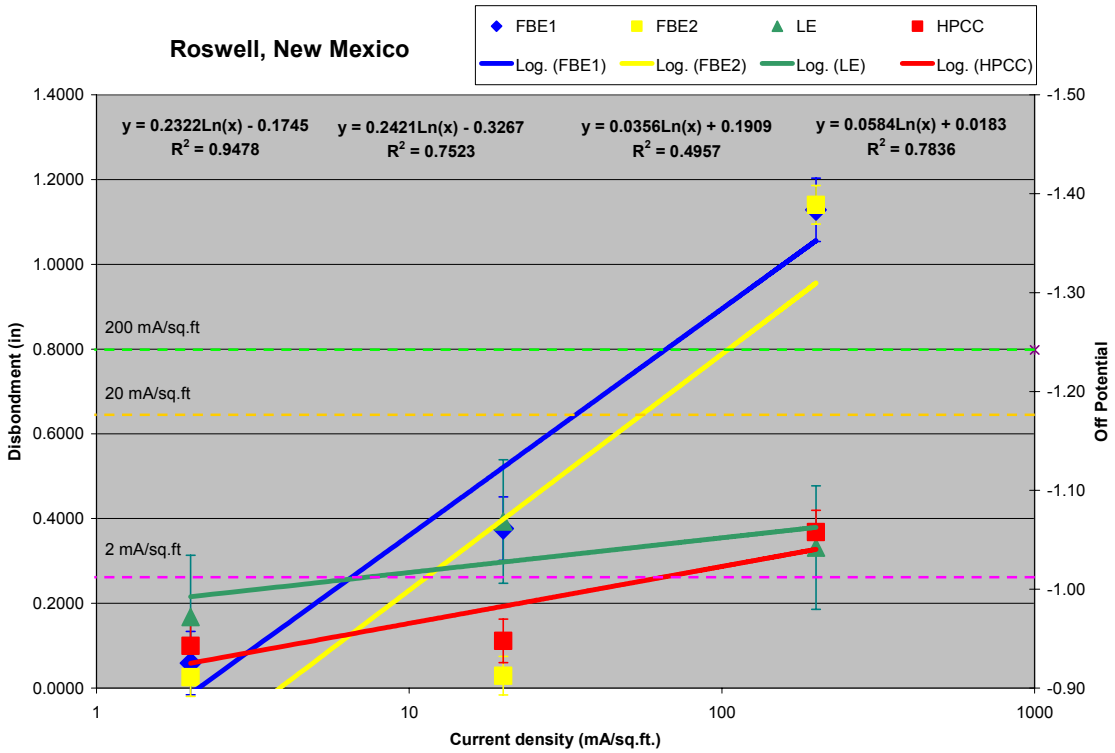

Figure 26. Cathodic disbondment vs. CP current density for RNM soil. Color coded lines illustrate regression analysis results. Dashed lines show average off-potential values for each applied current density.

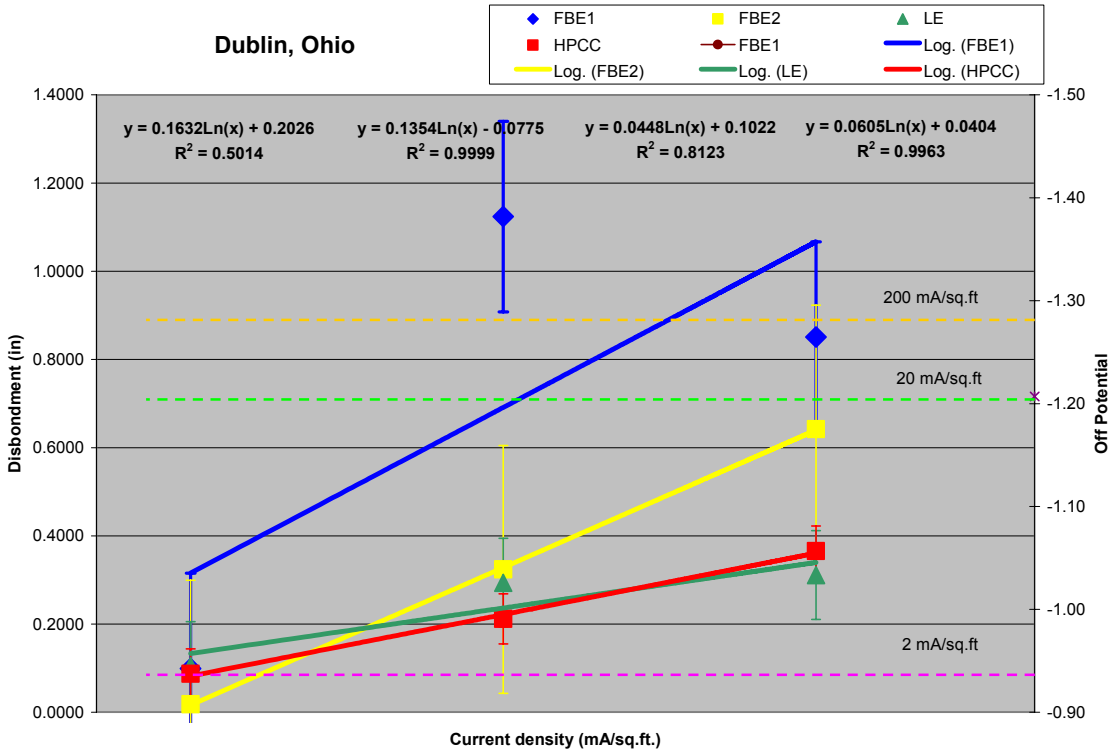

Figure 27. Cathodic disbondment vs. CP current density for DOH soil. Color coded lines illustrate regression analysis results. Dashed lines show average off-potential values for each applied current density.

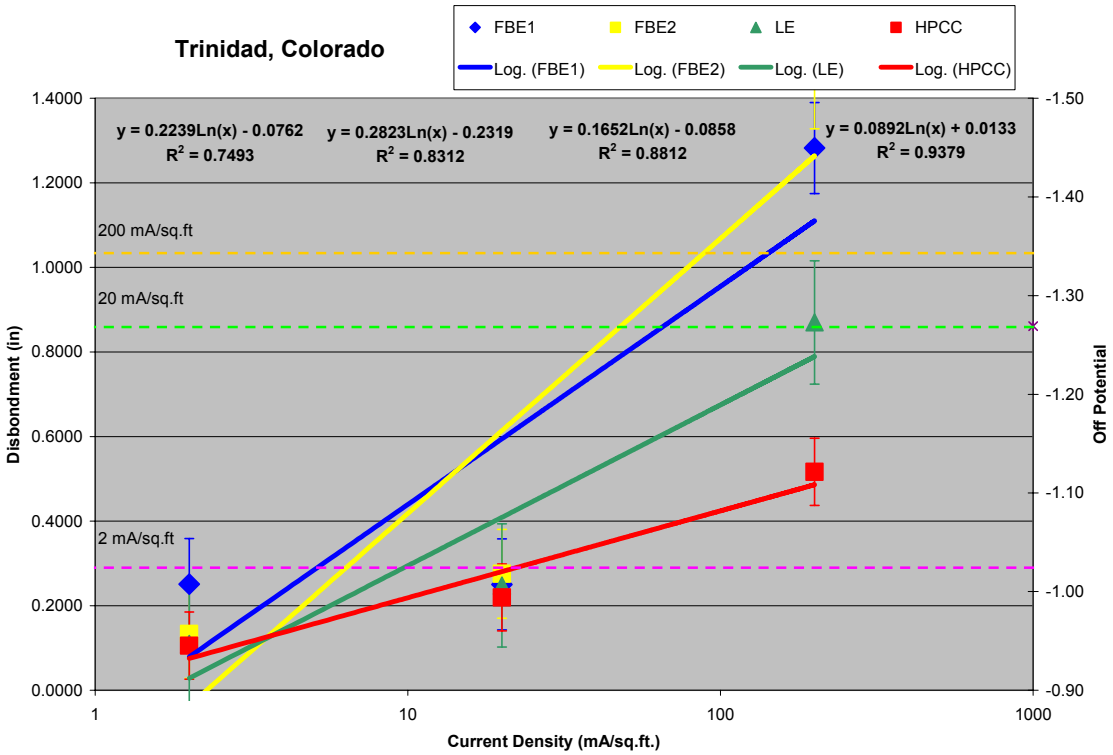

Figure 28. Cathodic disbondment vs. CP current density for TCO soil. Color coded lines illustrate regression analysis results. Dashed lines show average off-potential values for each applied current density.

Effect of current density

The primary observed trend is that all coatings exhibit an increased propensity to disbond with an increase in the applied cathodic protection current density. Based on the regression analysis, HPCC exhibited the least pronounced dependence of the disbondment values on the imposed current density.

The readers should note that whereas the logarithm trend appears to describe the observed dependence adequately (R^2 values are predominantly greater than 0.75, i.e., 75% (or more) of the observed trend can be explained by the linear correlation between the two variables), it is not certain that the trend can be extrapolated further. It is likely that the derivative of the function is going to decrease (the extent of disbondment is going to be limited at the very high current densities). Another limitation (experimental) of the regression is that it incorporates the disbondment data from the cells where the coating disbonded up to the edge of the cell wall; the question that remains is, if there were no restrictions to the disbondment (e.g., a much larger cell or no cell at all), how far would the coating disbond. [See also 'Conclusions' section.]

The higher slopes of the disbondment vs. current density curves for the FBE coatings are largely the result of the higher disbondment observed at 200 mA/ft^2. In all the tested conditions, disbondment at low (2 mA/ft^2) current density was no greater than the disbondment measured for the "controls". The results of the medium (20 mA/ft^2) current density tests exhibited disbondment no greater than ASTM sodium chloride solution-based tests.

Effect of potential

As the values of the applied polarization potential are linked to the applied current density values through the Tafel equation, the effect of the off-potential on the disbondment is similar to that of the effect of the current density, i.e., at higher (more negative) potentials there was greater disbondment. Also, the relationship between the two parametric values is also a function of the environment characteristics. Table 22 represents the averaged values for the off-potentials recorded for each current density for each tested soil.

Table 22. Per-soil average off-potential values

	2 mA/sq.ft.	20 mA/sq.ft.	200 mA/sq.ft.
RNM	-1.009	-1.177	-1.242
DOH	-0.935	-1.283	-1.207
TCO	-1.025	-1.342	-1.269

As seen, the same current density has produced polarization potentials in different soils which vary by more than 150 mV. Furthermore, ten-fold increase in the applied current density from 20 to 200 mA/ft^2 in two out of three soils did not lead to further increase in

potential (the potential-current relationships are graphed in Figure 29 and expressed as mV/decade of current in Table 23).

The observed slopes between 2 and 20 mA/ft^2 are rather low (compared to approximately 300-500 mV/decade, which is common for typical cathodic polarization curves in soil). This is likely an indication that, at the examined current densities, cathodic reaction related to the hydrogen production begins to dominate oxygen depolarization reaction; this explanation is further supported by the even lower slope for the 20-200 mA/ft^2. The low slope suggests kinetic control (i.e., the speed of reaction determines the amount of reactant produced by the reaction).

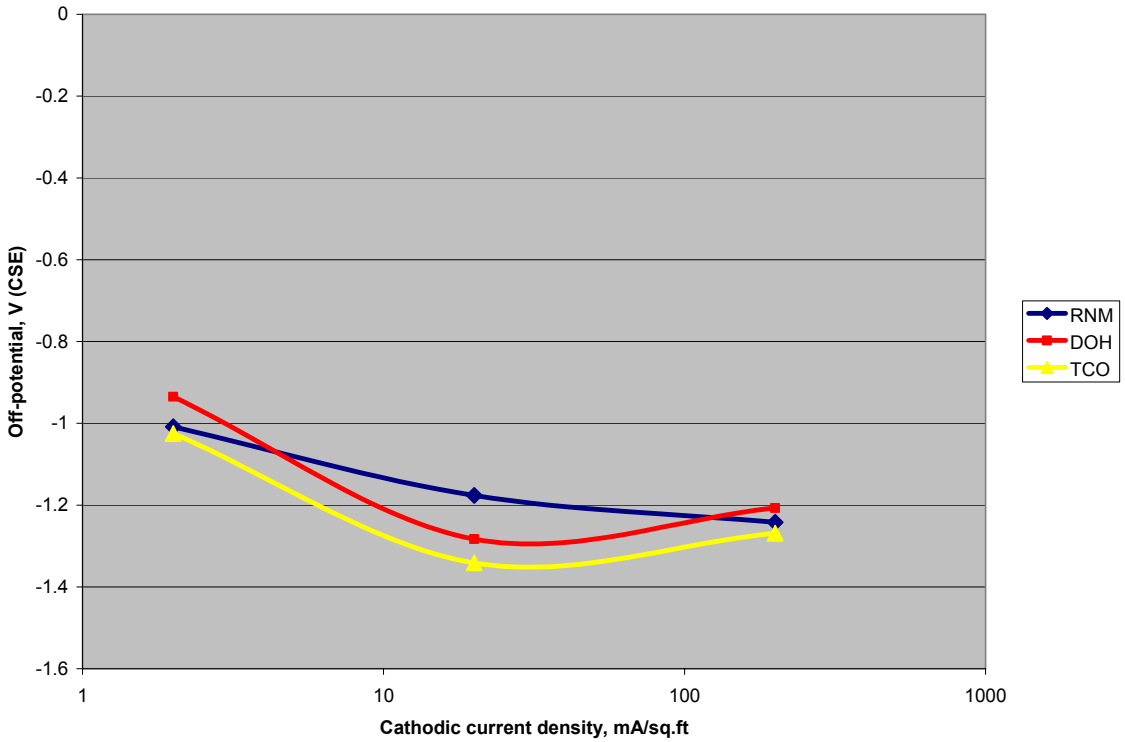

Figure 29. Average off-potential vs. current density for the three tested soils.

Table 23. Potential-current density slopes based on average off-potentials.

	Slope 2-20 mA/ft^2, mV/decade	Slope 20-200 mA/ft^2, mV/decade
RNM	-73	-28
DOH	-151	33
TCO	-138	32

Thermodynamic considerations show that, using the Nernst equation, the equilibrium potential for the hydrogen evolution (through water electrolysis, line (a) on the Pourbaix diagram for steel in water shown in Figure 30) is related as (for saturated copper/copper sulfate reference electrode scale):

$$e_{H^+/H_2} = -0.318 - 0.059\,pH$$

Experimental observations show that, at higher applied current densities, pH was significantly elevated (estimated at 11-12+ using indicator paper – see Figure 31 for an illustration). The ordinates (y-axes) are in reference to a standard hydrogen electrode (SHE); to convert to saturated copper/copper sulfate (CSE) electrode, subtract 0.318V from the SHE potential value.

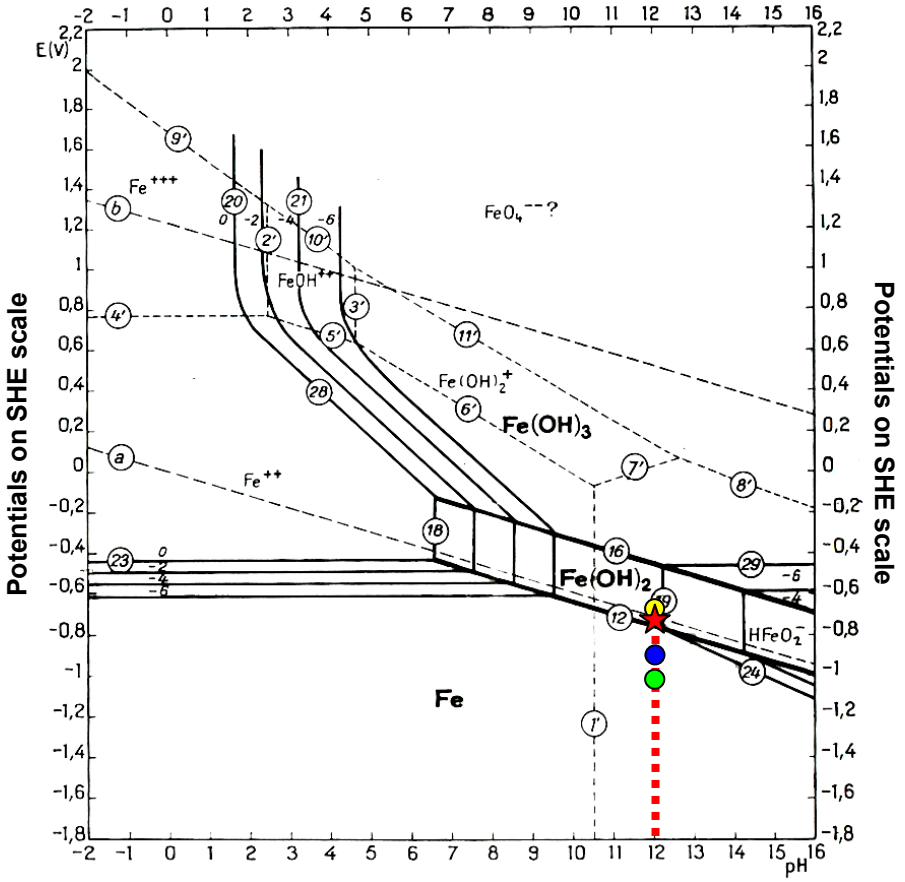

Figure 30. Potential/pH (Pourbaix) diagram showing conditions of stability for water, oxygen, and hydrogen at 25°C or 77°F (line (a)). Potential values are in reference to standard hydrogen electrode.

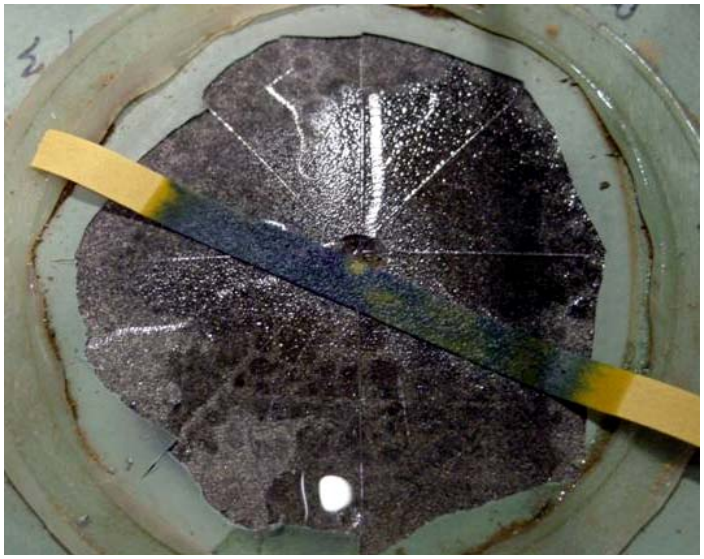

Figure 31. Elevated pH under disbonded coating in RNM soil at 200 mA/ft^2. Deep blue color indicates pH of 11-12+.

Using the value of pH 12 and substituting in the equation above, the equilibrium potential for hydrogen evolution is approximately -1.030V (CSE) (denoted by the star in Figure 30). Therefore, the evolution of hydrogen at the low current density of 2 mA/ft^2 is not very likely (corresponding 'average' potential is shown as the yellow dot in Figure 30, but may be taking place at the higher (20 and 200 mA/ft^2) densities (blue and green dots, respectively, in Figure 30).

The purpose of the preceding discussion is not, however, to suggest that the evolution of hydrogen is the primary driver behind the cathodic disbondment process. It is offered as an illustration for the argument that the heavy reliance on the potential measurements alone may lead to underestimation of the disbondment hazards. For example, all of the tested coatings have shown increased (significantly for some) disbondment values at 200 mA/ft^2 when compared to 20 mA/ft^2 and yet in two soils the potential shift between the two conditions was actually in the positive direction (using *average* off-potentials), however, in both cases being more negative than -1.2V (CSE).

Under the circumstances, the preferred approach would be to adopt a more conservative stance. The cathodic protection criteria outlined in the NACE Recommended Practice RP0169 are being currently reviewed by the NACE Task Group TG 285. The value often mentioned in regard to the upper CP limit with respect to hydrogen evolution is -1.1V (CSE), although this ceiling is typically discussed with regard to the hydrogen embrittlement. However, given the above, it may be appropriate to use the -1.1V (CSE) criterion as the cathodic disbondment criterion as well.

Ranking of coatings

Given the scatter in the disbondment observed on the tested specimens, the ranking on the basis of the projected trend (above) is augmented by ranking the coatings using the *average* disbondment data.

Using the *average values plus/minus one standard deviation*, the coatings were ranked on the basis of their performance for each current density/soil combination (receiving the score of 1.0 for the best performance and 4.0 for the worst performance). The resultant scoring and the ranking are shown Table 24 and Figure 32.

Table 24. Ranking of tested coatings (average disbondment with standard deviation).

	RNM	DOH	TCO	Score	Rank
HPCC	4.0	3.5	3.0	10.5	**1**
LE	6.0	3.5	4.0	13.5	**2**
FBE2	6.0	5.5	5.5	17.0	**3**
FBE1	8.0	8.5	5.5	22.0	**4**

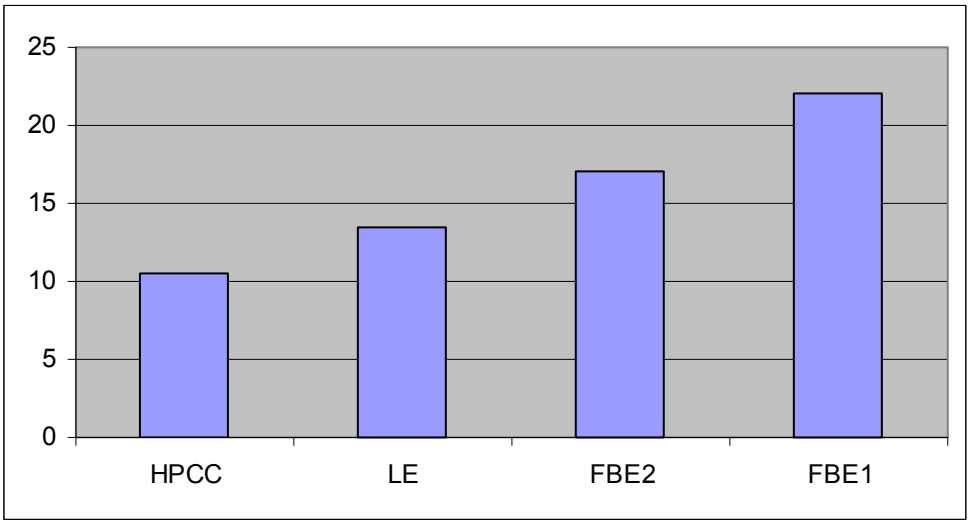

Figure 32. Performance score of tested coatings using average disbondment values with one standard deviation.

The above analysis suggests that in the tested conditions, the best performer of the group (using cumulative rankings) is HPCC, followed by FBE2/LE, and FBE1.

However, this conclusion requires several important qualifications. Although all coatings were supplied in the form of the product applied to a pipe, the sources were different. The HPCC coating was supplied by its manufacturer (Shaw Pipe Protection Limited, the Canadian division of the Bredero Shaw Group), FBE 1 and FBE 2 coatings were furnished by the gas pipeline operators, and LE coating was applied in the laboratory by CC Technologies. Therefore, there was no control for such factors as the age/prior history of the coating (such as UV damage during storage) and the surface preparation. This may explain why the thicker FBE coating (FBE1), while presumed to be the same formulation as FBE2 (the thinner coating) has apparently produced poorer results, which is contrary to some of the earlier published findings.

Consistency of performance

To further characterize the coatings' performance in the tests, the standard deviation values were used as a proxy for the consistency of the coatings performance (the degree of scatter in the disbondment values). The standard deviation (expressed as a percentage of the average value for each current density/soil condition) is plotted on the abscissae of the charts shown in Figure 33.

Coating-specific scatter as the result of imposed current density (left charts)

FBE2 formulation exhibited greater scatter than the other three coatings in RNM and DOH soils; it also tended to perform less consistently at the lower current densities. At the high current density, HPCC tended to display the most consistent results.

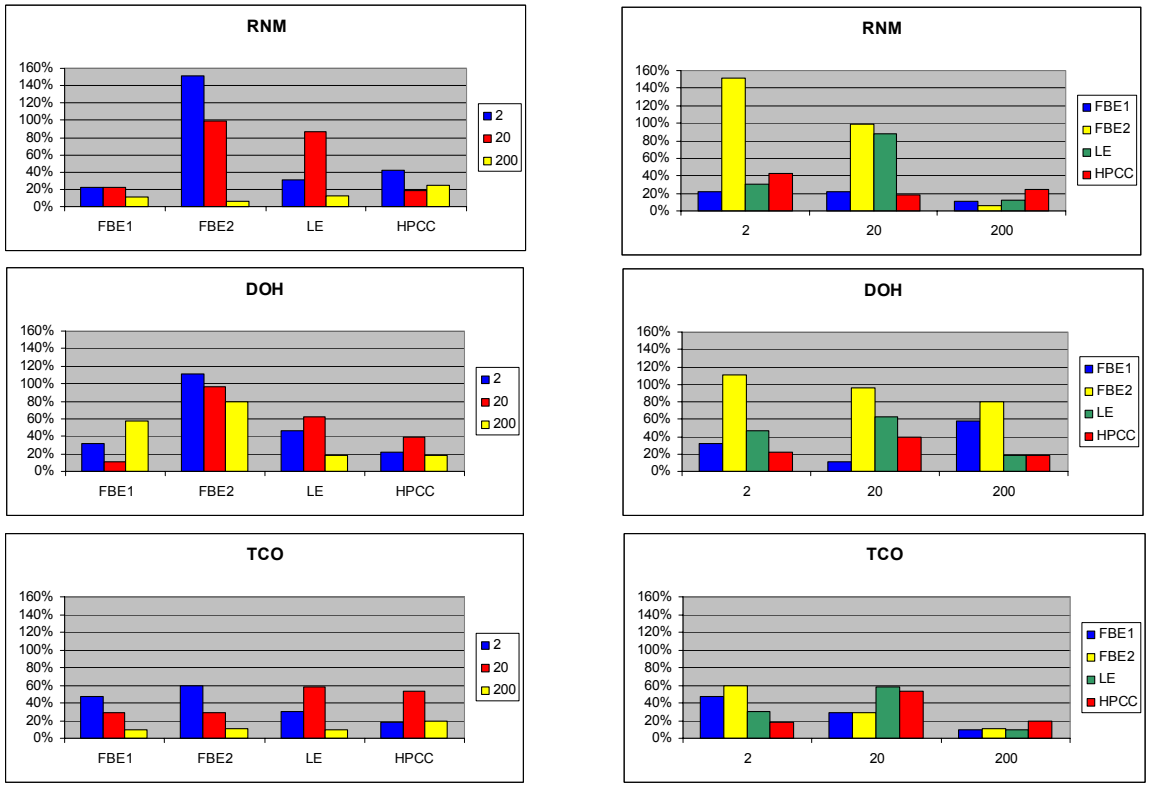

Figure 33. Standard deviation of disbondment results in the tested conditions.

Current-specific scatter in different tested soils (right charts)

As a group, the coatings exhibited more consistent performance in each of the tested soils at 200 mA/ft^2 than at the lower densities for a given soil. The behavior at 2 and 20 mA/ft^2 was not statistically different. The lowest scatter for all coatings was observed in the TCO soil.

The comparison uses the subset of data array employed for the ranking of the coatings with the help of the standard deviation and therefore, reaffirms the preceding conclusions.

Blistering

None of the tested coatings exhibited any propensity to blister under the applied voltage, even after a prolonged (1-year plus) exposure.

ASTM testing vs. soil-based testing

One of the comparisons that can be made on the basis of the results is with regard to the comparison between the ASTM standard test and the soil-based tests. The findings corroborate the notion that the ASTM test should be used merely as a screening/ranking test and should not be utilized as the basis for the prediction of the tested coatings' field-based performance. As shown in Figure 22, Figure 23, Figure 24, and Figure 25, the disbondment values in the ASTM test were in the same range as the disbondment 2 - 20 mA/ft^2 soil tests. The soil tests show that under the more extreme conditions, coating disbondment caused by high CP can be far greater than the one observed in the ASTM tests.

Testing temperature considerations for cathodic disbondment

Temperature influences the performance of coating. In this work, a single test temperature (ambient) was used to represent the value commonly used in laboratory experiments and stipulated by many ASTM procedures (including the ones used in this project). Although the test temperature is expected to represent a large portion of pipeline in the field and results can be compared to those of other researchers, it should be recognized that the results may not represent pipelines at significantly different temperatures.

In general, if all other circumstances are the same, higher temperatures typically decrease the performance of organic coatings, resulting in lower adhesion and increased water absorption and diffusivity. For the temperature range expected on a 'typical' pipeline (between 40º and 80ºF), the effect of the temperature on cathodic disbondment is likely to be eclipsed by variations in the coatings characteristics (e.g., local thickness, as-produced bond strength, etc) and environmental factors (e.g., local chemistry, moisture content, wet/dry cycling, etc.). The research published by PRCI in 2001 (Cathodic Disbondment of Pipeline Coatings Under Realistic Field Conditions) concluded that elevated temperature often increases disbonding, but the effect is complex and can depend upon the specifics of the coating system. Depending on the coating system, a temperature exists where severe loss of adhesion can occur. This temperature is typically greater than 120, 150, and 200ºF for tape, coal tar, and FBE systems respectively. These temperatures are not common on gas transmission systems unless directly downstream of a compressor.

The primary focus of the cathodic disbondment tests was to evaluate the effect of cathodic current density on CD; therefore, the tests were conducted at the constant temperature; the ambient conditions simplified the experimental apparatus, allowed results to be compared to other work, and represented the majority of pipelines in the field.

With respect to disbondment, the results may be conservative for the pipelines in colder environments. Accurate determination of the level of conservatism inherent in the results with respect to disbondment will require further study

Summary

- The results confirm the commonly accepted trend that the increase in the applied cathodic protection current leads to increased cathodic disbondment of the coatings. The CD of the tested coatings was most pronounced at the high (200 mA/ft^2) current density.

  The primary question at this stage is whether the observed trends could be used for a quantitative prediction of the effect of CP on coatings in the field. In other words, is the disbondment versus current density trend (1) accurate, (2) sustainable, and (3) universal? It is important to stress that the linear regression results for the CD - current density dependence should not be used to calculate the expected CD values in the field conditions. As shown, for some conditions, considerable scatter was observed which affects the precision of the empirically derived equation.

  The results are based on the extensive testing of several experimental conditions (88 tests); however, the linear regression fit is based on three data points per each coating/soil combination, which may affect the degree of accuracy. From the practical standpoint, the range of the examined density values is likely to cover the high end of the CP potentials observed in the field (approximately -1.250V (CSE)) and thus provides a valid “order of magnitude” approximation for the coatings’ performance under high CP conditions on the actual pipelines. It is not likely that the slope of the regression curve can be sustained at the yet higher currents.

  Further, the results are based on the test configuration that limits the maximum disbondment to the physical size of the test cell. In this regard, the findings are a low estimate for some of the testing conditions where disbonded coating extended to the edge of the cell area. Also, the results are applicable only to the tested coatings/soil conditions. It is known that moisture content affects disbondment (higher moisture content increases propensity to CD); hence, in this respect, the CD values represent the ‘worst case’ scenario for the tested soils.

- The findings show that the three-layer coating appears to perform better than the other tested formulations. However, the results do not take into considerations such very important disbondment-affecting parameters as the coating age and surface preparation.

- None of the tested coatings displayed susceptibility to blistering under the tested conditions in the absence of a holiday.

- The proposed approach to monitoring for conditions conducive to CD should include monitoring both current density (through the use of Coupon Test Stations placed next to the underground pipeline) and off-potential values. If all cathodic disbondment data from the laboratory tests are averaged for each current density, the following trend emerges (see Figure 34 below).

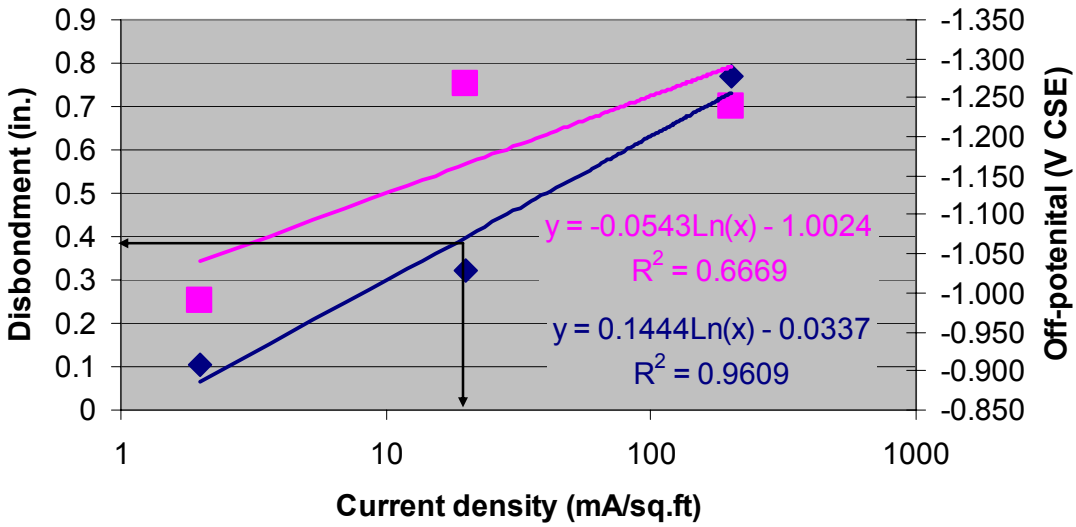

Figure 34. Cathodic disbondment and off-potential values versus applied cathodic protection current density.

The graph in Figure 34 superimposes the CD data and the off-potential values. The arrows in the graph point to the CD value which NACE PR0394 "Application, Performance and Quality Control of Plant-Applied Fusion Bonded Epoxy External Pipe Coating" considers acceptable (CD radius of 10 mm or 0.39 inch). [Note: This value is applicable to the test similar to the ASTM G95 Standard test method (28 day exposure of a 3 mm diameter holiday to a sodium chloride solution and a polarization of -1.5V. With the exception of FBE2 (see Table 17) all tested coatings met this criterion.] Using the linear regression equation correlating the CP current density and the CD values (lower equation) to back-calculate the "limiting" current density, one arrives at a value of 19 mA/ft^2. Substituting this number in the linear regression for the off-potential/CP current density (upper equation), one calculates the "limiting" value of -1.16V (CSE). As it is based on averaging the data for different soils and coatings, the preceding example is meant to merely provide the reader with a reference point; it is not intended to serve as a 'hard and fast' criterion for cathodic disbondment. Furthermore, the current density limits should take into consideration the effect of CP on mechanical properties of the linepipe steels (see above).

Hence, as a *general* guideline, the use of the -1.1V (CSE) for upper limit on the off-potential value may be acceptable but in order to confirm the applicability of this value to the other existing coating systems (i.e., to evaluate the degree of the

universality of the criterion) and to establish the degree of the conservatism of this criterion further testing is necessary.

It should be also noted that the adoption of the -1.1V value as the CD criterion should be weighed against the issue of how extensive/localized the areas of the high CP potentials are with regard to the areas of the 'normal' CP potentials (i.e., those with the off-potential values below the -1.1V limit). In the attempt to bring the high CP potential areas into compliance with the -1.1V ceiling, the operator may run into the hazard of not complying with the NACE PR0169 protection criterion on more vast regions of the underground structure. One possible solution for resolving the dilemma of complying with both the RP0169 CP criteria and avoiding the local overprotection is to install additional anode groundbeds to achieve a finer control of the CP potential conditions and even out the potential distribution along the protected structure. The alternative is to reconfigure the CP system and/or to recoat selected sections of the pipeline.

One additional important consideration is that the assessment of the hazards of increased cathodic disbondment area at existing holidays at higher CP currents should be considered with regard to the ability of the imposed CP to mitigate corrosion at the larger holiday(s). In other words, the fact that the holiday area is increased due to overprotection does not necessarily imply that this location will no longer be cathodically protected. For example, Worthingham et al (R. Worthingham, M. Cetiner, "Long Term Performance of Fusion Bonded Epoxy Coated Pipelines", International Pipeline Conference, Calgary, Alberta, Candad, 2004, IPC 04-0570) indicates that FBE fails in a "CP-friendly manner" and concludes that "as long as CP is operating on a pipeline, blistering and disbondment of FBE coatings does not present an integrity threat to the pipeline". [Note that the study evaluated the performance of FBE coatings only.] However, if the conditions of overprotection persist over an extended area of the pipeline, it is possible that with time CP output may not be sufficient for an effective CP protection. Further work is required to address the issue.

- Further testing is required to address various aspects of the observed trends and proposed guidelines. The applicability of this suggested CP criterion/CD density values to the other existing coating systems (i.e., to evaluate the degree of the universality of the criterion) and evaluation of the degree of conservatism of this criterion necessitates additional examination. Further testing is required to establish the impact of the CP potential cycling (as a result of e.g., seasonal changes it the soil resistivity) on the cathodic disbondment. The time during which high CP potentials exist on the pipeline needs to be related to the extent of disbonding. This issue is also closely related to the one noted in the preceding paragraph; the hazards of the high CP potentials in some pipeline regions should be regarded with respect to the hazards of low CP for the rest of the structure.

GENERAL CONCLUSIONS

The experimental program carried out under Task I and Task II activities indicate that:

1. The imposition of the cathodic protection current has an effect on the mechanical properties of the studied steels under the examined conditions. The primary observed effect is the increase of the brittle area on the fracture surface in response to the increase of the current density of the CP current, which is a proxy for the propensity to hydrogen-related damage (HRD). The most notable effect was observed on X100 steel.

2. The presence of hard spots, simulated by the heat treatment of the X65(HC) steel did not cause an appreciably different behavior regarding the susceptibility to the hydrogen-related damage when compared to the un-treated material. This unexpected result (in contrast to the field-based observations) is likely caused by the insufficient sensitivity of the testing method.

3. Whereas the increase in the cathodic protection current produced an effect on the mechanical properties of the studied materials, there is insufficient data to translate the observed effect into what could be expected in the field. It is not possible to draw definitive conclusions as to the quantified relationship between the CP current density and structural integrity of the pipelines. Further studies are mandatory to establish the influence of time on the observed effect, which includes the impact of the CP potential cycling.

4. The CP effect on the materials properties is material-specific and a 'one-size-fits-all' approach to choosing a 'hard and fast' criterion may not be adequate and will likely result in over-/underestimation of the danger in some circumstances. Notwithstanding the above, prolonged periods of 'overprotection' should be avoided. The value of less than 2 mA/ft^2 may serve as a target value for the CP current density (and can be monitored through the use of Coupon Test Stations); at this time, the use of the polarized off-potentials as the sole criterion for the assessment of the hazards of hydrogen-related damage is discouraged.

5. The increase in the applied cathodic protection current leads to increased cathodic disbondment of the coatings. The CD of the tested coatings was most pronounced at the high (200 mA/ft^2) current density. It is important to stress that the linear regression results for the CD - current density dependence should not be used to calculate the expected CD values in the field conditions. The range of the examined density values is likely to cover the high end of the CP potentials observed in the field (approximately -1.250V (CSE)) and thus provides a valid "order of magnitude" approximation for the coatings' performance under high CP conditions on the actual pipelines. One additional important consideration is that the assessment of the hazards of increased cathodic disbondment area at existing holidays at higher CP currents should be considered with regard to the ability of the imposed CP to mitigate corrosion at the larger holiday(s). In other

words, the fact that the holiday area is increased due to overprotection does not necessarily imply that this location will no longer be cathodically protected. However, if the conditions of overprotection persist over an extended area of the pipeline, it is possible that with time CP output may not be sufficient for an effective CP protection. Further work is required to address the issue.

6. Laboratory tests were carried out at an ambient temperature; it should be recognized that the results may not represent pipelines at significantly different temperatures. Accurate determination of the level of conservatism inherent in the experimental results (with respect to hydrogen related damage and coating disbondment) will require further study. .

7. The proposed approach to monitoring for conditions conducive to CD should include monitoring both current density (through the use of Coupon Test Stations placed next to the underground pipeline) and off-potential values. As a *general* guideline, the use of the -1.1V (CSE) and 2 mA/ft^2 for upper limit on the CP protection parameters may be acceptable, but in order to evaluate the degree of the universality and to establish the degree of the conservatism of this criterion further testing is necessary.

8. The adoption of the -1.1V value as the CD criterion should be weighed against the issue of how extensive/localized the areas of the high CP potentials are with regard to the areas of the 'normal' CP potentials (i.e., those with the off-potential values below the -1.1V limit). In the attempt to bring the high CP potential areas into compliance with the -1.1V ceiling, the operator may run into the hazard of not complying with the NACE PR0169 protection criterion on more vast regions of the underground structure. One possible solution for resolving the dilemma of complying with both the RP0169 CP criteria and avoiding the local overprotection is to install additional anode groundbeds to achieve a finer control of the CP potential conditions and even out the potential distribution along the protected structure. The alternative is to reconfigure the CP system and/or to recoat selected sections of the pipeline.

TASK III - GUIDELINES

Foreword

The results of an experimental program, which investigated the effects of cathodic protection on mechanical properties of pipeline materials and cathodic disbondment of several common types of external coatings, form the basis of suggested guidelines for the pipeline operators regarding monitoring the 'overprotection' conditions.

There is insufficient data to draw definitive conclusions as to the quantified relationship between the CP current density and structural integrity of the pipelines. The CP effect on the materials properties is material-specific and a 'one-size-fits-all' approach to choosing a 'hard and fast' criterion may not be adequate and will likely result in over-/underestimation of the danger in some circumstances.

Further testing is required to address various aspects of the observed trends and proposed guidelines. A quantitative relationship between the imposed CP current density and the expected extent of cathodic disbondment would require extensive additional testing to incorporate other coatings and other environmental conditions (i.e., evaluation of the degree of the universality and conservatism of this criterion). Further experimentation is required to establish the impact of the CP potential cycling (as a result of e.g., seasonal changes it the soil resistivity) on the cathodic disbondment. The time during which high CP potentials exist on the pipeline needs to be related to the extent of disbonding.

General guidelines for CP currents and potentials

The results of the extensive experimental program show that the imposition of the cathodic protection current has an effect on the mechanical properties of the studied steels under the examined conditions. The primary observed effect is the increase of the brittle area on the fracture surface in response to the increase of the current density of the CP current, which is a proxy for the propensity to hydrogen-related damage. The results also confirm the commonly accepted trend that the increase in the applied cathodic protection current leads to increased cathodic disbondment of the coatings.

The CP off-potentials, being a derivative of the applied current density, environmental characteristics, and material properties, serves merely as a convenient metric to assess the danger of the overprotection and not as the primary cause of the possible damage caused by overprotection. Heavy reliance on the potential measurements alone may lead to errors in the assessment of the actual threat of overprotection. Therefore, the use of the polarized off-potentials as the sole criterion for the assessment of the hazards of hydrogen-related damage is discouraged. Notwithstanding the above, prolonged periods of 'overprotection' (as manifested by the high negative potentials) should be avoided.

In the tests, cathodic disbondment of the tested coatings was most pronounced at the high (200 mA/ft^2) current density, which is not likely to be frequently encountered in the field. Experimental observations thus cover the high end of the CP off-potentials observed in the field (approximately -1.250V (CSE)) and provide an "order of magnitude" approximation for the coatings' performance under high CP conditions on the actual pipelines.

The proposed approach to monitoring for conditions conducive to CD includes monitoring current density (through the use of Coupon Test Stations placed next to the underground pipeline) augmented by the off-potential values. In practical terms, the experimental observations mean that increased current densities, while showing continuous detrimental influence on coatings' and linepipe steels' performance, do not cause an appreciable corresponding shift in the polarized potentials. Indeed, if the slope of the potential-vs.-current curve is, e.g., 60 mV, it would require a ten-fold increase in the imposed CP current to produce a 60 mV off-potential shift in the negative direction.

Therefore, it is suggested that the measurement of the current density (through the use of coupon test stations) be used as a primary metric for assessing the possible HRD hazards. The experimental results show that at the 2 mA/ft^2 plus current densities, the polarized potentials are close or more negative than -1.1V (CSE). The off-potential data is still useful, especially if used as a supplemental means of assessment or as a 'threshold' value. [The ongoing efforts of the NACE Task Group considering the criterion for overprotection are expected to contribute to the understanding of the issue.] Further testing is required to establish how universal the applicability of the experimental findings is to other coatings/environment/CP regimes.

As a *preliminary* and *general* guideline, the use of 2 mA/ft^2 and the off-potential of -1.1V (CSE) as a target upper limit on the CP current density and off-potential value may be acceptable, but in order to evaluate the degree of the universality and to establish the degree of the conservatism of this criterion further testing is necessary.

The adoption of the -1.1V value as the CD criterion should be weighed against the issue of how extensive/localized the areas of the high CP potentials are with regard to the areas of the 'normal' CP potentials (i.e., those with the off-potential values below the -1.1V limit). In the attempt to bring the high CP potential areas into compliance with the "2mA/ft^2/ -1.1V" 'ceiling', the operator may run into the hazard of not complying with the NACE PR0169 protection criterion on more vast regions of the underground structure. One possible solution for resolving the dilemma of complying with both the RP0169 CP criteria and avoiding the local overprotection is to install additional anode groundbeds to achieve a finer control of the CP potential conditions and even out the potential distribution along the protected structure. The alternatives are to reconfigure the CP system and/or to recoat selected sections of the pipeline.

APPENDIX A1

Hard Spots: Heat Treatment Technique.

The X65(HC)[8] steel (0.16% carbon) was subjected to a single-stage heat treatment to simulate hard spot conditions. The steel strips cut from the pipe were 12 in. long by 1 in. wide with a 0.388 in. wall thickness. The sample's long dimension was parallel to the pipe's longitudinal direction.

Continuous cooling transformation (CCT) diagrams (from M. Atkins, "Atlas of Continous Cooling Transformation Diagrams for Engineering Steels", 1980, ASTM, Metals Park, OH) for carbon steel with low carbon content (such as X65(LC) steel (0.049%C)) indicate that sufficient surface hardness (~35HRC) can not be achieved but that it is possible to heat treat X65(HC) steel (0.16% carbon) to arrive at the desired hardness. For an illustration, see CCT diagrams for 1016 (0.16% carbon) and 1005 (0.05% carbon) steels presented in Figure 35 and Figure 36, respectively. Based on the CCT charts, X65(HC) steel was chosen for the material to use in the tests simulating hard spots.

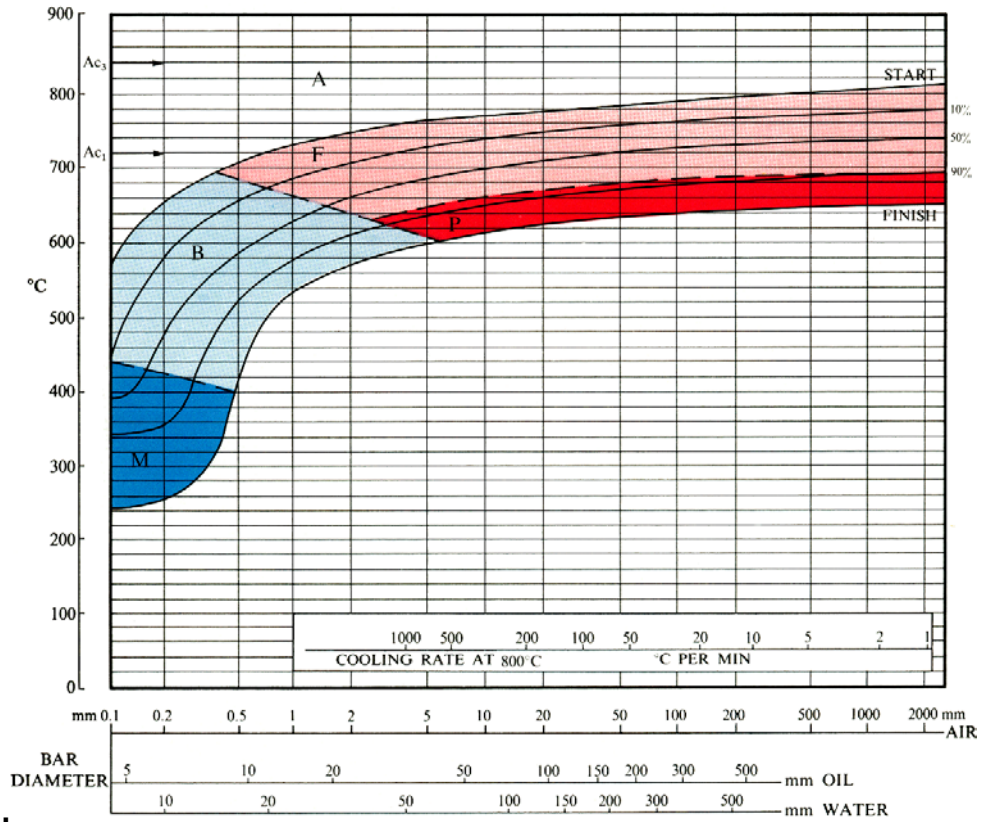

Figure 35. CCT diagram for 1016 carbon steel.

[8] Heat treated specimens are denoted as (HT) for 'heat treatment'.

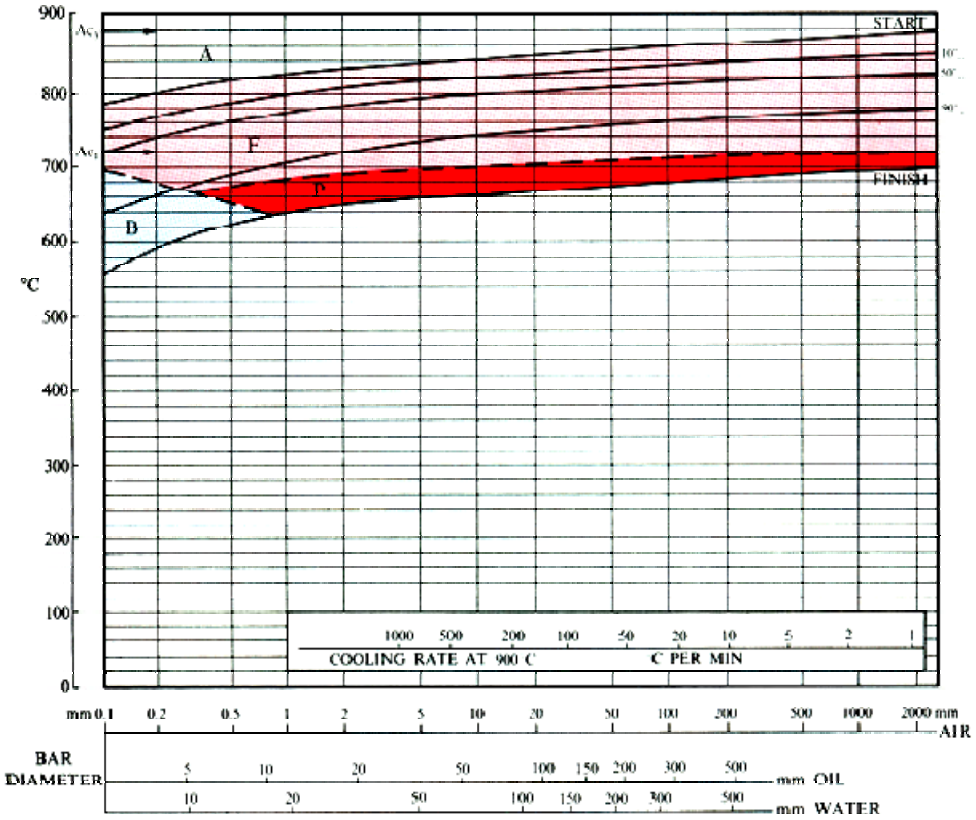

Figure 36. CCT diagram for 1005 carbon steel.

A furnace was pre-heated to 1600°F (872°C) and the samples were then inserted into the furnace and allowed to soak at temperature for 1 hour. After 1 hour, the samples were removed from the furnace and water quenched. Based on the literature data, the target mid-section hardness was 35 HRC. Due to the lack of availability of the Jominy end quench curve for the heat treated steel (X65(HC)), the Jominy chart for the hot rolled 1045 steel was used as a rough guide for the expected hardness (shown in Figure 37). The blue rectangle indicates the targeted area.

The estimated time to cool the X65(HC), 0.16% carbon, steel bars from 1600°F to room temperature was between one and ten seconds. The resultant microstructure contained mostly bainite with sparse islands of ferrite (SEE 'before and after' microstructure' in Figure 38). The achieved hardness was approximately 32HRC (see Figure 6).

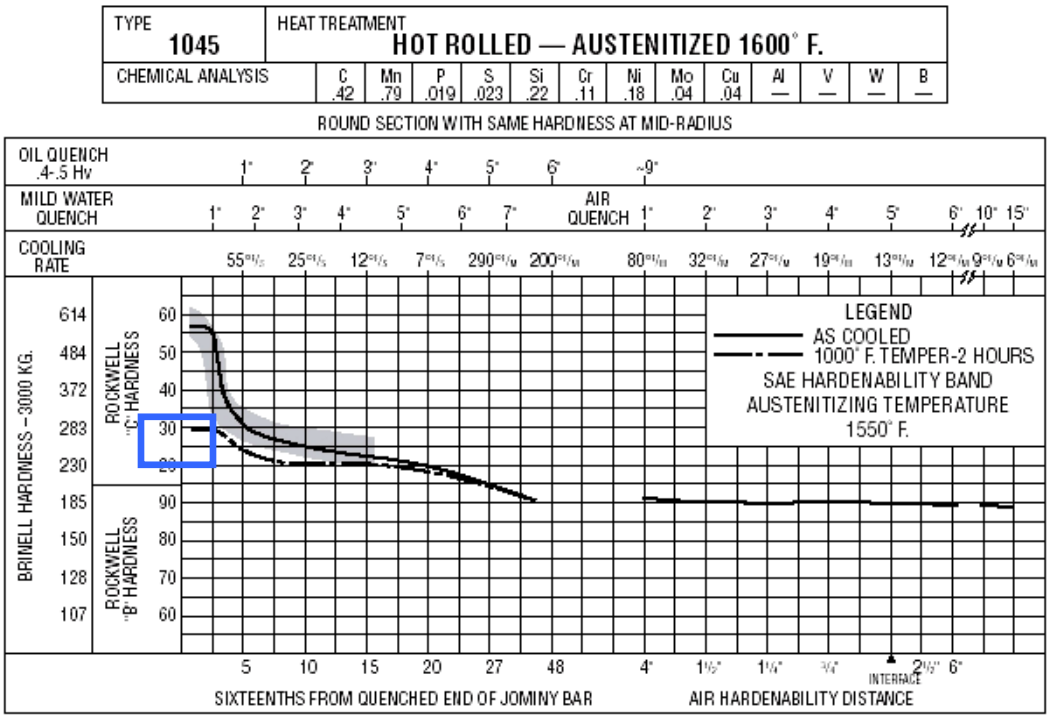

Figure 37. Jominy end quench curve for hot-rolled 1045 steel.

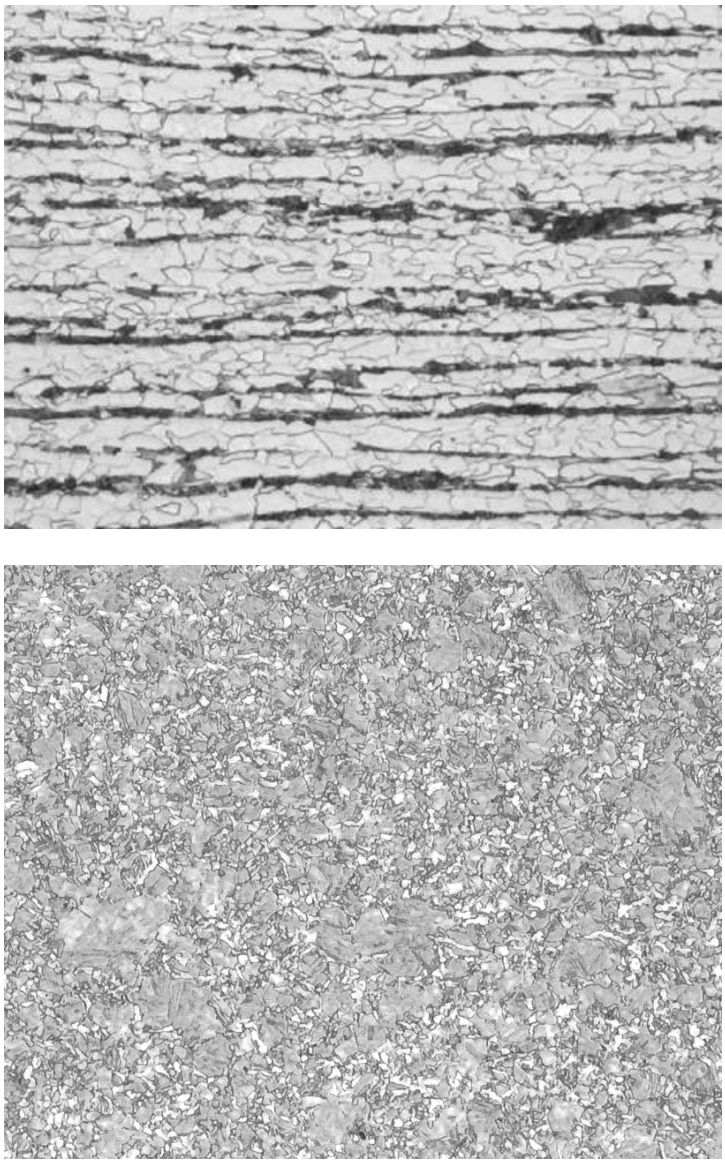

Figure 38. Microstructure of X65(HC) steel before (upper micrograph) and after (lower micrograph) the heat treatment.

APPENDIX A2

HIC Immersion Testing

HIC immersion testing was performed according to NACE TM0284 "Standard Test Method - Evaluation of Pipeline and Pressure Vessel Steels for Resistance to Hydrogen-Induced Cracking". NACE solution A was used, which consists of 3% NaCl and 0.5% CH_3OOH in deionized water. The ratio of solution volume to specimen surface area was greater than 3 mL/cm^2; the initial pH was 2.8.

The test specimens were standard HIC specimens with dimensions of 100 mm by 20 mm by actual material thickness. All specimens were taken from base metal in the parent material. The surface was ground using 320 grit silicon carbide paper after final machining. The specimens were wrapped in corrosion inhibiting paper and stored in a dessicator prior to testing. Each sample was cleaned with methanol, then with acetone, and handled with protective gloves on the test date.

The solution was placed in a sealed 50-liter glass vessel and purged with nitrogen for 2 hours to remove oxygen. The test specimens were placed in a container and the dry container was purged with nitrogen for 2 hours. The test solution was then introduced to the test chamber; to not allow oxygen ingress, positive pressure of nitrogen gas was maintained. The test solution was purged with pure H_2S at a rate greater than 200 mL/min per liter of solution for 1 hour. The 96-hour test period began after the initial 1-hour H_2S purge was complete. Immersion testing was carried out at approximately 75^{o}F. Each alloy was tested in triplicate with the narrow face pointing up in the test solution.

Upon completion of the test, each specimen was sectioned according to NACE TM0284. The sections were mounted in two-part epoxy, and ground successively with 80, 120, 240, 400, 800, and 1200 grit silicon carbide papers. Final polishing was performed using 6 micron, 3 micron, 1 micron, and 0.5 micron diamond suspension. The samples were then etched with 1% nitric acid. Each sample was examined using a light microscope at magnifications ranging from 25x to 400x.

SOHIC Immersion Testing

SOHIC testing was performed according to NACE TM0103-03 "Laboratory Test Procedures for Evaluation of SOHIC Resistance of Plate Steels Used in Wet H_2S Service". NACE solution A was used for the test solution, which consists of 3% NaCl and 0.5% CH_3OOH in deionized water. The ratio of solution volume to specimen surface area was kept greater than 3mL/cm^2. The initial pH was 2.8, measured using a pH electrode. The solution was placed in a sealed 50-liter glass vessel and purged with nitrogen for 2 hours to remove oxygen. The test specimens were placed in a container and the dry container was purged with nitrogen for 2 hours. The test solution was then introduced to the test chamber; to prevent oxygen ingress, positive pressure of nitrogen gas was maintained. The test solution was purged with pure H_2S at a rate greater than 200 mL/min per liter of solution for 1 hour. The 96-hour test period began after the initial 1-hour H_2S purge was complete.

The test specimens were as described in the NACE TM0103-03 procedure with dimensions of 146 mm by 25 mm by 7.6mm. All specimens were taken from base metal in the parent material. The spacers used to separate the upper and lower double beams and the bolts used to stress the beams were made of 1018 carbon steel to avoid galvanic corrosion effects. The dimensions of the individual SOHIC beams fabricated from the vessel plate material were 38 mm wide (1.5 inches) by 13 mm (0.5 inch) thick. The minimum length was 305 mm (12 inches). The steel spacers were 0.5 inch in diameter and spaced at positions one inch from the middle of the specimen. The notch was 2.0 mm deep and was machined with an EDM using 0.2 mm wire (0.008 in.). The notch root radius is 0.13 mm + 0.01 mm (0.0051 + 0.0004 in.). Figure 39 shows examples of SOHIC double beam assemblies.

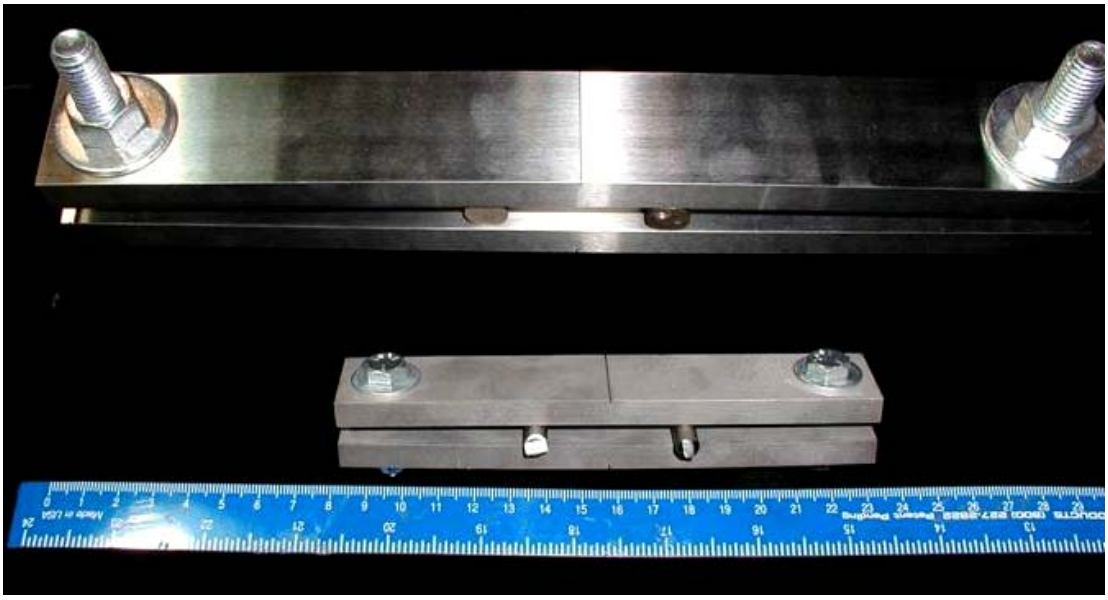

Figure 39. Examples of SOHIC double-beam assemblies.

shows the test matrix used for SOHIC screening tests. Some of the materials were tested at different levels of stress (as a percentage of yield strength). Each alloy/stress combination was tested in duplicate.

Table 25. SOHIC testing matrix.

Pipe Steel (API 5L)	SOHIC Beam Pseudo Stress (% Yield Strength)
X65	72%, 90%
X65(HT)	72%
X70	72%, 90%
X100	72%

APPENDIX B1

Table 26. Time-to-failure in SSRT experiments.

	Current density, mA/ft^2	Time-to-failure, hours
X65(HC)	Air	56
	0	66
	0.2	65
	2	25
	200	27
X65(LC)	0.2	49
	2	56
	200	33
X65(HC)(HT)	Air	48
	2	15
	200	20
X100	Air	20
	2	21
	200	17

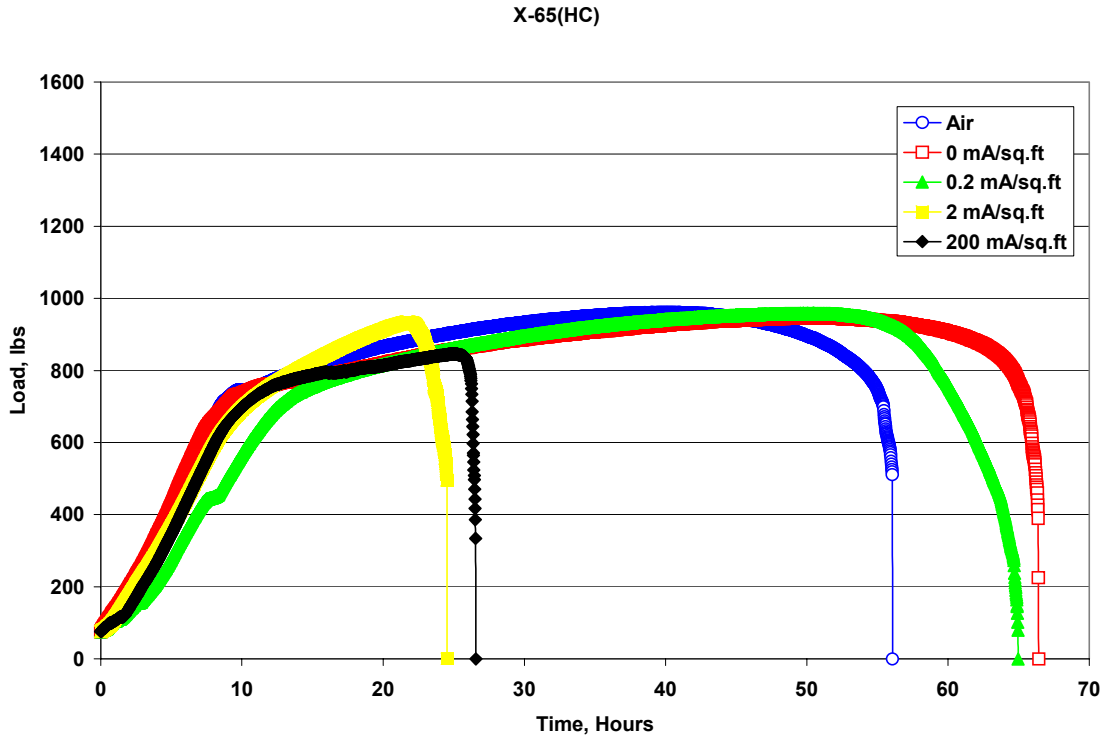

Figure 40. Load vs. time plot for X65 (HC) steel.

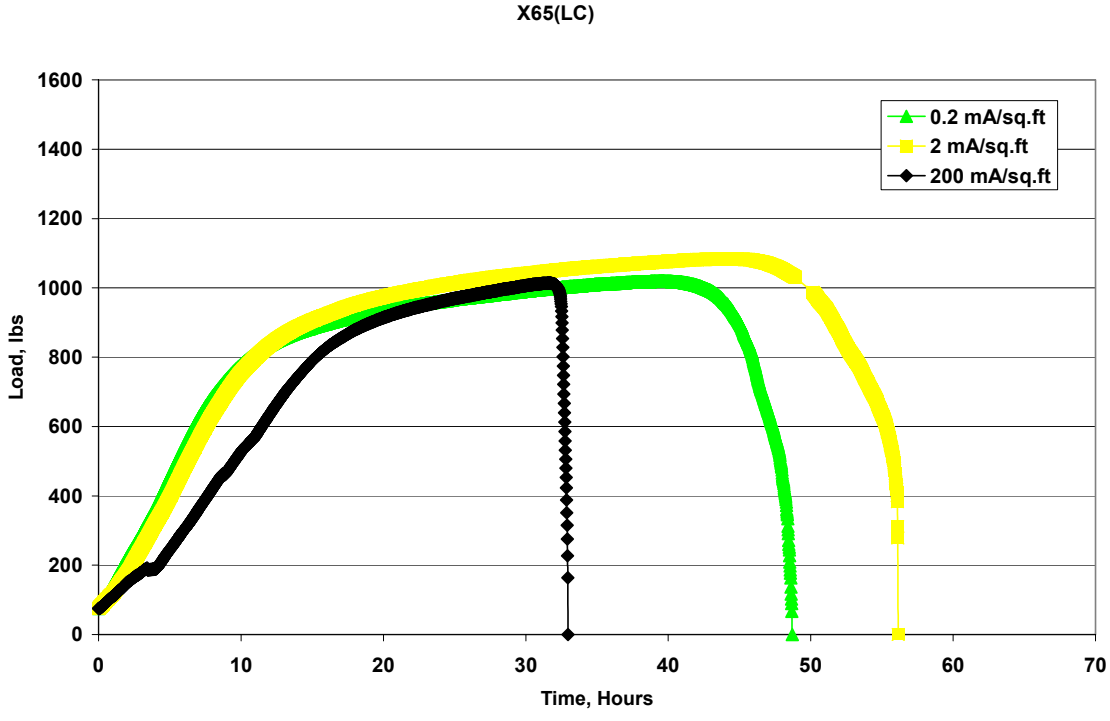

Figure 41. Load vs. time plot for X65 (LC) steel.

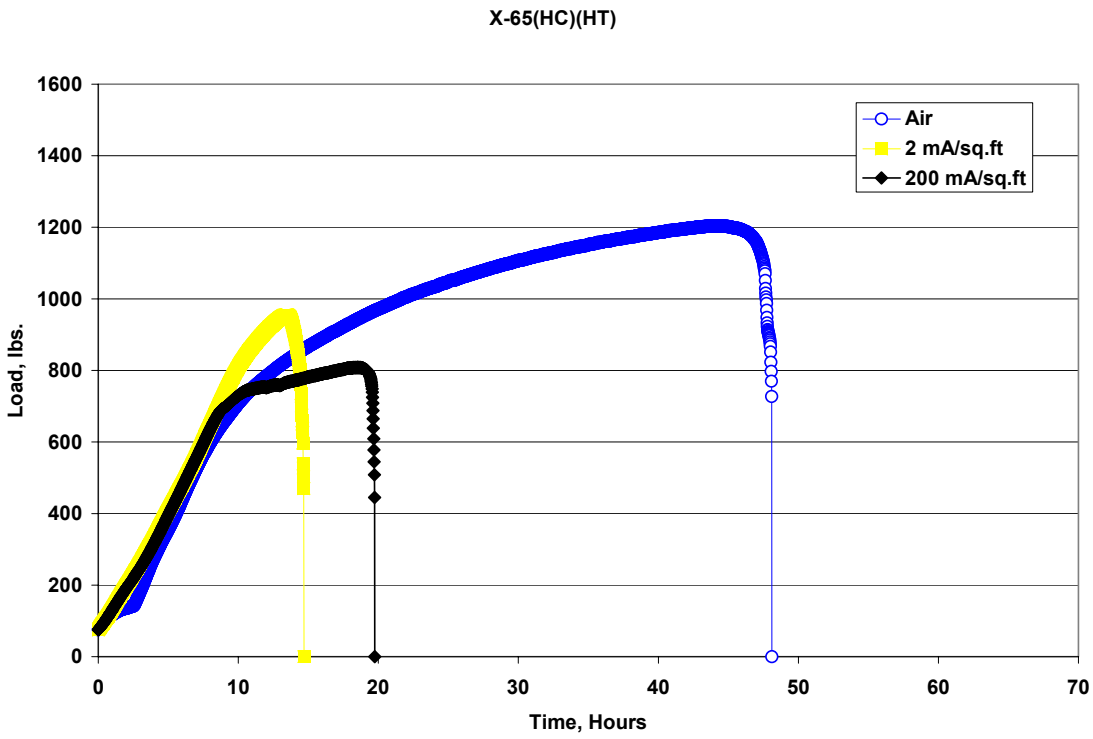

Figure 42. Load vs. time plot for X65 (HC)(HT) steel.

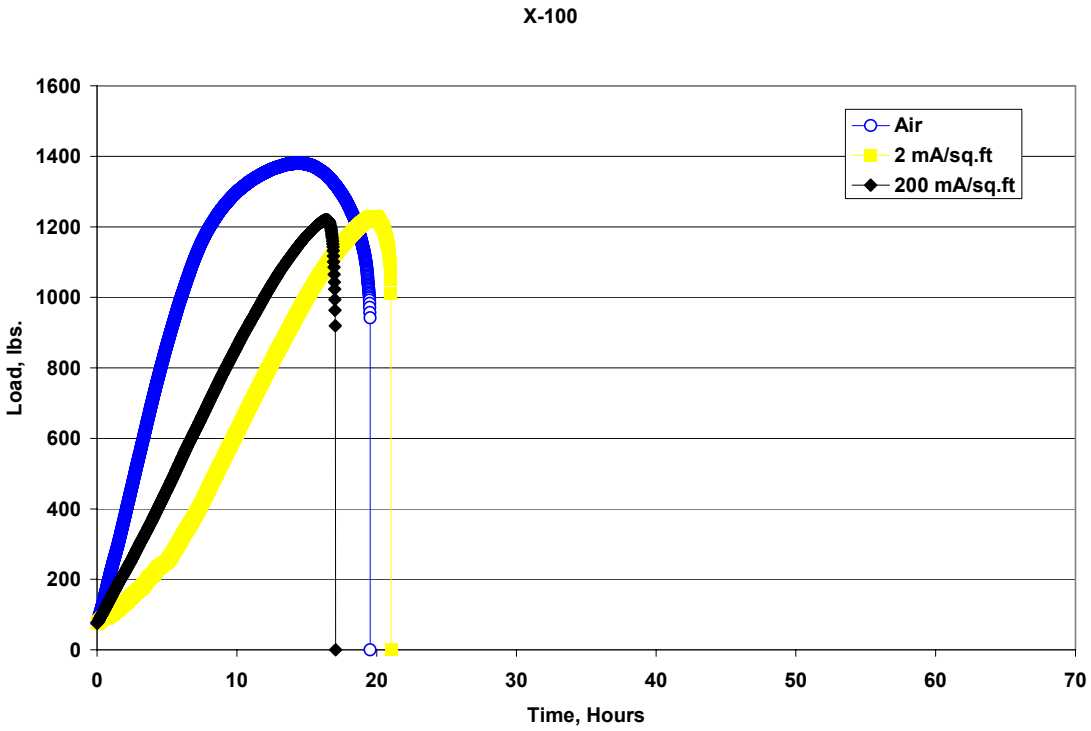

Figure 43. Load vs. time plot for X100 steel.

APPENDIX B2

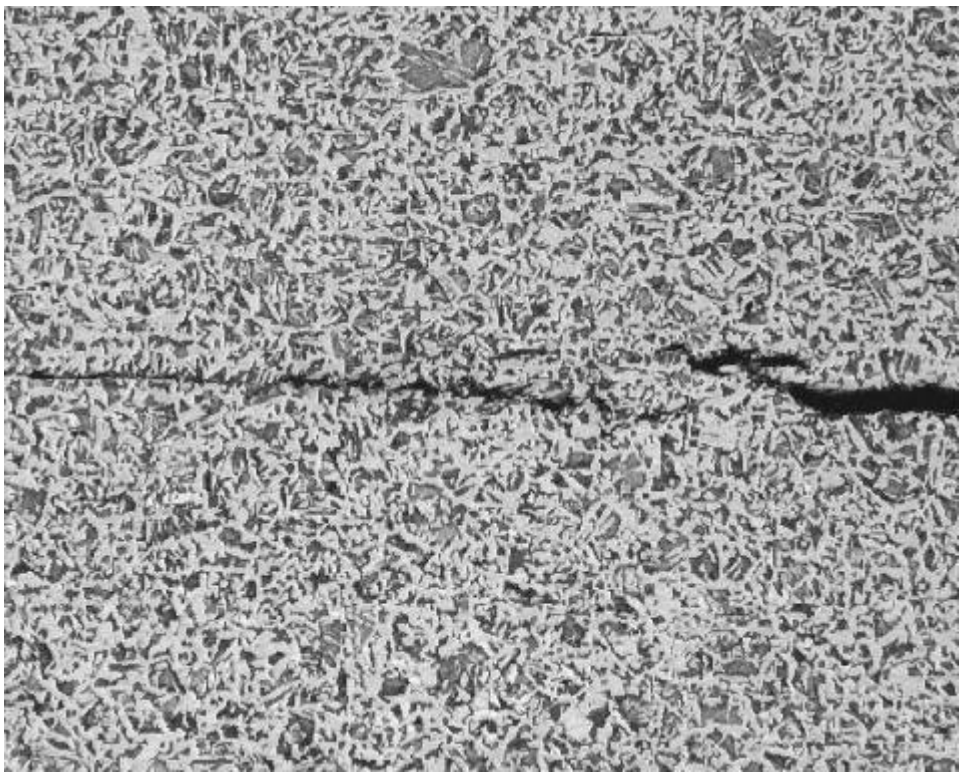

X65 (Vessel plate), 0.23% C, HIC, 50X magnification.

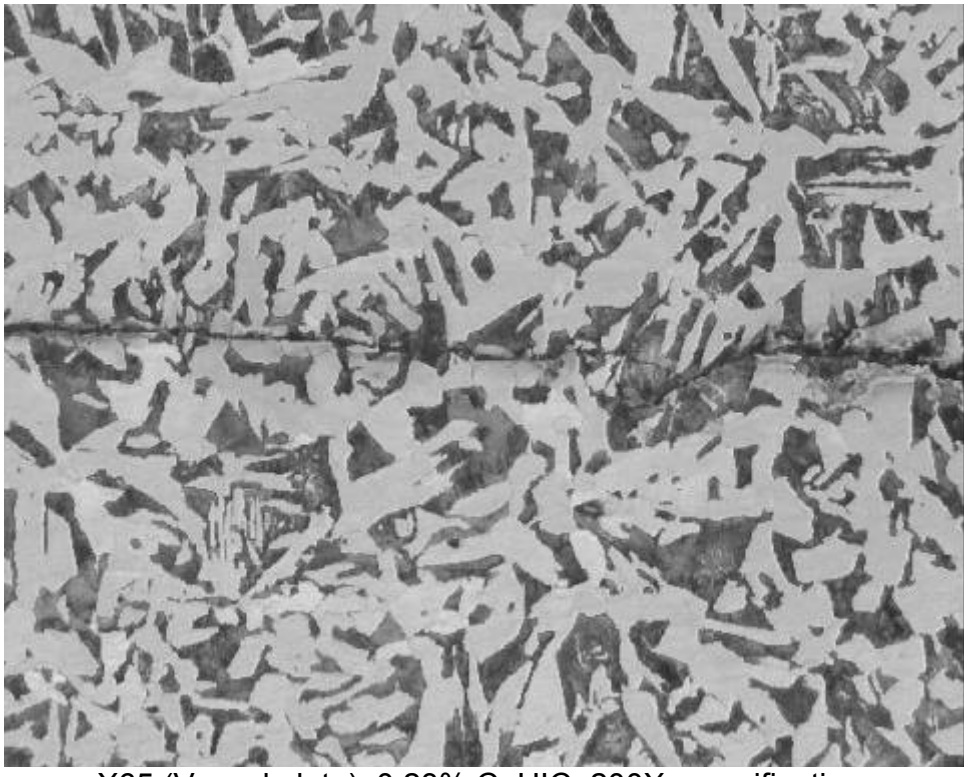

X65 (Vessel plate), 0.23% C, HIC, 200X magnification.

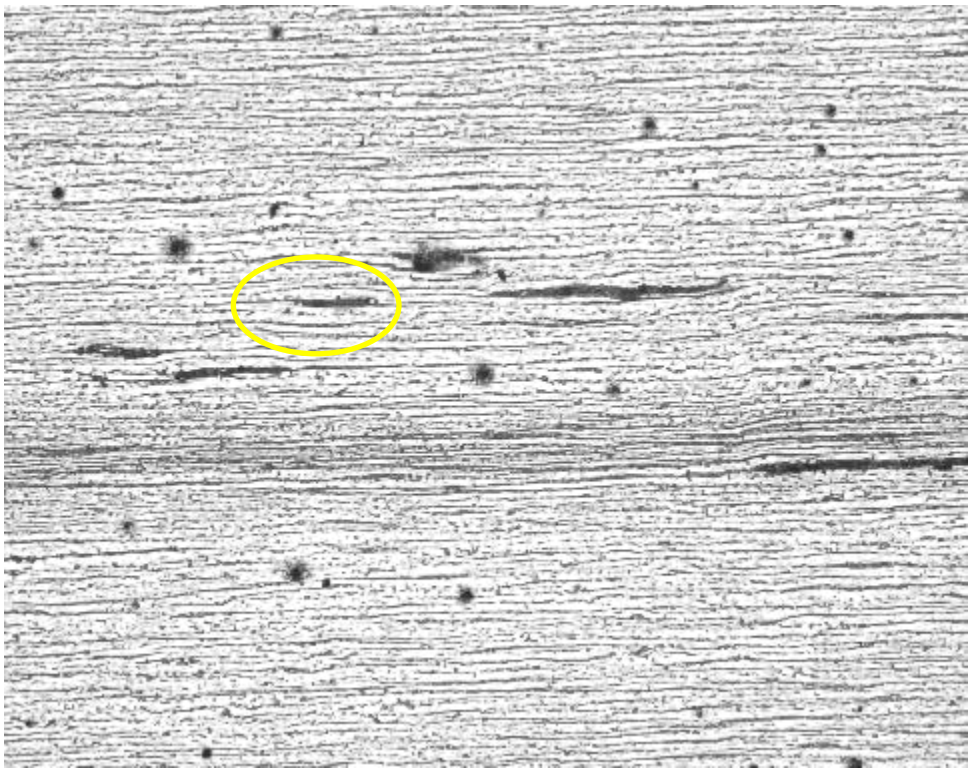

X65 (HC), 0.16% C, HIC, 50X magnification.

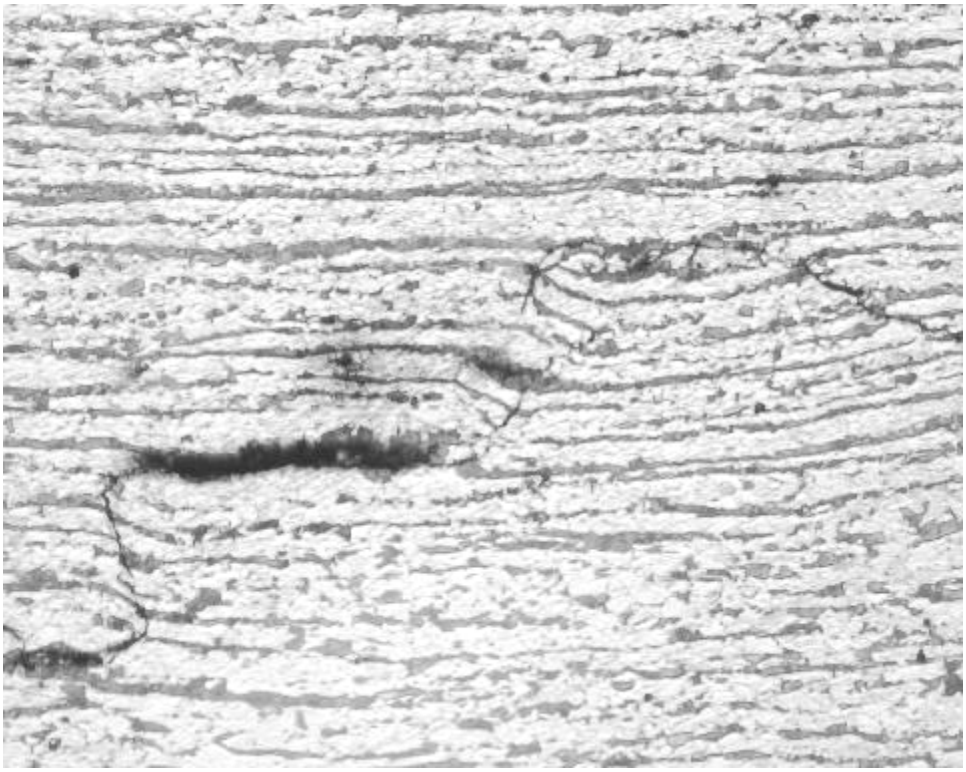

X65 (HC), 0.16% C, HIC, 200X magnification.

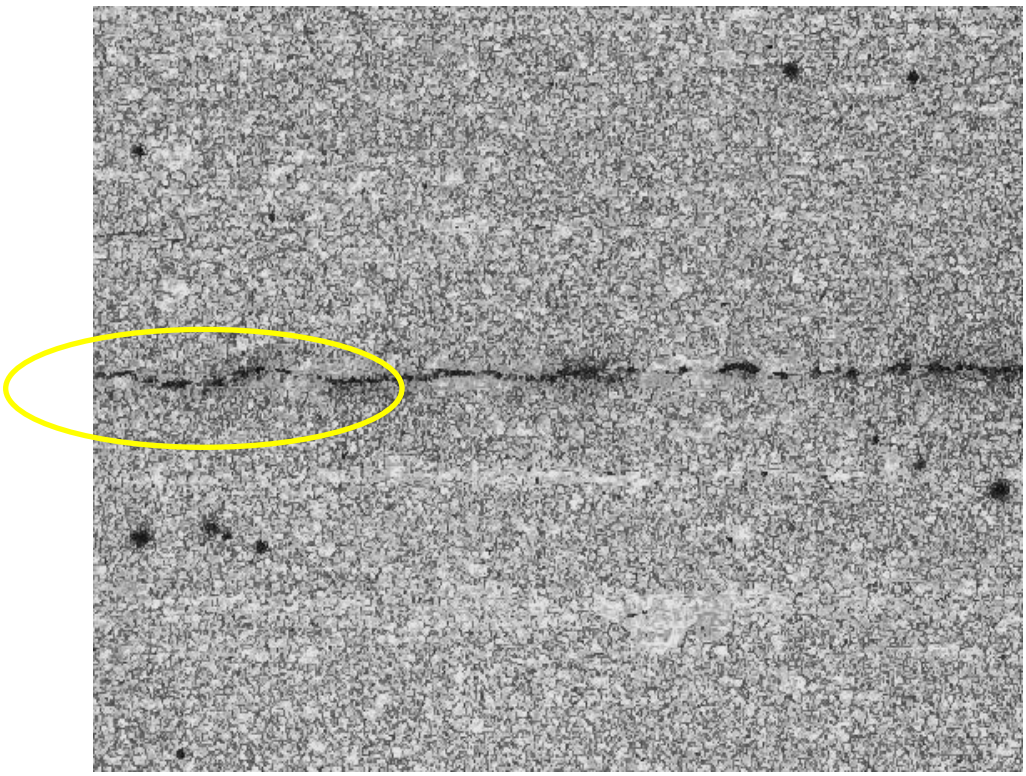

X65(HC) (HT), 0.16% C, heat treated, HIC, 100X magnification.

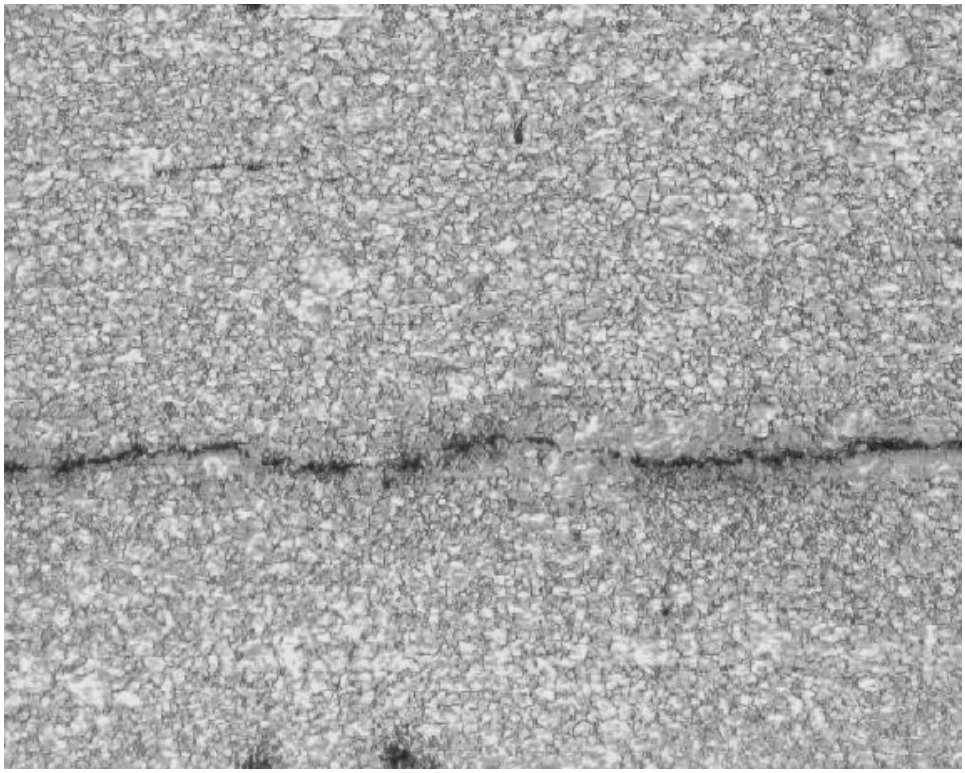

X65 (HC) (HT), 0.16% C, heat treated, HIC, 200X magnification.

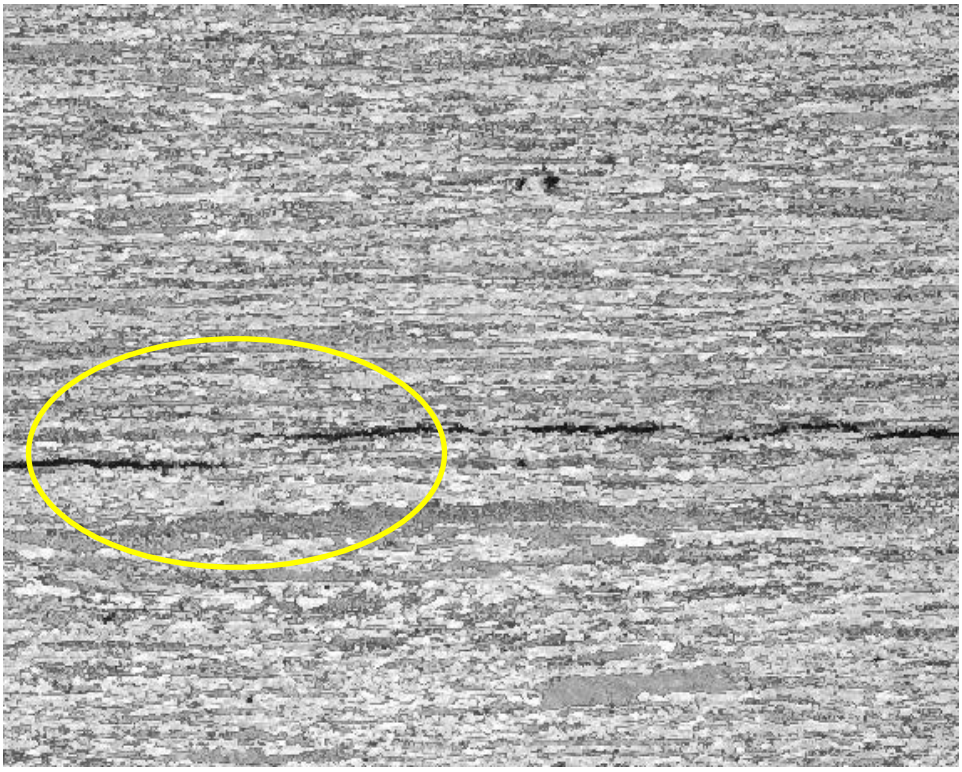

X100, HIC, 100X magnification.

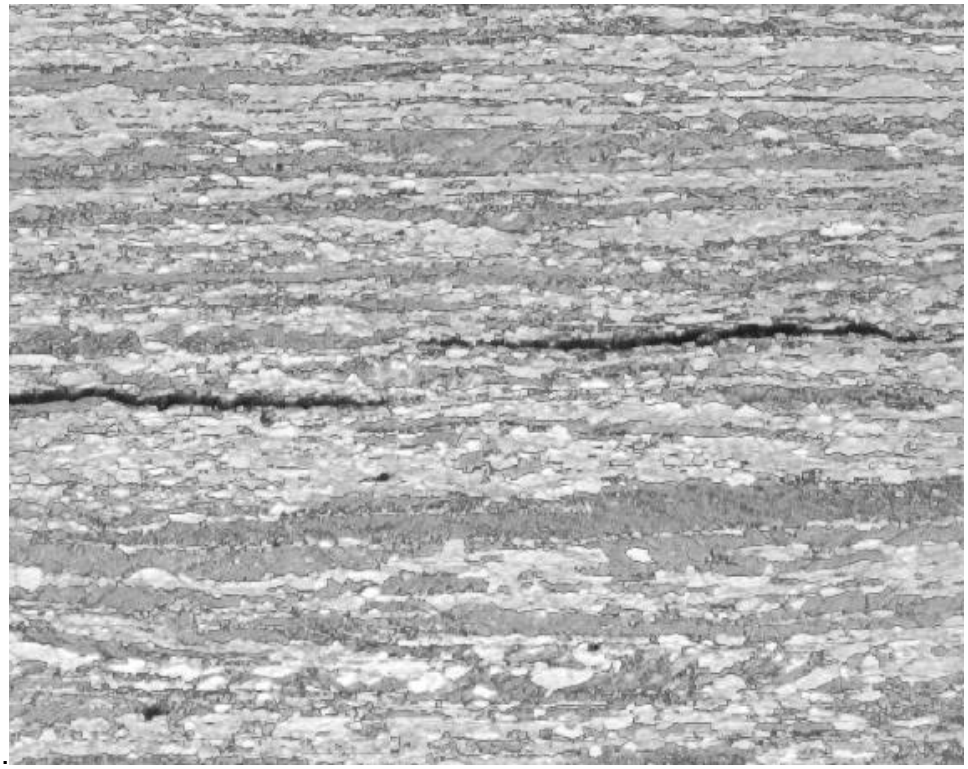

X100, HIC, 200X magnification

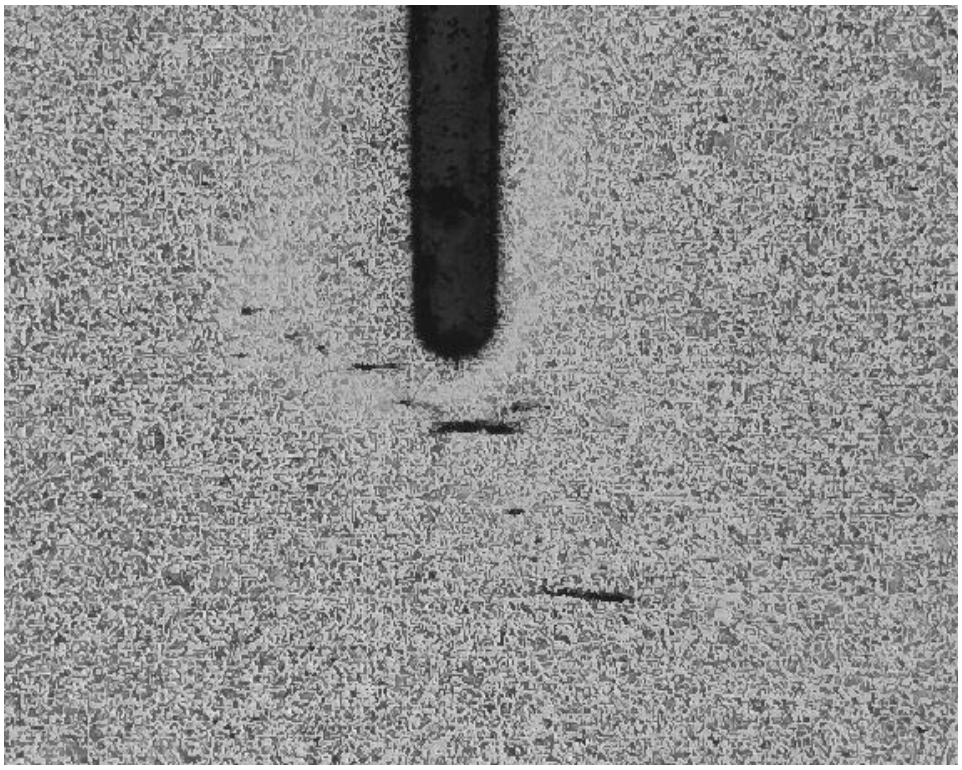

X65 (Vessel plate), 0.23%C, SOHIC, 25X magnification.

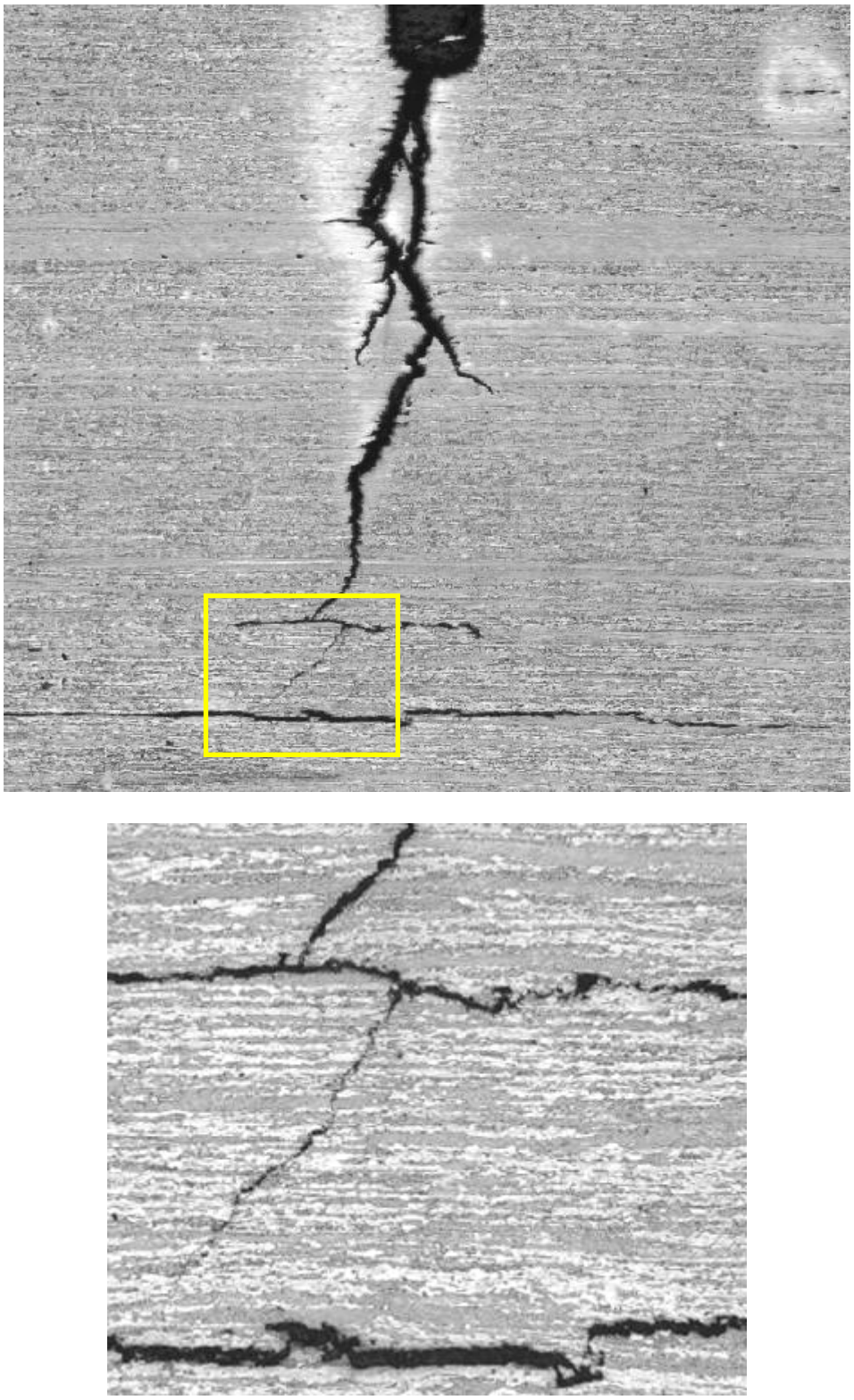

X100, SOHIC, 25X magnification (upper), 100X magnification (lower).

APPENDIX B3

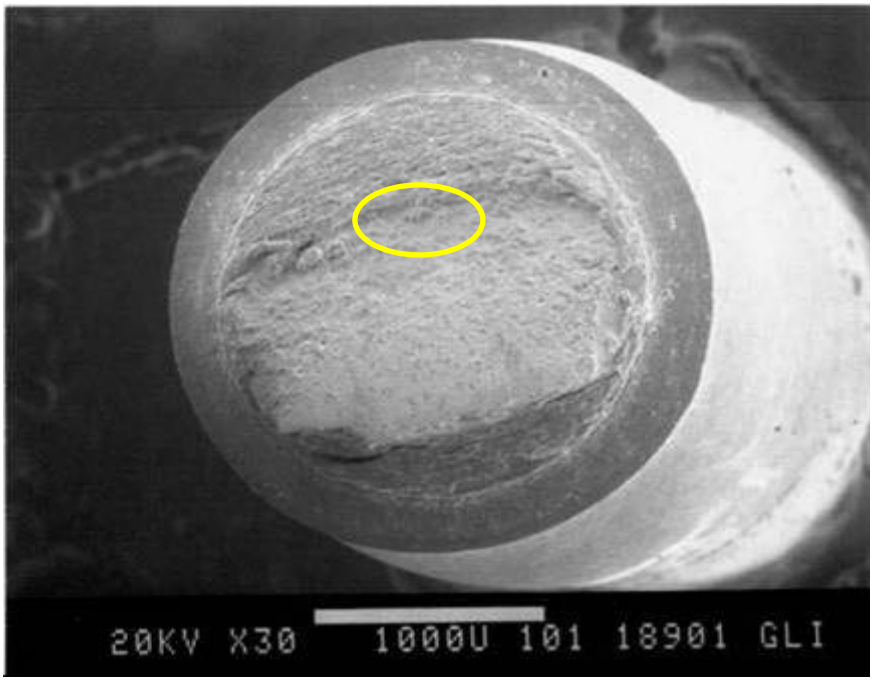

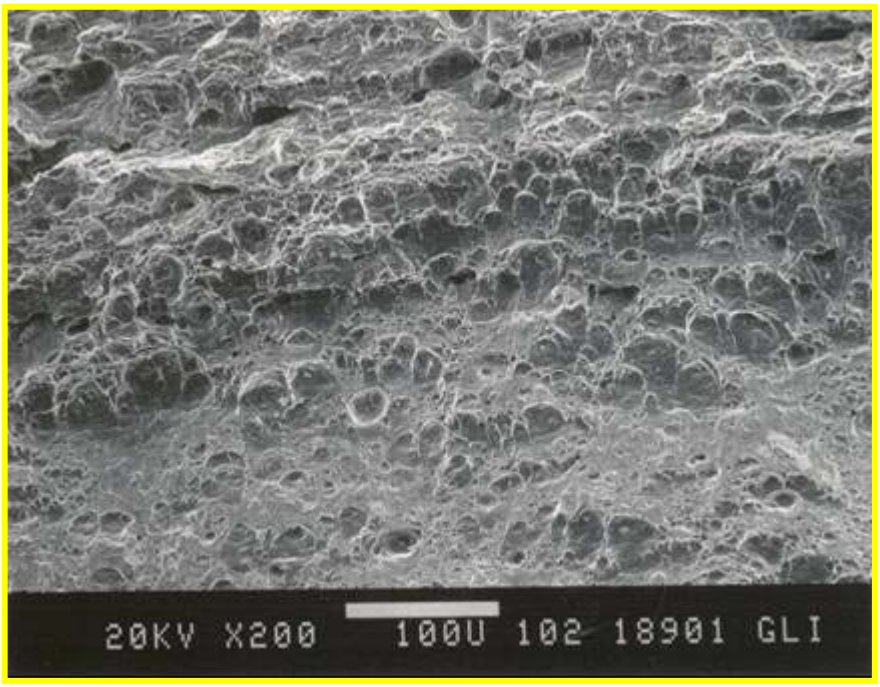

X100 steel, air (top – 30X, bottom – 200X)

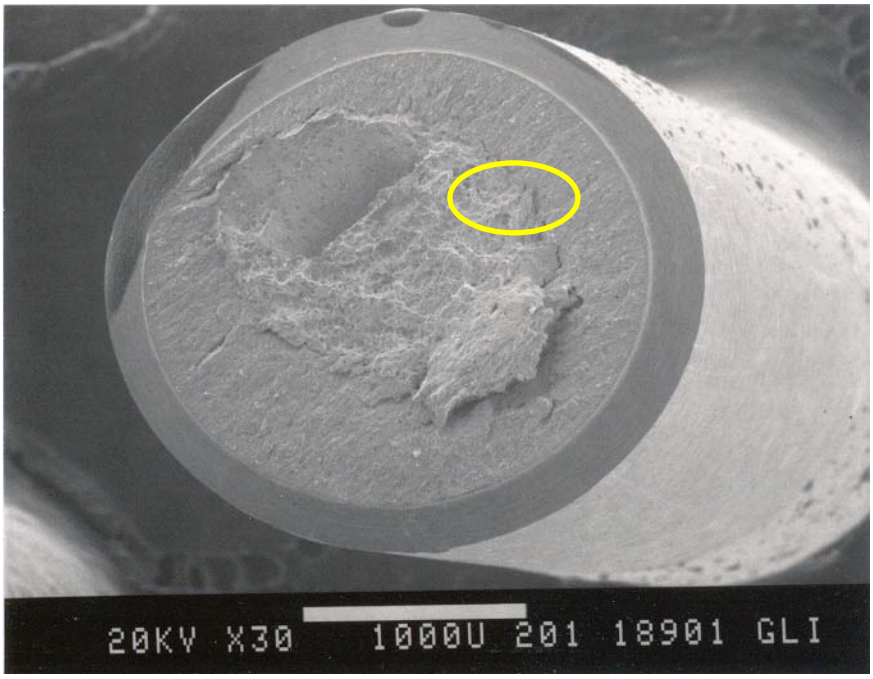

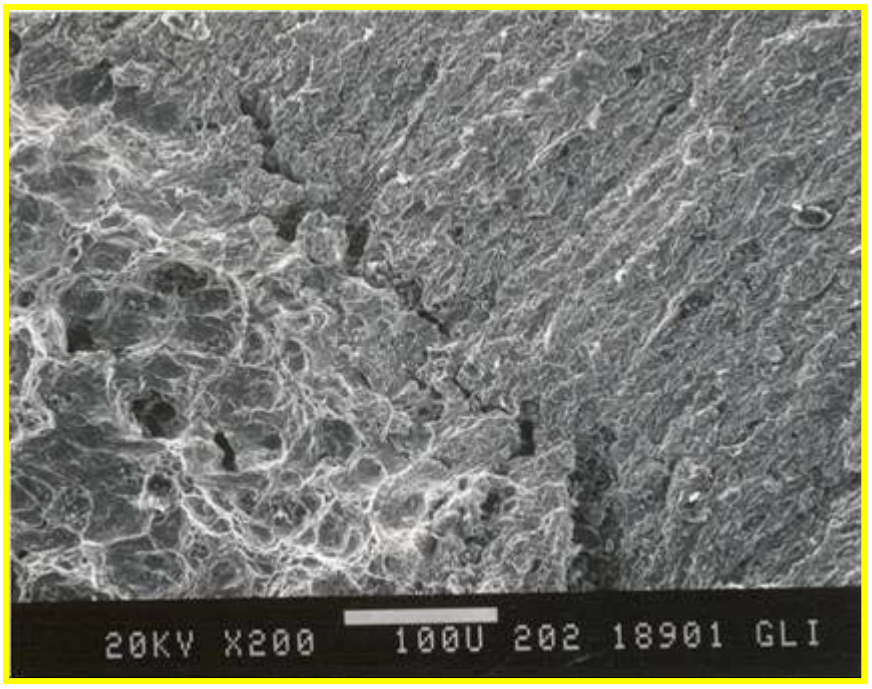

X100 steel, 200 mA/ft^2 (top – 30X, bottom – 200X)

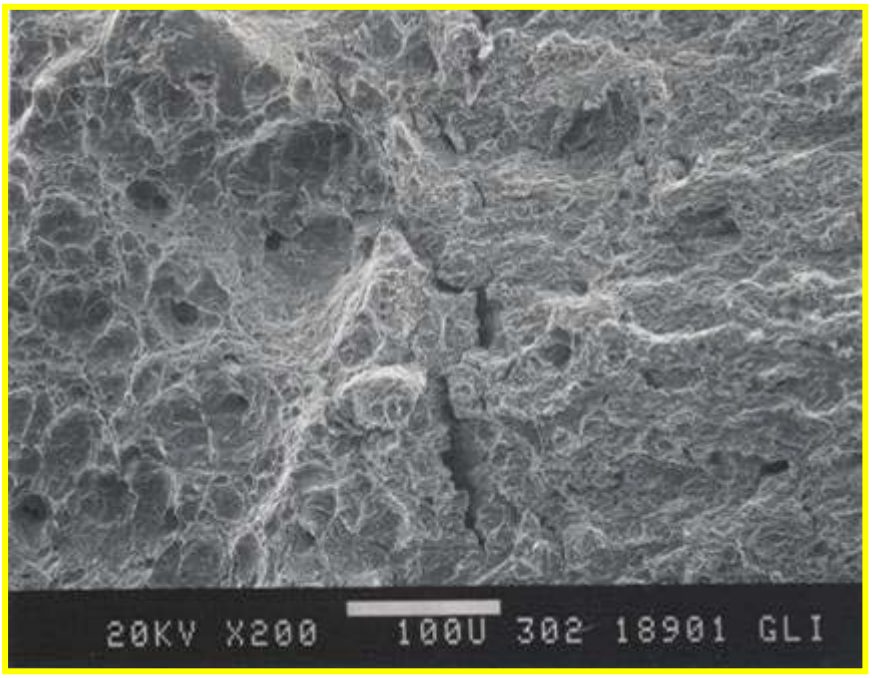

X100 steel, 2 mA/ft^2 (top – 30X, bottom – 200X)

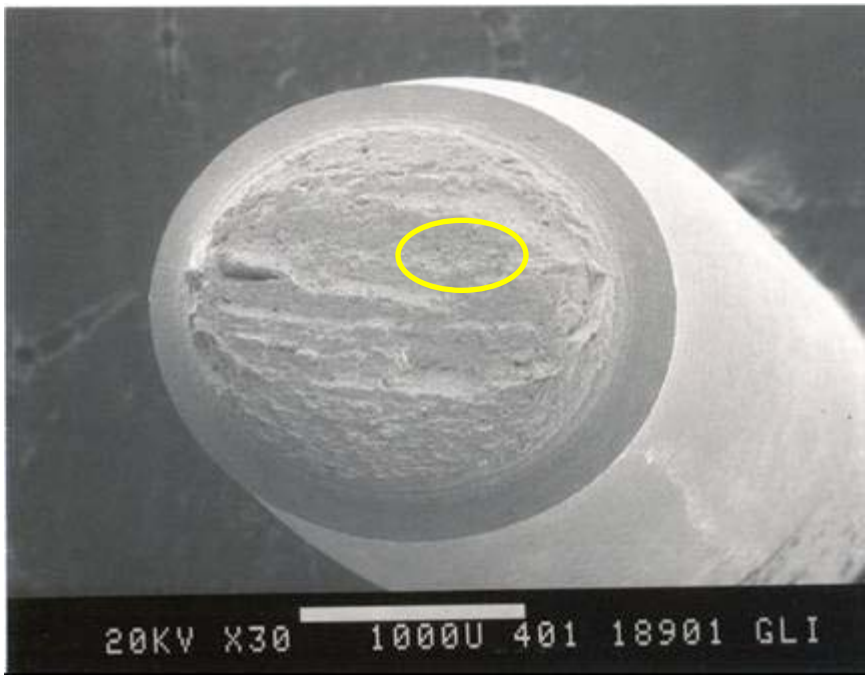

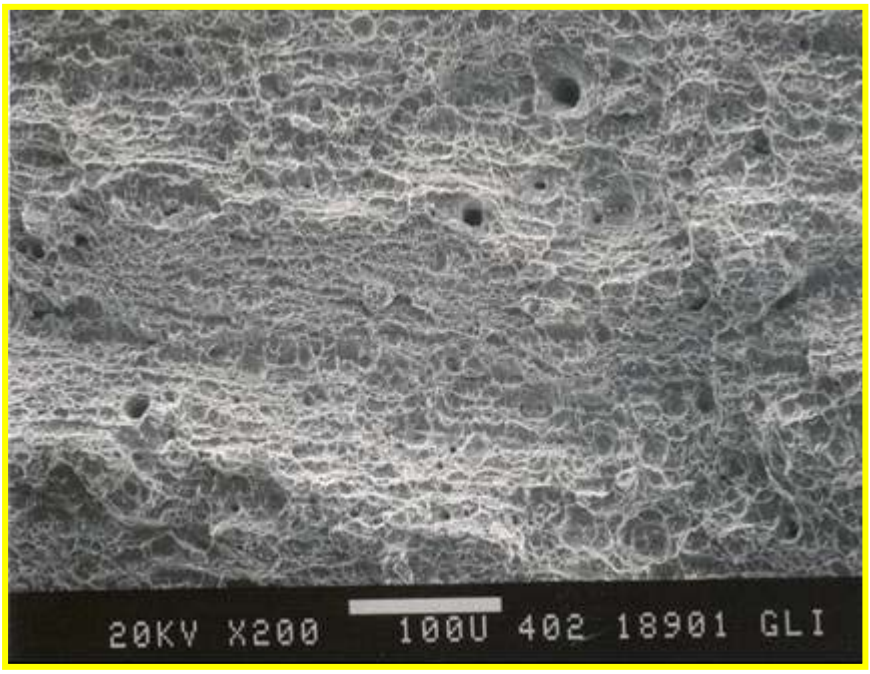

X65 HC steel, air (top – 30X, bottom – 200X)

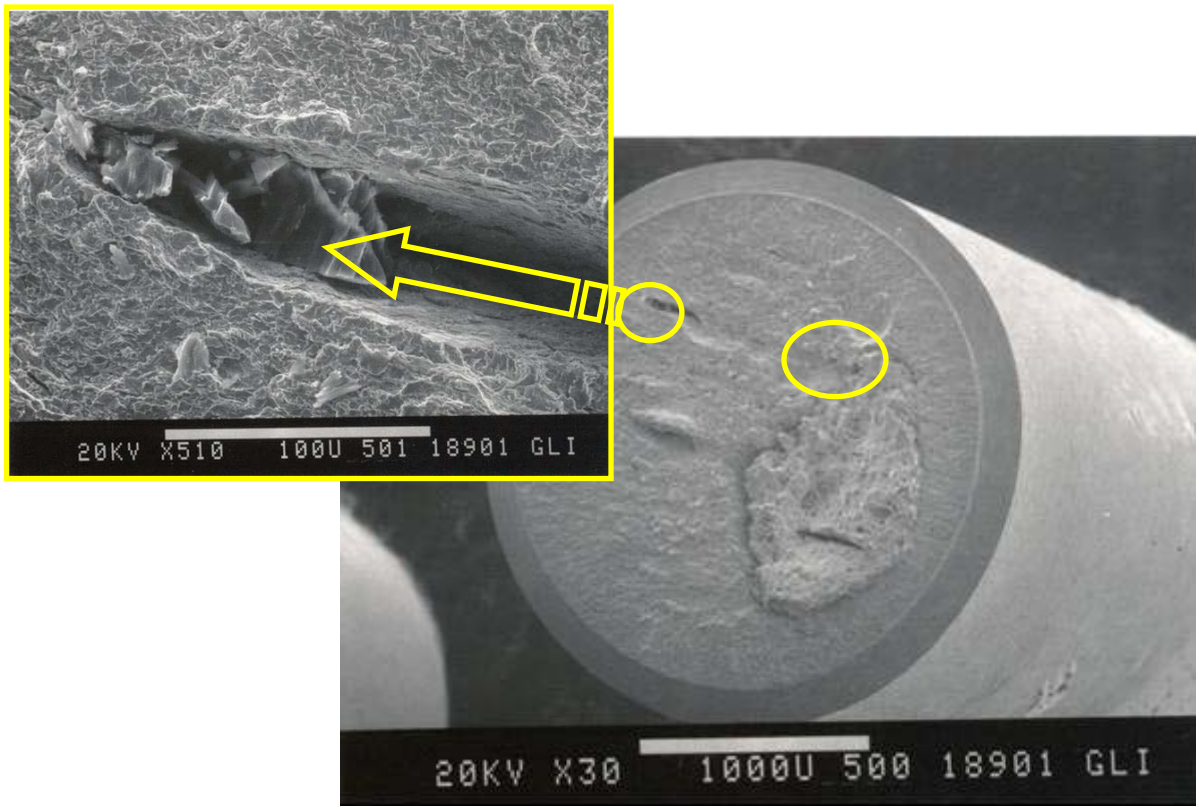

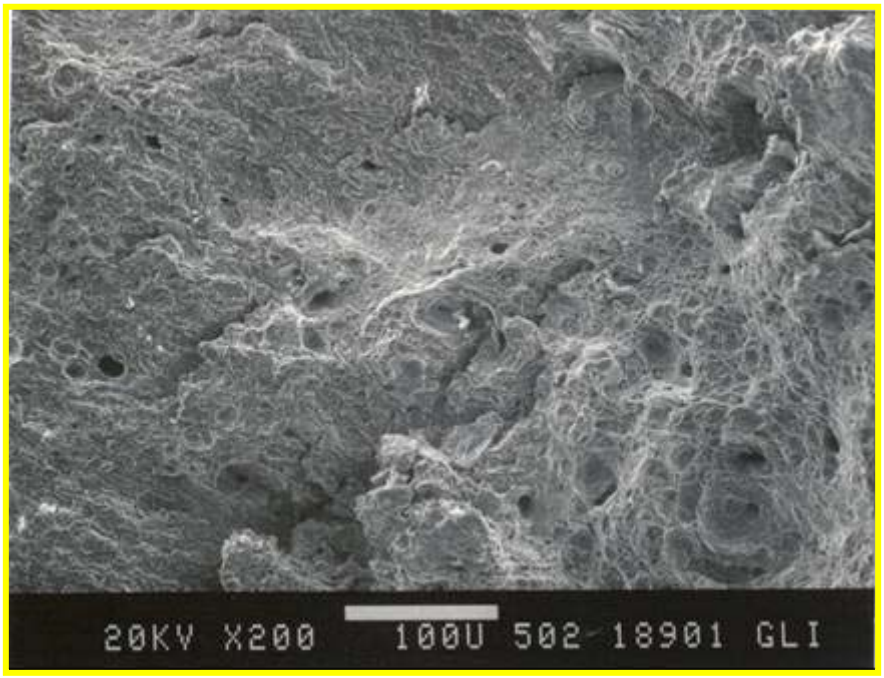

X65 HC steel, 200 mA/ft^2 (top – 30X, bottom – 200X). Inset – 360X.

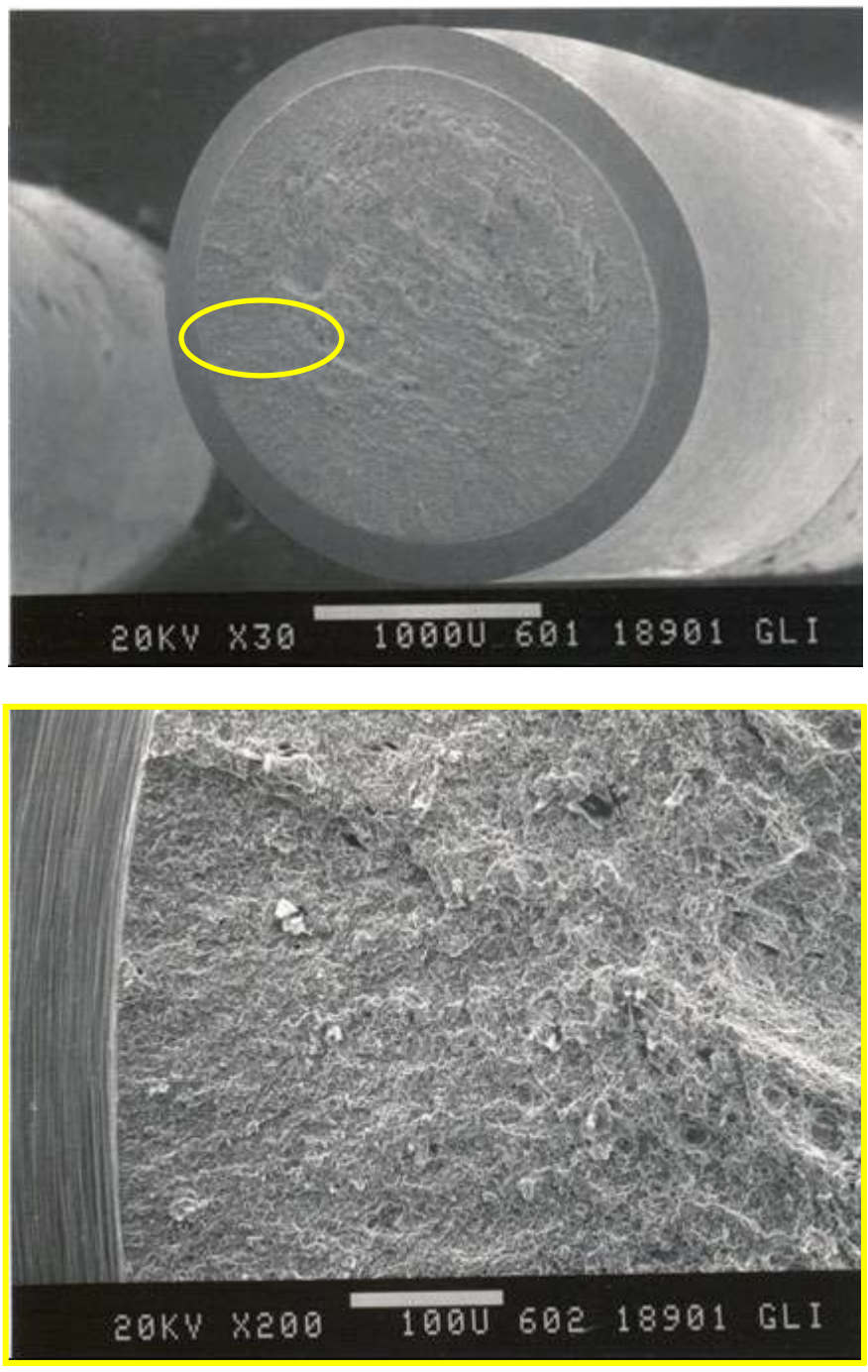

X65 HC steel, 2 mA/ft^2 (top – 30X, bottom – 200X)

X65 HC steel, 0.2 mA/ft^2 (top – 30X, bottom – 200X)

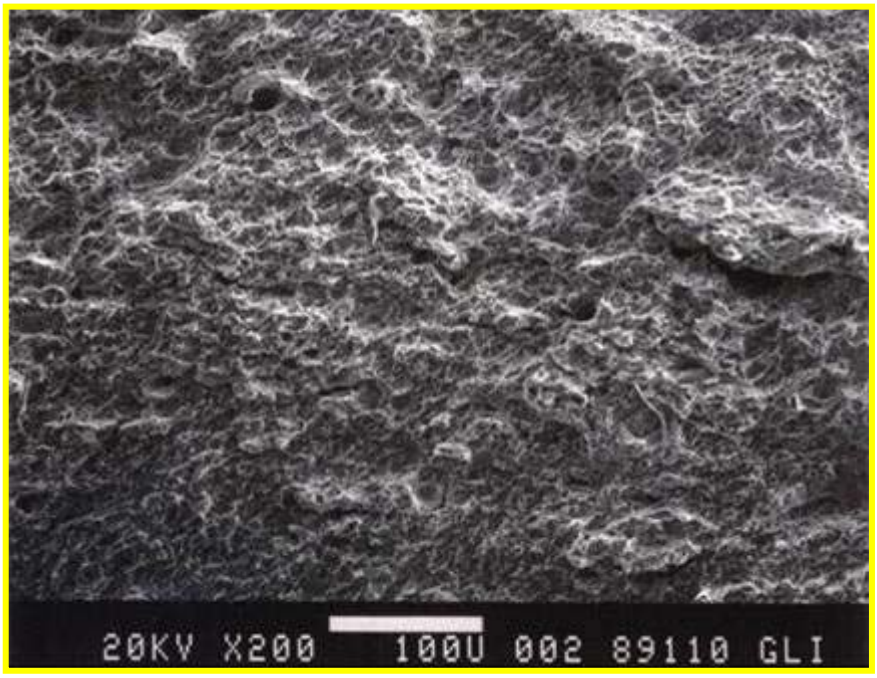

X65 HC steel, 0 mA/ft^2, (top – 31X, bottom – 200X)

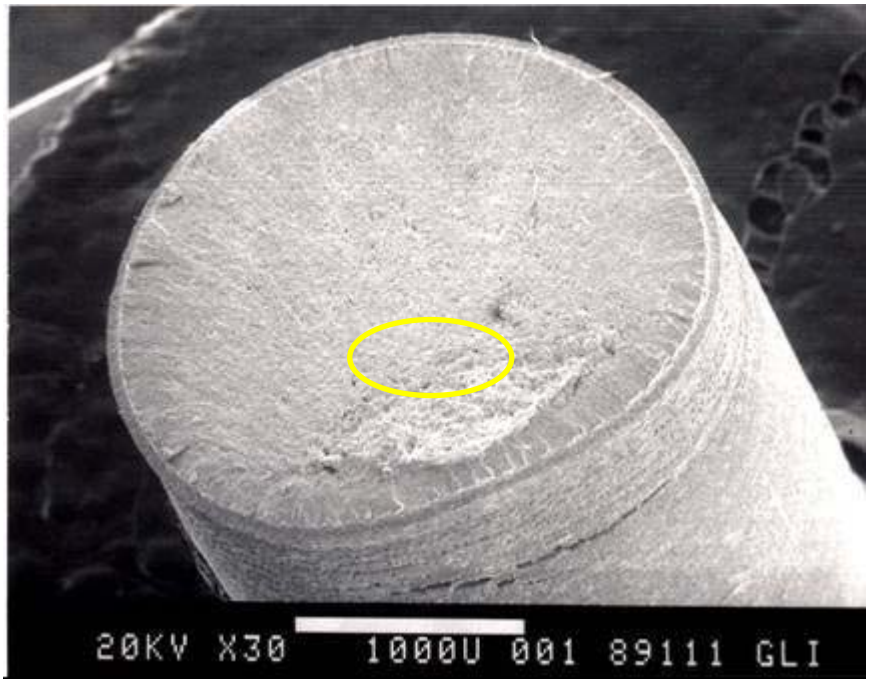

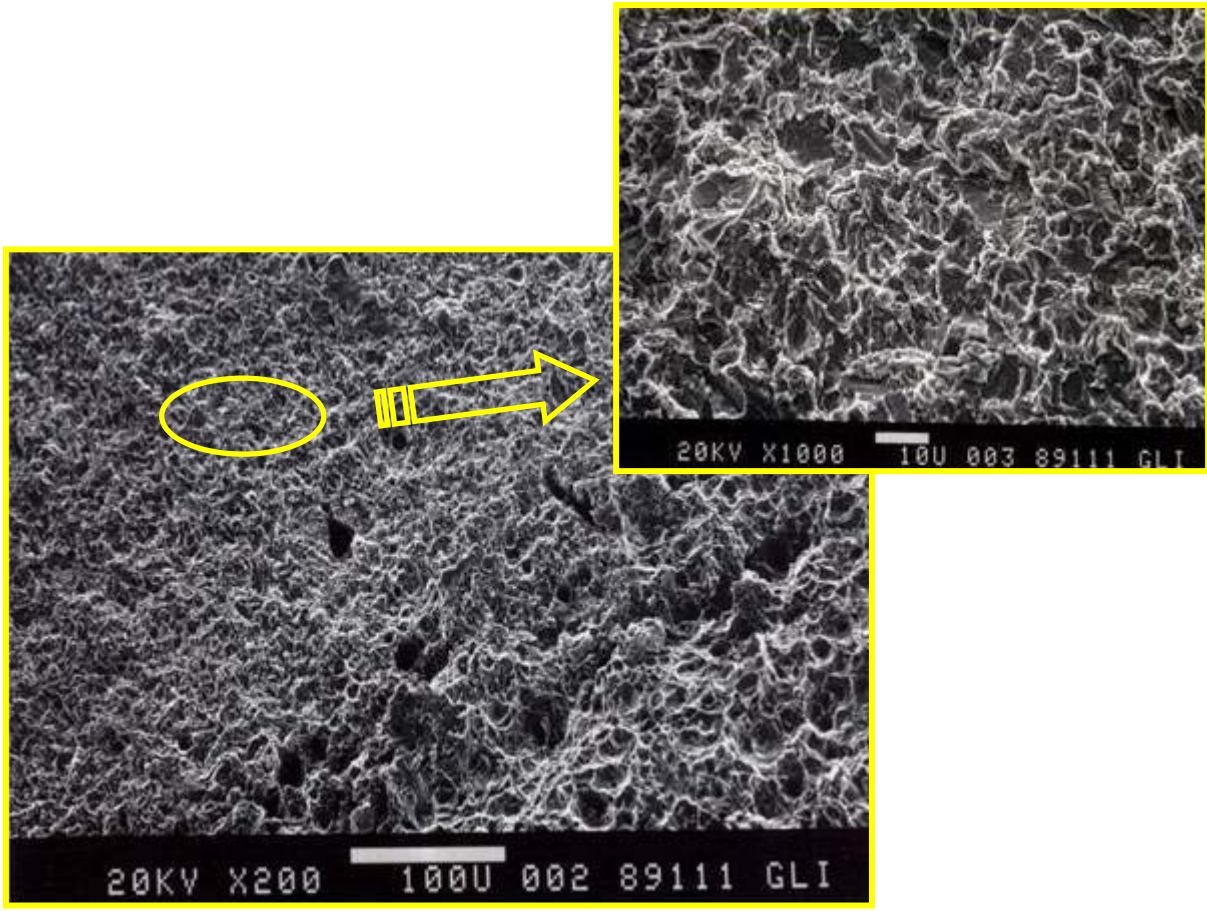

X65 LC steel, 200 mA/ft^2 (top – 30X, bottom – 200X). Inset – 1000X.

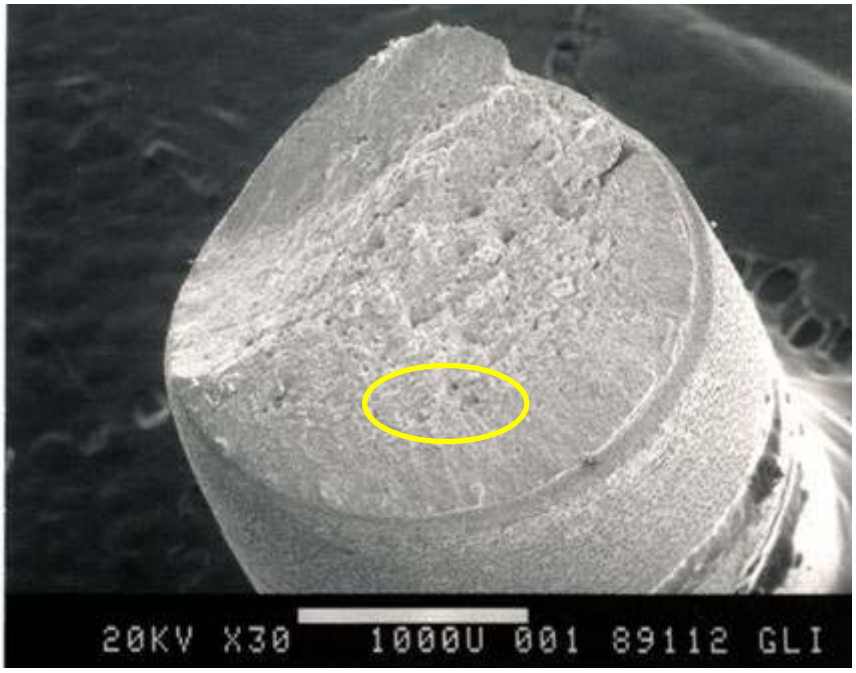

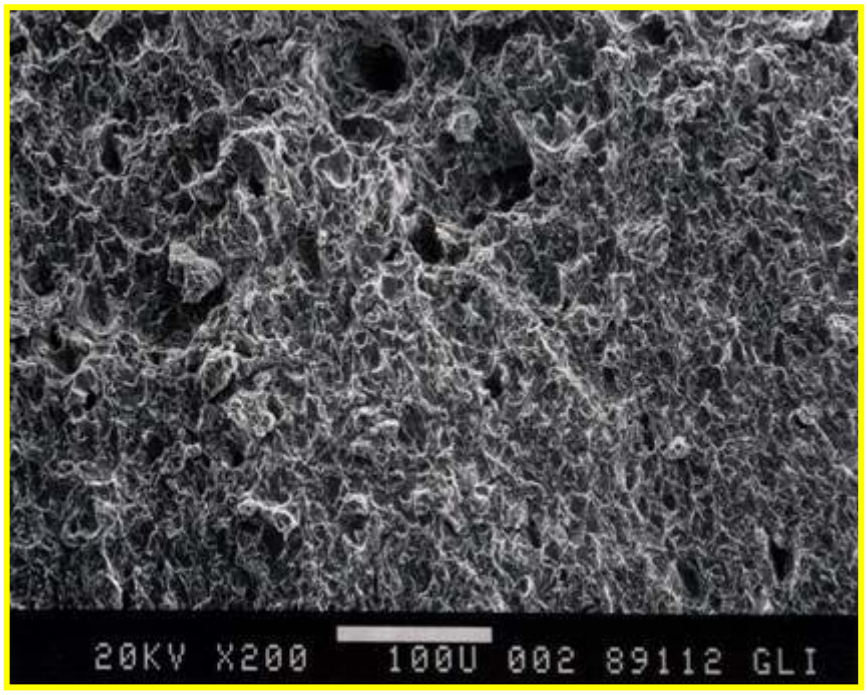

X65 LC steel, 2 mA/ft^2 (top – 30X, bottom – 200X)

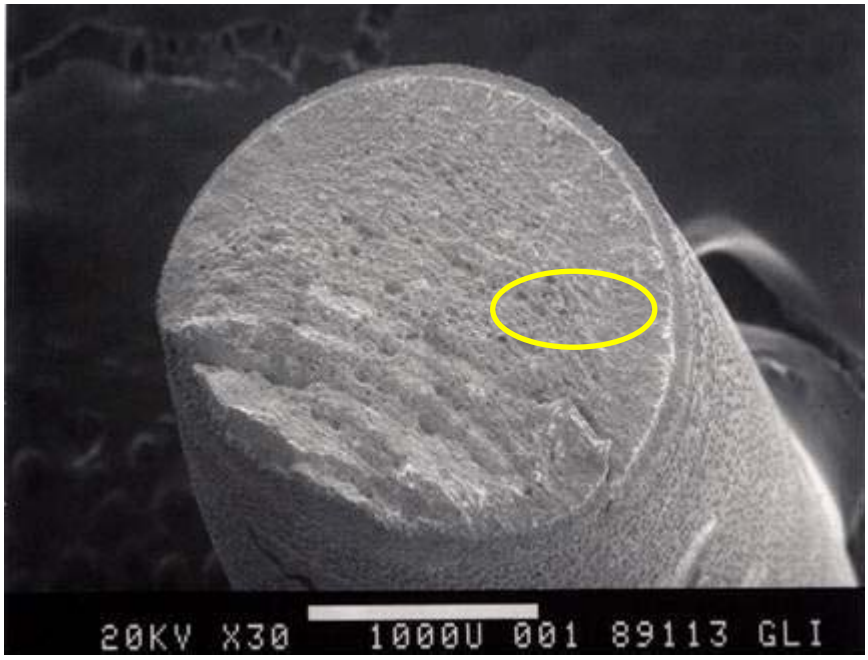

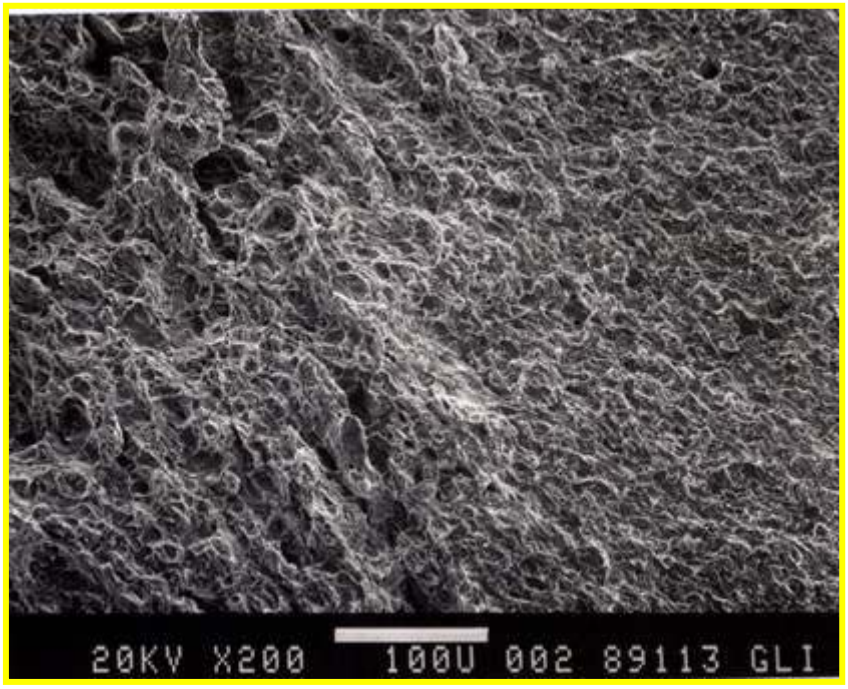

X65 LC steel, 0.2 mA/ft^2 (top – 30X, bottom – 200X)

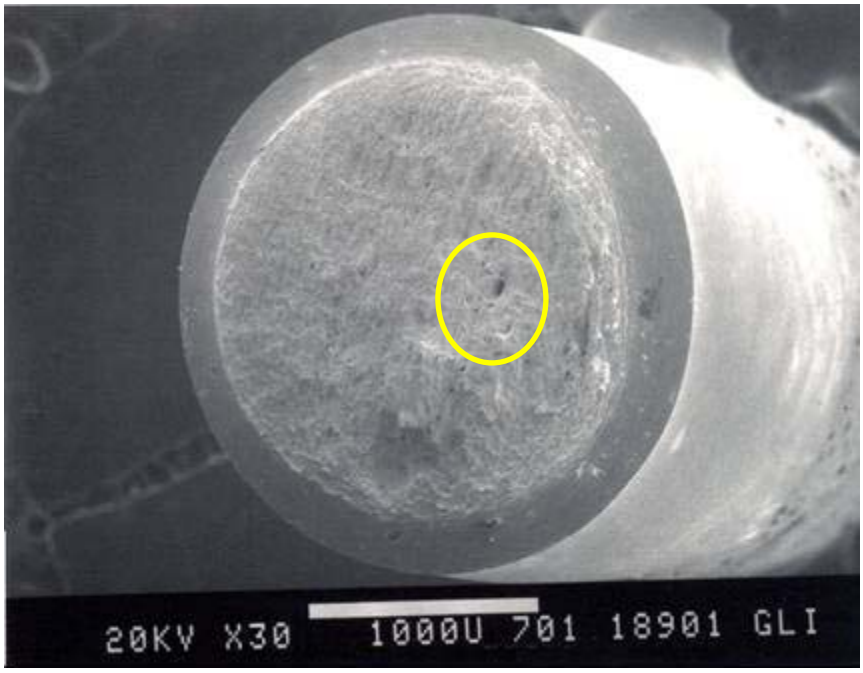

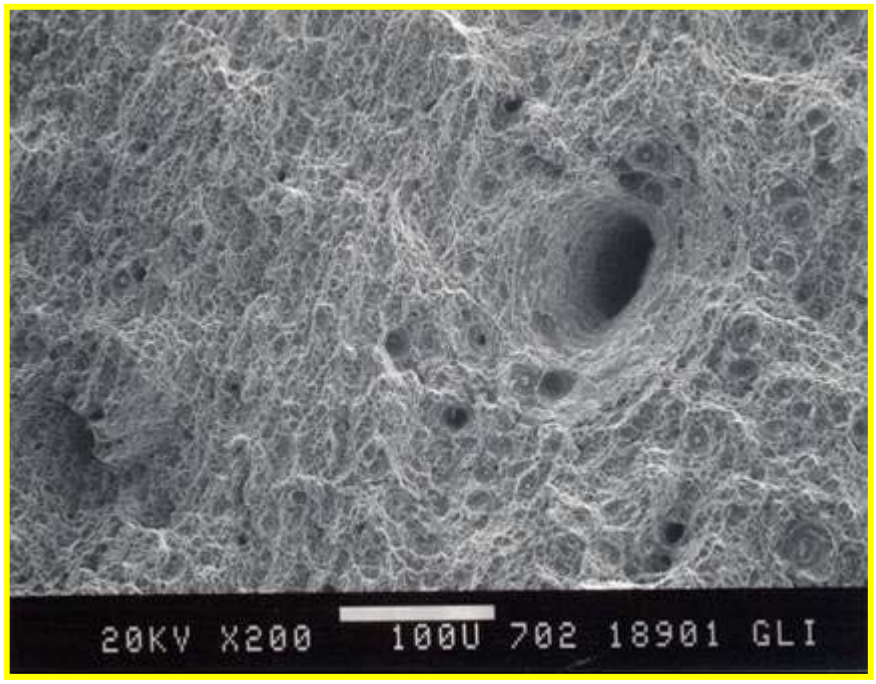

X65 steel with heat treatment, air (top – 30X, bottom – 200X)

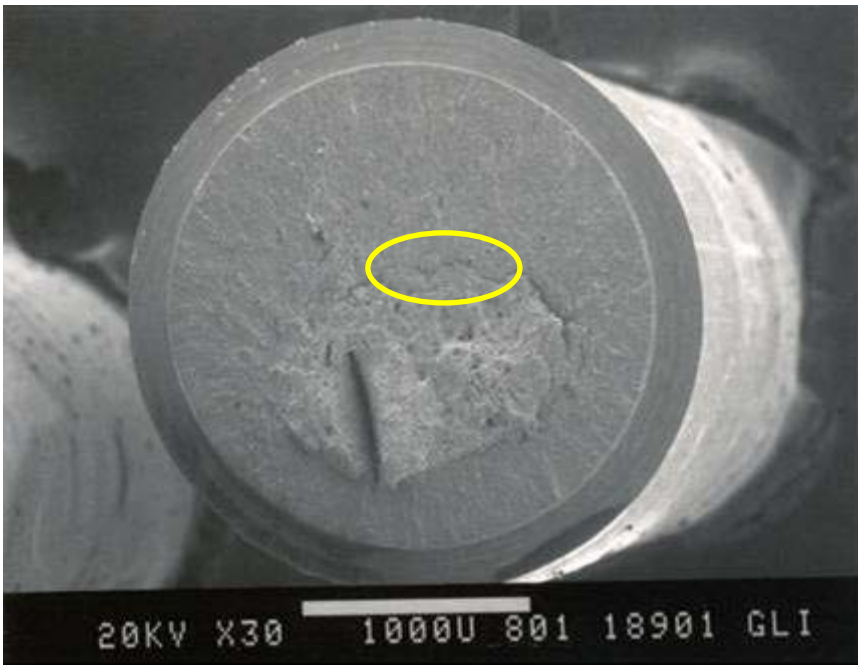

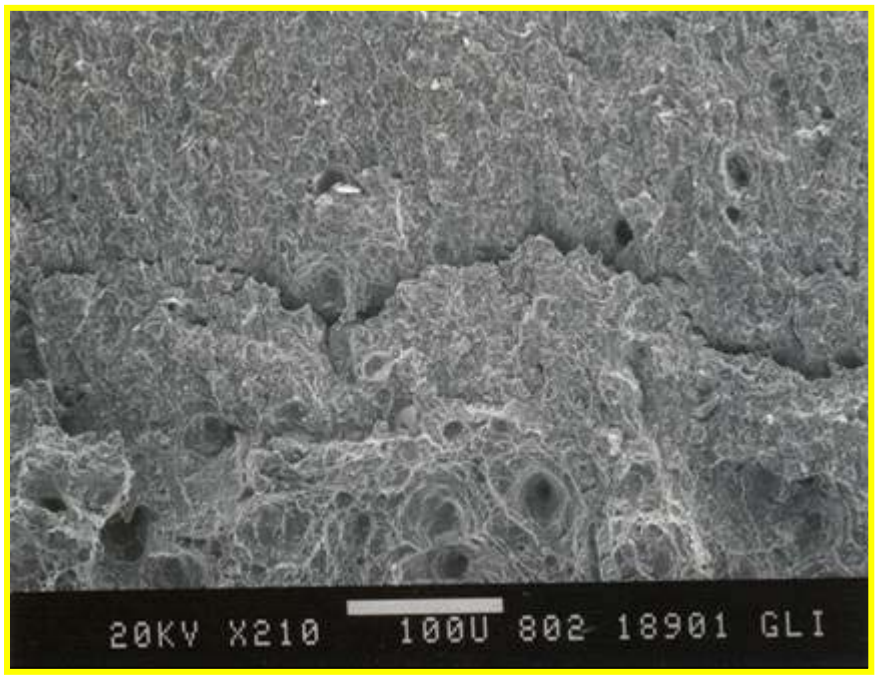

X65 steel with heat treatment, 200 mA/ft^2 (top – 30X, bottom – 200X)

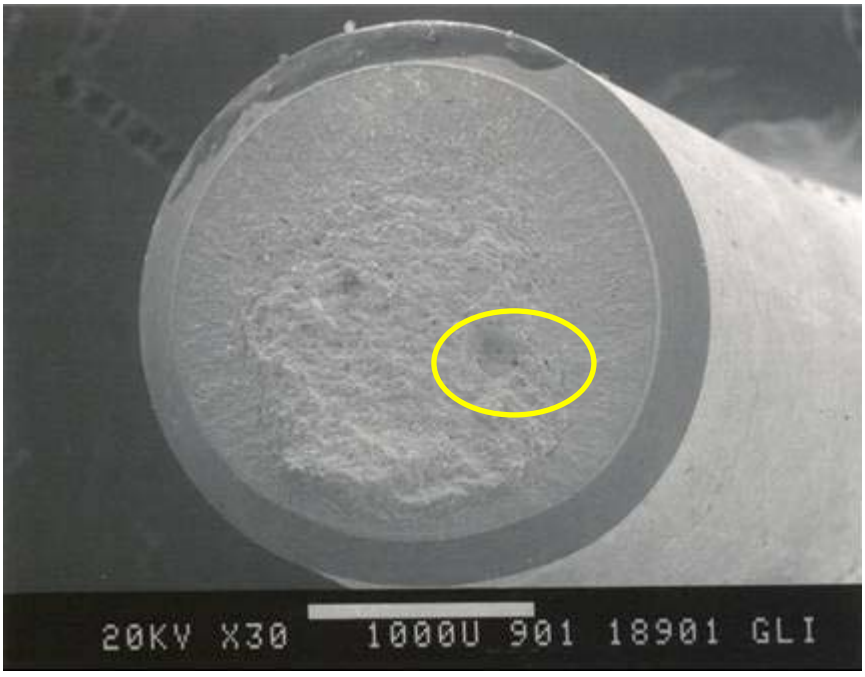

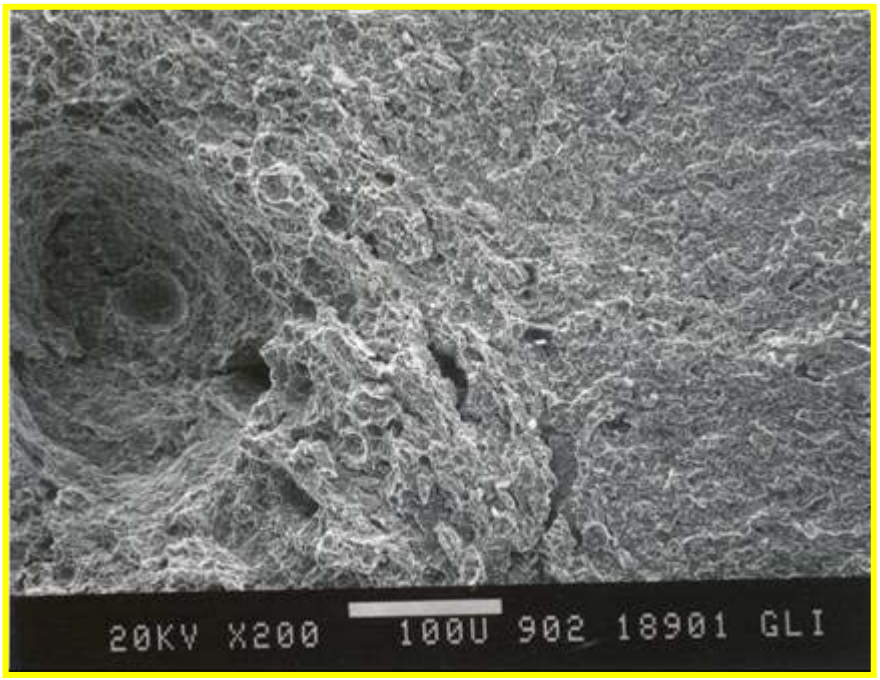

X65 steel with heat treatment, 2 mA/ft^2 (top – 30X, bottom – 200X)

APPENDIX B4

FBE 1

Soil	Current Density, mA/sq.ft	Cell	1	2	3	4	5	6	7	8	Average Disbondment
Control	na	1	0.0000	0.0680	0.0000	0.0555	0.0605	0.0695	0.0000	0.0900	**0.0429**
ASTM	na	1	0.7670	0.8215	0.7685	0.7985	0.7795	0.7350	0.7282	0.7160	**0.7643**
ASTM	na	2	0.8375	0.8965	0.9370	1.4690	1.5095	0.8995	0.8675	0.8140	**1.0288**
DOH	2	1	0.1090	0.1620	0.0955	0.0580	0.0920	0.0890	0.1670	0.1320	**0.1131**
DOH	2	2	0.1090	0.0560	0.0820	0.0710	0.0950	0.0725	0.0975	0.1020	**0.0856**
DOH	20	1	1.2820	1.2390	1.1890	1.2500	1.2380	1.1850	1.1210	1.3475	**1.2314**
DOH	20	2	0.9900	1.0800	1.0000	0.9925	1.0890	1.0095	0.9660	1.0040	**1.0164**
DOH	200	1	0.3555	0.3610	0.2850	0.3810	0.4955	0.4140	0.4000	0.3420	**0.3793**
DOH	200	2	1.3705	1.3840	1.3510	1.2620	1.2550	1.2190	1.2745	1.4610	**1.3221**
RNM	2	1	0.0750	0.0685	0.0630	0.0600	0.0520	0.0465	0.0525	0.0380	**0.0569**
RNM	2	2	0.0650	0.0645	0.0530	0.0670	0.0430	0.0440	0.0880	0.0640	**0.0611**
RNM	20	1	0.3040	0.2870	0.2900	0.2515	0.3890	0.4355	0.3900	0.2340	**0.3226**
RNM	20	2	0.4195	0.4230	0.5355	0.3960	0.4045	0.4220	0.3635	0.4770	**0.4301**
RNM	200	1	0.9115	1.2035	1.2505	1.3020	1.2200	1.1430	0.9875	0.8860	**1.1130**
RNM	200	2	1.1880	1.0740	0.9530	1.1265	1.2390	1.1915	1.1735	1.2045	**1.1438**
TCO	2	1	0.5245	0.4055	0.3145	0.2265	0.2310	0.2840	0.3380	0.3925	**0.3396**
TCO	2	2	0.1450	0.1725	0.1530	0.2650	0.1825	0.1910	0.0930	0.1005	**0.1628**
TCO	20	1	0.3245	0.3515	0.2990	0.2680	0.2560	0.2970	0.3355	0.3450	**0.3096**
TCO	20	2	0.1625	0.2310	0.2685	0.2365	0.1620	0.1885	0.1435	0.1355	**0.1910**
TCO	200	1	1.2375	1.4415	1.2365	1.1790	1.2210	1.2265	1.1360	1.3435	**1.2527**
TCO	200	2	1.1365	1.2420	1.2145	1.5815	1.3610	1.4775	1.3215	1.1615	**1.3120**
RNM	No Holiday	1	0.1655	0.1215	0.0850	0.1095	0.1135	0.0980	0.0770	0.1275	**0.1122**
RNM	No Holiday	2	0.1965	0.1485	0.1695	0.1890	0.1620	0.1035	0.1325	0.1155	**0.1521**

FBE 2

Soil	Current Density, mA/sq.ft	Cell	1	2	3	4	5	6	7	8	Average Disbondment
Control	na	1	0.0805	0.0430	0.0340	0.0375	0.0440	0.0385	0.0000	0.0000	**0.0347**
ASTM	na	1	0.3430	0.3250	0.3600	0.3890	0.3885	0.3845	0.3880	0.3805	**0.3698**
ASTM	na	2	0.2240	0.2160	0.2380	0.2785	0.2575	0.2250	0.2185	0.2140	**0.2339**
DOH	2	1	0.0550	0.0215	0.0430	0.0000	0.0000	0.0000	0.0380	0.0280	**0.0232**
DOH	2	2	0.0470	0.0315	0.0320	0.0000	0.0000	0.0000	0.0000	0.0000	**0.0138**
DOH	20	1	0.0000	0.0485	0.0660	0.0495	0.0575	0.0485	0.0295	0.0000	**0.0374**
DOH	20	2	0.5880	0.5080	0.4510	0.4245	0.6730	0.6410	0.7745	0.8230	**0.6104**
DOH	200	1	0.1140	0.1420	0.1200	0.2055	0.1985	0.1565	0.1315	0.1325	**0.1501**
DOH	200	2	1.1390	1.1460	1.1545	1.1365	1.1890	1.0190	1.1415	1.1480	**1.1342**
RNM	2	1	0.0590	0.0000	0.0000	0.0000	0.0000	0.0000	0.0000	0.0000	**0.0074**
RNM	2	2	0.0720	0.0415	0.0675	0.1295	0.0000	0.0000	0.0420	0.0000	**0.0441**
RNM	20	1	0.0450	0.0380	0.0270	0.0360	0.0750	0.0635	0.0595	0.0635	**0.0509**
RNM	20	2	0.0595	0.0000	0.0000	0.0000	0.0000	0.0000	0.0000	0.0000	**0.0074**
RNM	200	1	1.2440	1.2570	1.2080	1.1295	1.0805	1.1735	1.1125	1.0910	**1.1620**
RNM	200	2	1.1340	1.0970	1.0250	1.1605	1.1815	1.2125	1.0525	1.0885	**1.1189**
TCO	2	1	0.2720	0.2115	0.1885	0.1595	0.1580	0.1705	0.1930	0.2565	**0.2012**
TCO	2	2	0.0695	0.0585	0.0000	0.0480	0.0720	0.0900	0.1010	0.0785	**0.0647**
TCO	20	1	0.2825	0.2045	0.1765	0.1815	0.2370	0.2255	0.2455	0.2965	**0.2312**
TCO	20	2	0.4080	0.2875	0.2080	0.1945	0.3235	0.3470	0.3920	0.3985	**0.3199**
TCO	200	1	1.5815	1.6035	1.6305	1.5985	1.5650	1.4905	1.3540	1.5590	**1.5478**
TCO	200	2	1.2300	1.4300	1.4000	1.2135	1.2315	1.4695	1.4110	1.1605	**1.3183**
RNM	No Holiday	1	0.0920	0.0520	0.0490	0.0000	0.0000	0.0000	0.0515	0.0760	**0.0401**
RNM	No Holiday	2	0.0685	0.0081	0.0805	0.0020	0.7200	0.0410	0.0155	0.0910	**0.1283**

LE

Soil	Current Density, mA/sq.ft	Cell	1	2	3	4	5	6	7	8	Average Disbondment
Control	na	1	0.1545	0.0000	0.1320	0.1120	0.0915	0.1335	0.0735	0.1210	**0.1023**
ASTM	na	1	0.1350	0.1320	0.1245	0.1370	0.1395	0.1305	0.1505	0.1635	**0.1391**
ASTM	na	2	0.1650	0.1380	0.1305	0.1645	0.1505	0.1545	0.1405	0.1445	**0.1485**
DOH	2	1	0.1545	0.1110	0.1200	0.1560	0.1290	0.1010	0.0960	0.0495	**0.1146**
DOH	2	2	0.1595	0.1075	0.1145	0.1240	0.1330	0.0000	0.0000	0.1185	**0.0946**
DOH	20	1	0.0965	0.1150	0.1665	0.1405	0.1265	0.1830	0.1870	0.1610	**0.1470**
DOH	20	2	0.4610	0.4265	0.4100	0.3695	0.4230	0.4565	0.4815	0.7970	**0.4781**
DOH	200	1	0.3690	0.3940	0.3630	0.3475	0.3525	0.3245	0.3390	0.3295	**0.3524**
DOH	200	2	0.3430	0.2195	0.1960	0.2190	0.2690	0.2900	0.2925	0.3275	**0.2696**
RNM	2	1	0.1800	0.0980	0.0720	0.1605	0.1735	0.1420	0.1615	0.1705	**0.1448**
RNM	2	2	0.2685	0.1955	0.2300	0.1995	0.1285	0.1185	0.2405	0.1470	**0.1910**
RNM	20	1	0.8095	0.7720	0.6720	0.7075	0.6760	0.6655	0.6860	0.7885	**0.7221**
RNM	20	2	0.0660	0.1110	0.0385	0.0540	0.0975	0.0740	0.0000	0.0665	**0.0634**
RNM	200	1	0.3590	0.3715	0.4020	0.3700	0.3605	0.3375	0.3305	0.3805	**0.3639**
RNM	200	2	0.3240	0.3070	0.3005	0.3170	0.2495	0.2595	0.3040	0.3330	**0.2993**
TCO	2	1	0.1040	0.1260	0.1260	0.1410	0.1370	0.1005	0.1760	0.0935	**0.1255**
TCO	2	2	0.0720	0.0585	0.1240	0.1490	0.1155	0.0775	0.0760	0.0725	**0.0931**
TCO	20	1	0.3700	0.3775	0.3525	0.3785	0.3915	0.4195	0.3975	0.4070	**0.3868**
TCO	20	2	0.1190	0.1075	0.1195	0.1215	0.1225	0.0860	0.1015	0.0930	**0.1088**
TCO	200	1	0.7485	0.7880	0.8715	0.8455	0.7755	0.7695	0.8770	0.8705	**0.8183**
TCO	200	2	1.0320	0.8990	0.9315	0.8705	0.8356	0.8950	0.8980	1.0115	**0.9216**
RNM	No Holiday	1	0.4015	0.3665	0.3415	0.4525	0.4990	0.4330	0.4030	0.3565	**0.4067**
RNM	No Holiday	2	0.2840	0.2850	0.2620	0.2610	0.2465	0.2590	0.2150	0.1880	**0.2501**

HPCC

Soil	Current Density, mA/sq.ft	Cell	1	2	3	4	5	6	7	8	Average Disbondment
Control	na	1	0.0730	0.0460	0.0765	0.0610	0.0635	0.0475	0.0890	0.0780	**0.0668**
ASTM	na	1	0.2217	0.2217	0.2233	0.2233	0.1993	0.1993	0.2142	0.2142	**0.2146**
ASTM	na	2	0.1931	0.1931	0.1971	0.1971	0.1959	0.1959	0.1923	0.1923	**0.1946**
DOH	2	1	0.0900	0.0985	0.0850	0.1160	0.0555	0.0330	0.0825	0.1030	**0.0829**
DOH	2	2	0.0770	0.0890	0.0895	0.1030	0.1015	0.0890	0.0945	0.0895	**0.0916**
DOH	20	1	0.0980	0.1430	0.1465	0.1455	0.1225	0.1405	0.1505	0.1130	**0.1324**
DOH	20	2	0.3055	0.2925	0.3010	0.2895	0.2870	0.2790	0.3010	0.2755	**0.2914**
DOH	200	1	0.3515	0.3600	0.4050	0.4140	0.4350	0.4725	0.4685	0.4405	**0.4184**
DOH	200	2	0.3290	0.3430	0.3430	0.3370	0.3060	0.2570	0.2670	0.3240	**0.3133**
RNM	2	1	0.1365	0.1220	0.1550	0.1130	0.1445	0.1415	0.1045	0.1280	**0.1306**
RNM	2	2	0.0455	0.0560	0.0000	0.0650	0.0775	0.1250	0.0840	0.0945	**0.0684**
RNM	20	1	0.1090	0.1520	0.1230	0.1320	0.1105	0.1125	0.1165	0.0865	**0.1178**
RNM	20	2	0.1050	0.0800	0.1005	0.1240	0.1330	0.1200	0.0675	0.1125	**0.1053**
RNM	200	1	0.2710	0.2705	0.2670	0.2985	0.2875	0.3015	0.2875	0.2915	**0.2844**
RNM	200	2	0.4310	0.4365	0.4605	0.5170	0.4855	0.4535	0.4230	0.4100	**0.4521**
TCO	2	1	0.1210	0.1125	0.0725	0.1170	0.0770	0.0960	0.1045	0.0980	**0.0998**
TCO	2	2	0.1060	0.0890	0.1415	0.1305	0.0970	0.0870	0.1195	0.1220	**0.1116**
TCO	20	1	0.1365	0.1250	0.0860	0.1040	0.1025	0.1110	0.0985	0.1000	**0.1079**
TCO	20	2	0.3330	0.3200	0.3065	0.3485	0.3450	0.3295	0.3330	0.3360	**0.3314**
TCO	200	2	0.6240	0.6395	0.6405	0.6195	0.6135	0.5990	0.5705	0.5765	**0.6104**
TCO	200	1	0.4480	0.4710	0.3985	0.3535	0.3780	0.4380	0.4410	0.4560	**0.4230**
RNM	No Holiday	1	0.1055	0.1115	0.0970	0.0860	0.1160	0.1260	0.1105	0.0800	**0.1041**
RNM	No Holiday	2	0.0590	0.0670	0.0000	0.0680	0.0920	0.0000	0.0405	0.0610	**0.0484**

ASTM (NaCl)

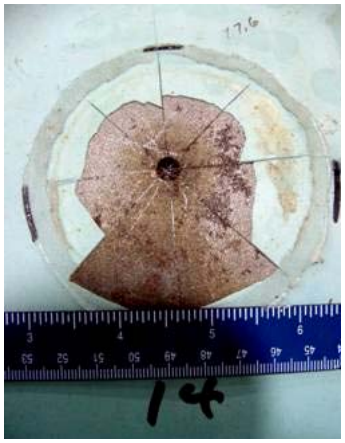

ASTM (NaCl)

No Holiday, Roswell, New Mexico

No Holiday, Roswell, New Mexico

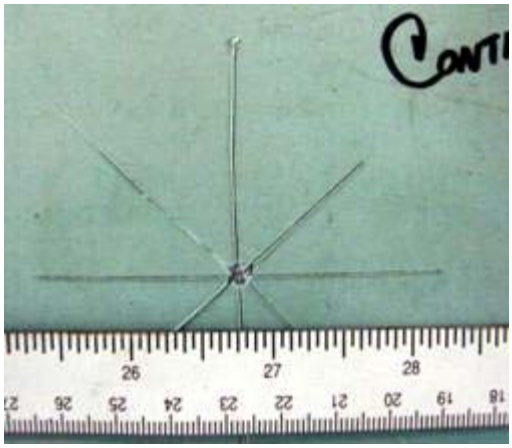

Control

FBE 1

2 mA/ft^2

2 mA/ft^2

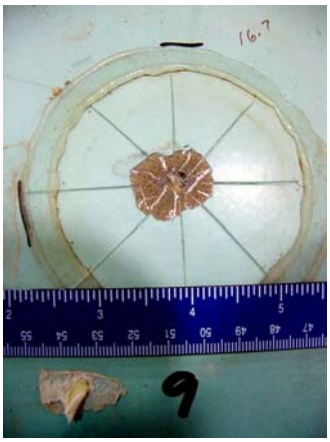

20 mA/ft^2

20 mA/ft^2

200 mA/ft^2

200 mA/ft^2

FBE 1, Roswell, New Mexico

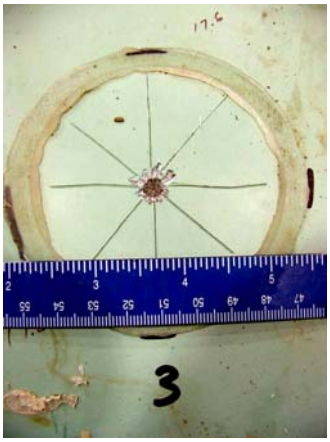

2 mA/ft^2

2 mA/ft^2

20 mA/ft^2

20 mA/ft^2

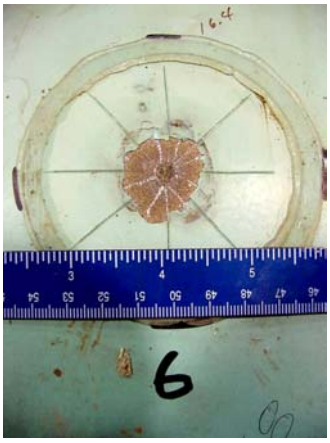

200 mA/ft^2

200 mA/ft^2

FBE 1, Dublin, Ohio

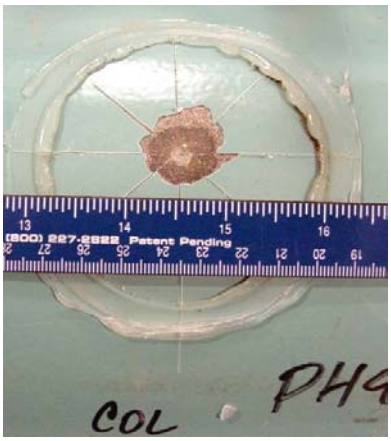

2 mA/ft^2

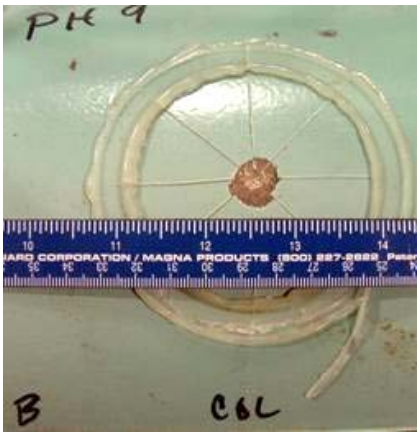

2 mA/ft^2

20 mA/ft^2

20 mA/ft^2

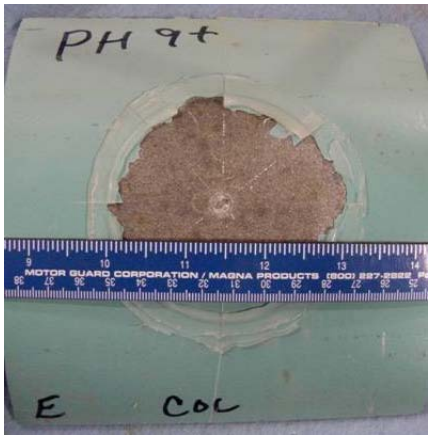

200 mA/ft^2

200 mA/ft^2

FBE 1, Trinidad, Colorado

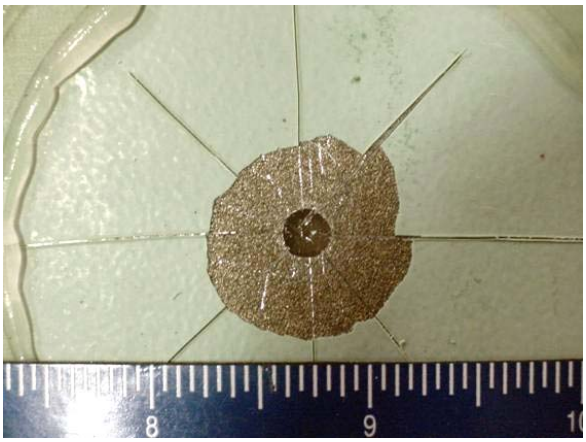

ASTM (NaCl)

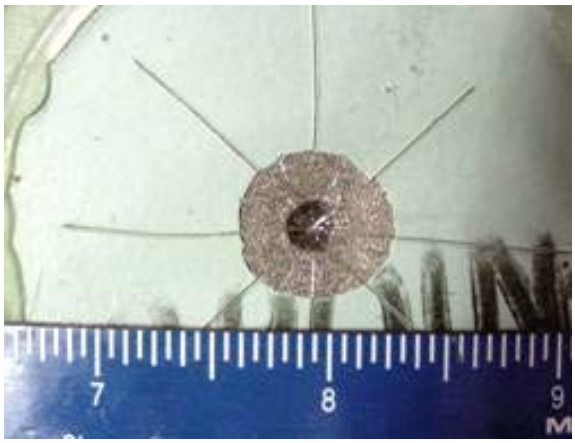

ASTM (NaCl)

No Holiday, Roswell, New Mexico

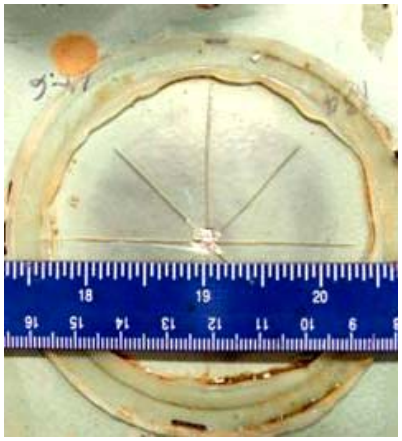

No Holiday, Roswell, New Mexico

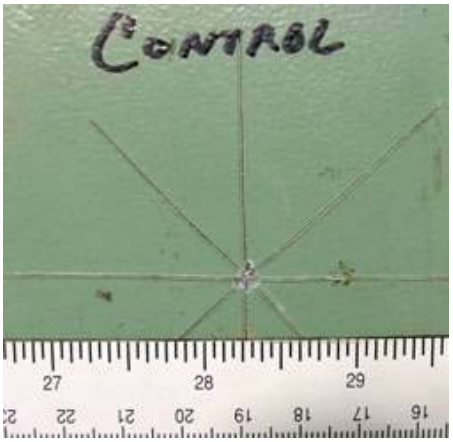

Control

FBE 2

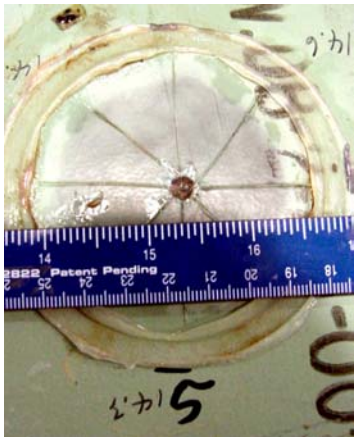

2 mA/ft^2

2 mA/ft^2

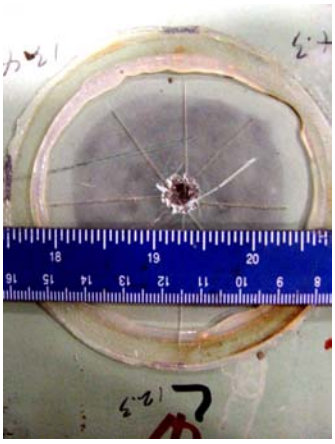

20 mA/ft^2

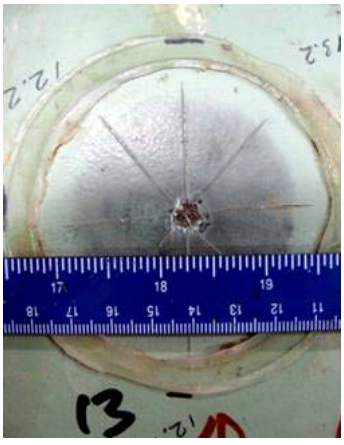

20 mA/ft^2

200 mA/ft^2

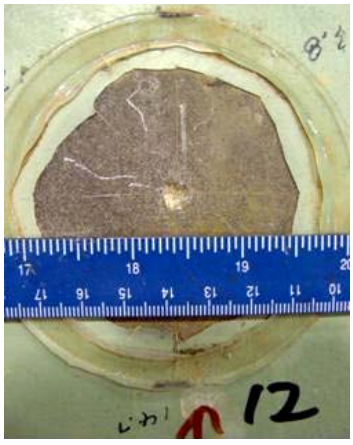

200 mA/ft^2

FBE 2, Roswell, New Mexico

2 mA/ft^2

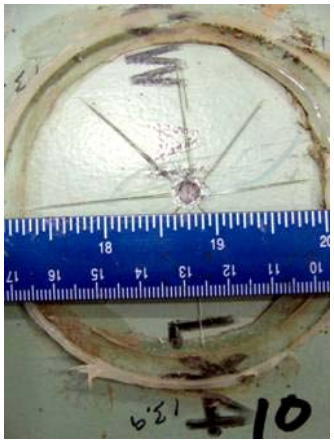

2 mA/ft^2

20 mA/ft^2

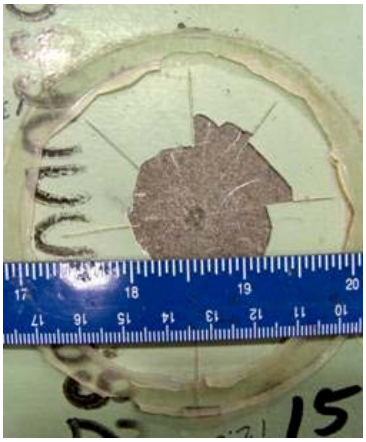

20 mA/ft^2

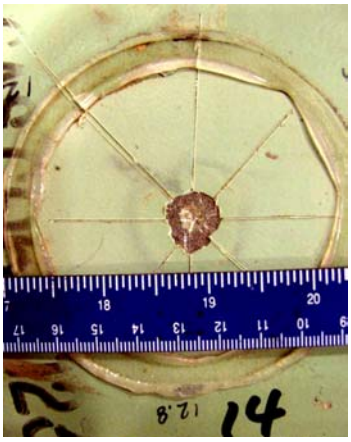

200 mA/ft^2

200 mA/ft^2

FBE 2, Dublin, Ohio

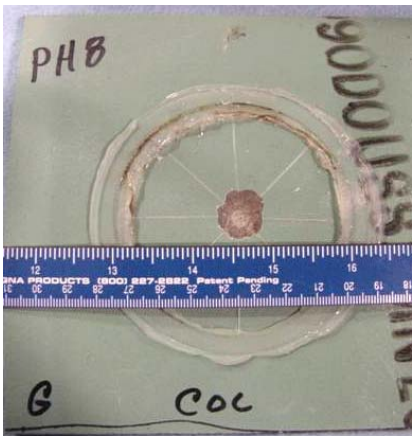

2 mA/ft^2

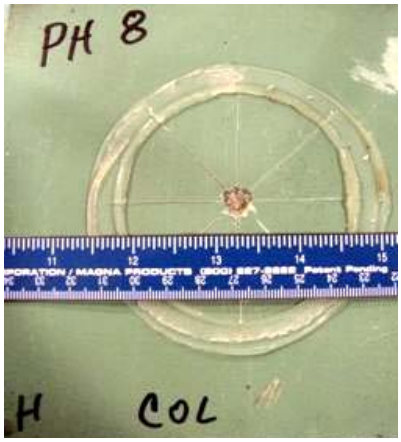

2 mA/ft^2

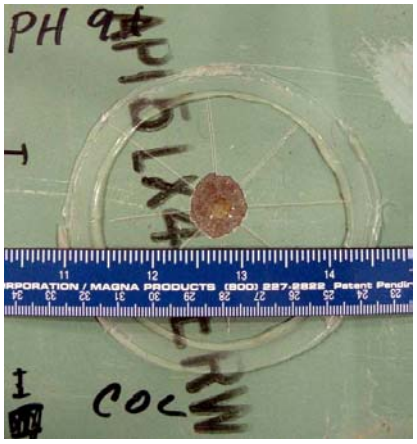

20 mA/ft^2

20 mA/ft^2

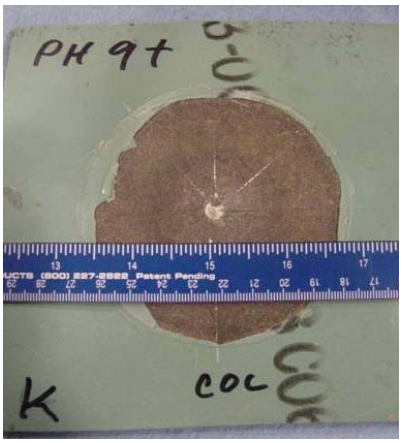

200 mA/ft^2

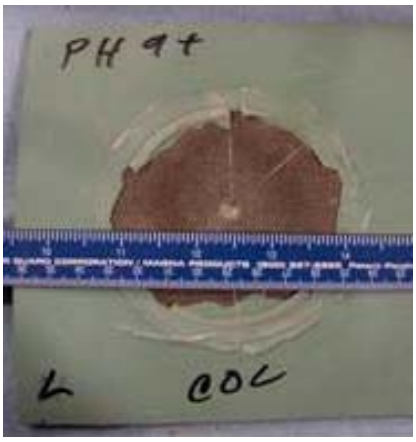

200 mA/ft^2

FBE 2, Trinidad, Colorado

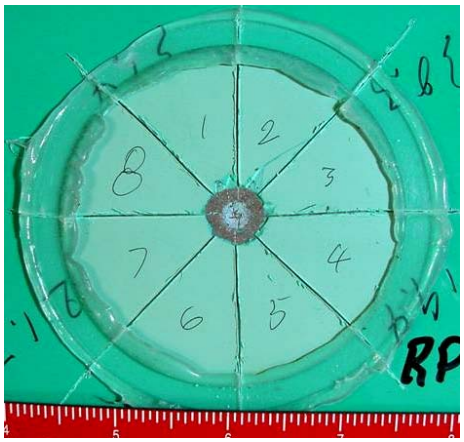

ASTM (NaCl)

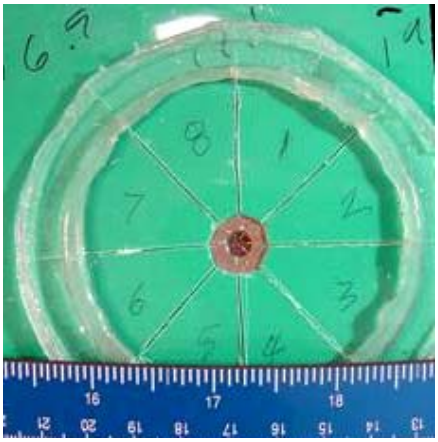

ASTM (NaCl)

No Holiday, Roswell, New Mexico

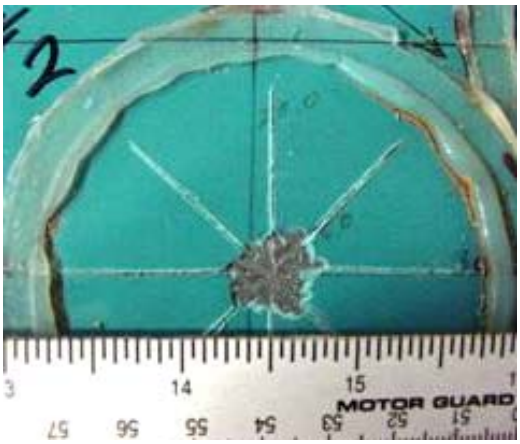

No Holiday, Roswell, New Mexico

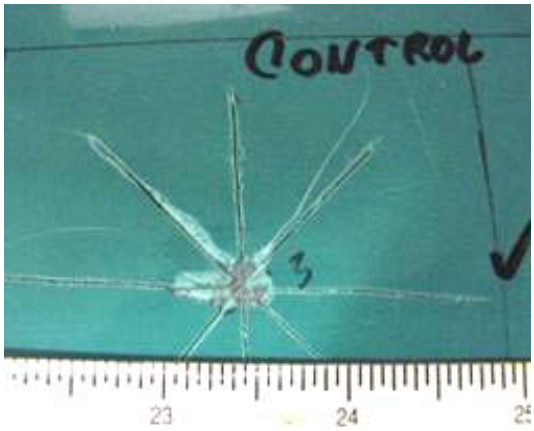

Control

LE (Repair)

2 mA/ft^2

2 mA/ft^2

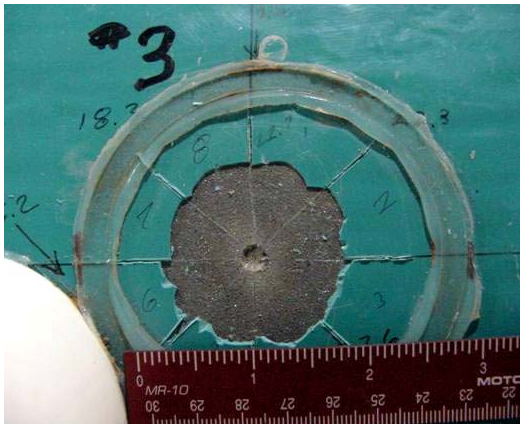

20 mA/ft^2

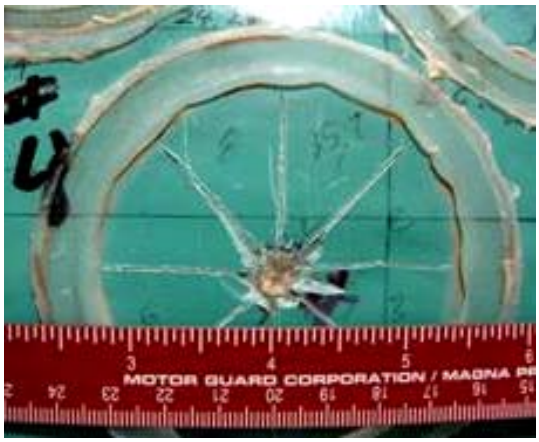

20 mA/ft^2

200 mA/ft^2

200 mA/ft^2

LE (Repair), Roswell, New Mexico

2 mA/ft^2

2 mA/ft^2

20 mA/ft^2

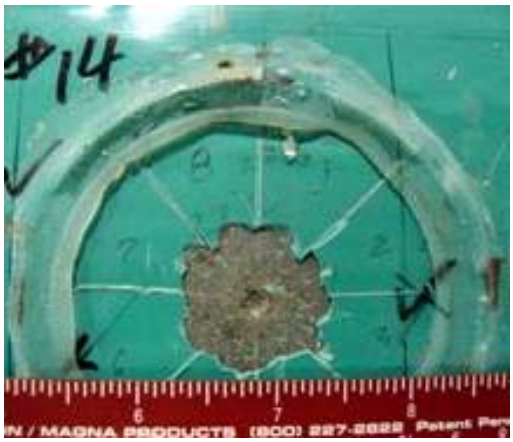

20 mA/ft^2

200 mA/ft^2

200 mA/ft^2

LE (Repair), Dublin, Ohio

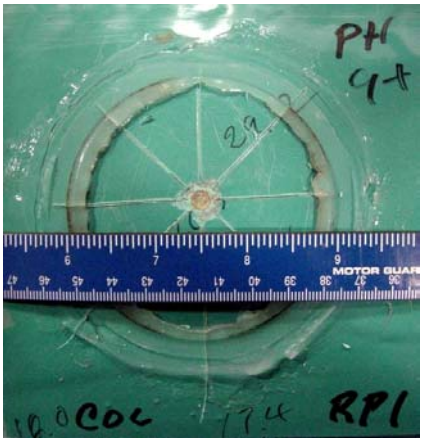

2 mA/ft^2

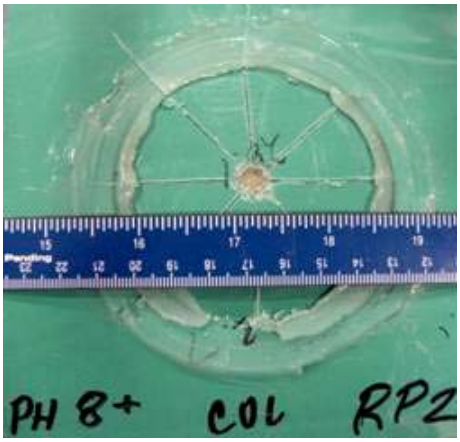

2 mA/ft^2

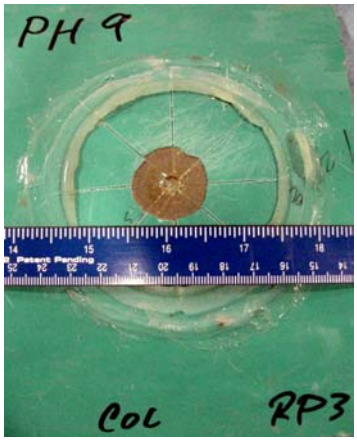

20 mA/ft^2

20 mA/ft^2

200 mA/ft^2

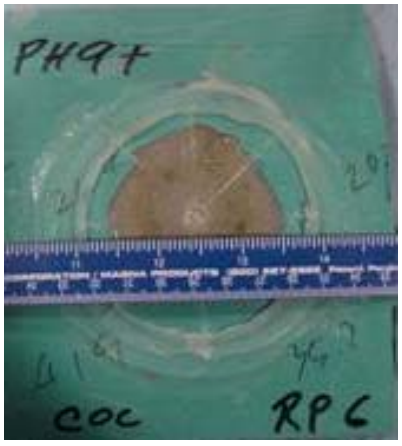

200 mA/ft^2

LE (Repair), Trinidad, Colorado

ASTM (NaCl)

ASTM (NaCl)

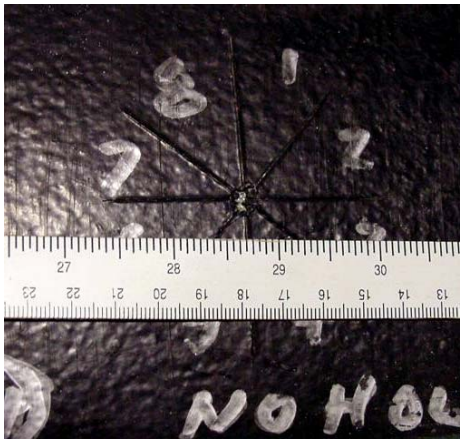

No Holiday, Roswell, New Mexico

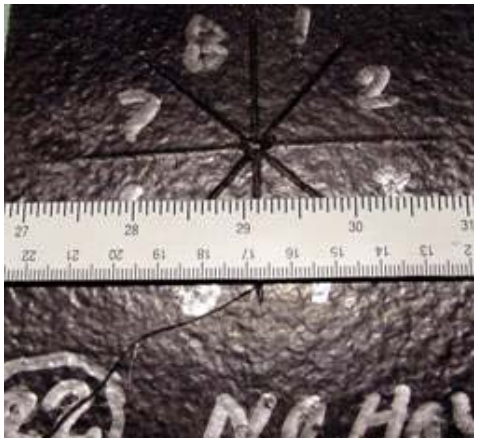

No Holiday, Roswell, New Mexico

Control

HPCC

2 mA/ft^2

2 mA/ft^2

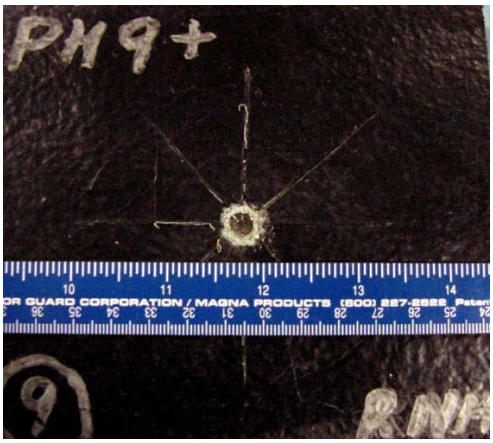

20 mA/ft^2

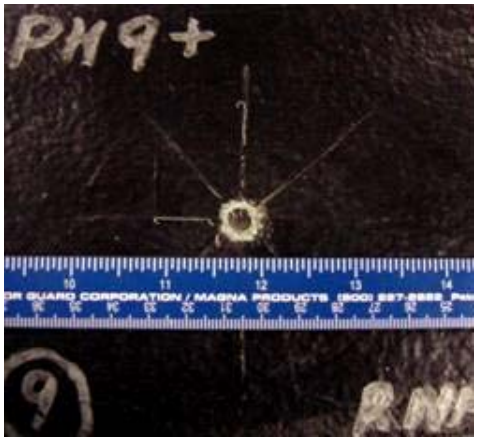

20 mA/ft^2

200 mA/ft^2

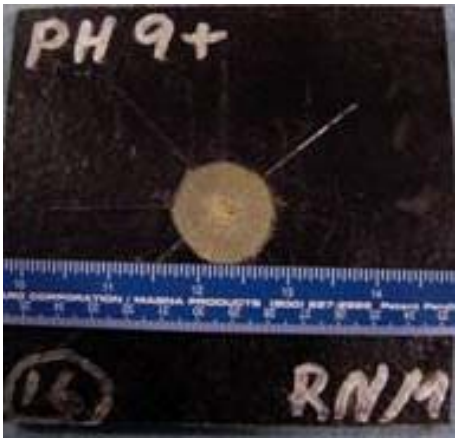

200 mA/ft^2

HPCC, Roswell, New Mexico

2 mA/ft^2

2 mA/ft^2

20 mA/ft^2

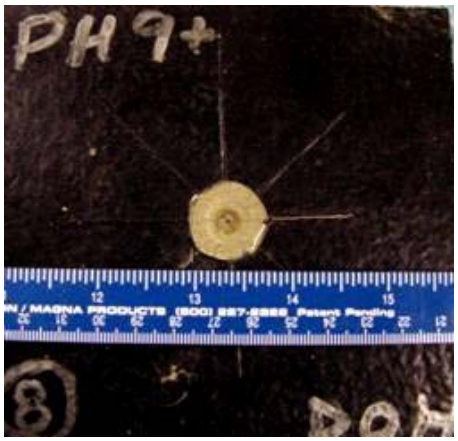

20 mA/ft^2

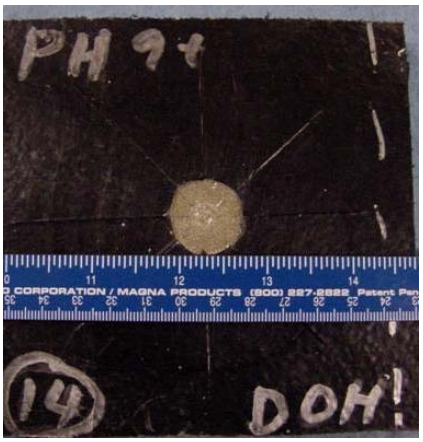

200 mA/ft^2

200 mA/ft^2

HPCC, Dublin, Ohio

2 mA/ft^2

2 mA/ft^2

20 mA/ft^2

20 mA/ft^2

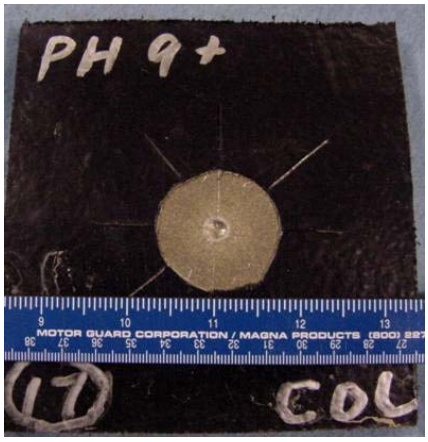

200 mA/ft^2

200 mA/ft^2

HPCC, Trinidad, Colorado